US Army Corps of Engineers

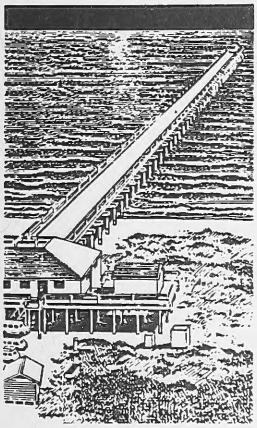

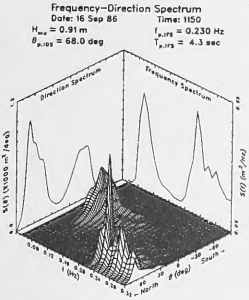




TECHNICAL REPORT CERC-91-1

# DIRECTIONAL CHARACTERISTICS OF WAVES IN SHALLOW WATER

by

Charles E. Long

Coastal Engineering Research Center

DEPARTMENT OF THE ARMY
Waterways Experiment Station, Corps of Engineers
3909 Halls Ferry Road, Vicksburg, Mississippi 39180-6199

and

Joan M. Oltman-Shay

College of Oceanography

Oregon State University
Oceanography Administration Building 104
Corvallis, Oregon 97331-5503



March 1991
Final Report



Prepared for DEPARTMENT OF THE ARMY
US Army Corps of Engineers
Washington, DC 20314-1000

Under Civil Works Research Work Unit 32484

Destroy this report when no longer needed. Do not return it to the originator.

The findings in this report are not to be construed as an official Department of the Army position unless so designated by other authorized documents.

The contents of this report are not to be used for advertising, publication, or promotional purposes. Citation of trade names does not constitute an official endorsement or approval of the use of such commercial products.

# REPORT DOCUMENTATION PAGE

*Form Approved*
*OMB No. 0704-0188*



| 1. AGENCY USE ONLY *(Leave blank)* | 2. REPORT DATE | 3. REPORT TYPE AND DATES COVERED |
|---|---|---|
| | March 1991 | Final report |

**4. TITLE AND SUBTITLE**
Directional Characteristics of Waves in Shallow Water

**5. FUNDING NUMBERS**
Civil Works Research
Work Unit 32484

**6. AUTHOR(S)**
Charles E. Long
Joan M. Oltman-Shay

**7. PERFORMING ORGANIZATION NAME(S) AND ADDRESS(ES)**
USAE Waterways Experiment Station, Coastal Engineering Research Center, 3909 Halls Ferry Road, Vicksburg, MS 39180-6199; Oregon State University, College of Oceanography, Oceanography Administration Building 104, Corvallis, OR 97331-5503

**8. PERFORMING ORGANIZATION REPORT NUMBER**
Technical Report
CERC-91-1

**9. SPONSORING/MONITORING AGENCY NAME(S) AND ADDRESS(ES)**
US Army Corps of Engineers
Washington, DC 20314-1000

**10. SPONSORING/MONITORING AGENCY REPORT NUMBER**

**11. SUPPLEMENTARY NOTES**
Available from National Technical Information Service, 5285 Port Royal Road, Springfield, VA 22161

**12a. DISTRIBUTION/AVAILABILITY STATEMENT**
Approved for public release; distribution unlimited

**12b. DISTRIBUTION CODE**

**13. ABSTRACT** *(Maximum 200 words)*

Proper coastal engineering design relies ultimately on a complete description of sea states to which natural or man-made structures are exposed. The character of directionally distributed wind wave energy is an intuitively and demonstrably important aspect of sea state definition, yet no long-term high-resolution coastal observations exist upon which to base engineering guidance. To remedy this, a multi-year series of directional wind sea and swell measurements has been undertaken at the Field Research Facility (FRF) of the US Army Engineer Waterways Experiment Station, Coastal Engineering Research Center (CERC). This report contains a preliminary analysis of 1,046 directional observations obtained during the first year of data collection. The climate during this year was typical of this site based on longer time series observations of winds, waves, and currents at the FRF.

(Continued)

**14. SUBJECT TERMS**
Directional spectra
Nearshore processes
Wave climate
Wave measurements
Wind waves

**15. NUMBER OF PAGES**
154

**16. PRICE CODE**

| 17. SECURITY CLASSIFICATION OF REPORT | 18. SECURITY CLASSIFICATION OF THIS PAGE | 19. SECURITY CLASSIFICATION OF ABSTRACT | 20. LIMITATION OF ABSTRACT |
|---|---|---|---|
| UNCLASSIFIED | UNCLASSIFIED | | |

13. (Concluded).

Bulk directional characteristics are deduced from a spread parameter, based on the angular arc which subtends the central half of the area under a wave energy directional distribution, and an asymmetry parameter, which indicates how evenly energy is distributed about the peak of a directional distribution. The spread parameter for energy integrated across all frequencies ranges from 20 to 60 deg with a distinct maximum occurrence near 40 deg. Unidirectional sea states do not exist in this data set. The same general behavior is found when data are evaluated frequency by frequency. The tendency for spread to be near 40 deg appears to occur under all conditions, being nearly independent of conventional sea state descriptors such as characteristic wave height, peak period, peak direction, and bulk steepness.

Multiple modes (distinct peaks in a directional distribution at a given frequency) occur in about one-third of the observations. Where multimodal distributions exist, energy tends to be evenly distributed among modes. Causes and effects of this feaure of wave climate are subjects for future research.

An indication of ordered structure in directional distributions at individual frequencies is apparent when select distributions are classed by ranges of spread and asymmetry parameter and then averaged to find mean shapes. Select distributions are those which are unimodal and contain enough wave energy to avoid noise contamination. The shapes thus found can be used as structural elements with which to constitute a complete sea state in numerical models or in signal generation algorithms for directional physical models. Only about one-third of all distributions are found to be symmetric. Symmetry is a common assumption in specifying analytic functions with which to model directionally distributed wave energy. The remaining two-thirds of observations are strongly asymmetric, a feature which is sure to have important consequences in wave dynamics inshore of the observation site.

# PREFACE

A paucity of observations of directionally distributed wave energy has hindered understanding and modeling of nearshore processes which affect coastal engineering projects. To help alleviate this dearth of knowledge, a long-term series of observations using a special, high-resolution directional wave gage has been initiated. This study was authorized by Headquarters, US Army Corps of Engineers (HQUSACE), under Civil Works Research Work Unit 32484, Directionality of Waves in Shallow Water, Coastal Flooding Program. Funds were provided through the US Army Engineer Waterways Experiment Station (WES), Coastal Engineering Research Center (CERC), under the program management of Dr. C. Linwood Vincent, CERC. Messrs. John H. Lockhart, Jr., John G. Housley, James E. Crews, and Charles W. Hummer were HQUSACE Technical Monitors.

The study was conducted by Dr. Charles E. Long at CERC's Field Research Facility (FRF) in Duck, NC, in cooperation with Dr. Joan M. Oltman-Shay of Oregon State University under the Inter-Governmental Personnel Act. The work was carried out under the direct supervision of Mr. William A. Birkemeier, Chief, FRF, and Mr. Thomas W. Richardson, Chief, Engineering Development Division, CERC; and under the general supervision of Dr. James R. Houston and Mr. Charles C. Calhoun, Jr., Chief and Assistant Chief, CERC, respectively.

Coordination of the initial installation of the directional gage was done by Messrs. Curt Mason, former Chief, and H. Carl Miller of the FRF. Installation and continued physical maintenance of the gage were done by the FRF dive team consisting of Messrs. Michael W. Leffler, William A. Birkemeier, H. Carl Miller, Eugene W. Bichner, and Brian L. Scarborough. Gage calibration has been maintained by Messrs. William E. Grogg (formerly) and Kent K. Hathaway (currently) of the FRF. Acquisition, monitoring, and storage of raw data have been done by Mr. Clifford F. Baron of the FRF. Substantial preparation of this manuscript was done by Mmes. Harriet M. Klein (formerly) and Dawn S. Miller (currently) of the FRF. This report was edited by Ms. Shirley A. J. Hanshaw, Information Technology Laboratory, WES.

Commander and Director of WES during the publication of this report was COL Larry B. Fulton, EN. Dr. Robert W. Whalin was Technical Director.

CONTENTS

# DIRECTIONAL CHARACTERISTICS OF WAVES IN SHALLOW WATER

## PART I: INTRODUCTION

### Basic Problem

1. Ocean waves in the so-called wind wave frequency band (roughly 0.04 to 0.3 Hz) are among the dominant forcing mechanisms in all coastal processes, acting on both natural and man-made boundary surfaces. An engineer designing a modification to the natural boundary needs to know the range and magnitude of these forces to ensure that the modification can withstand these forces and yet is economical to construct. Estimation of wave forces requires knowledge of the sea state in the vicinity of the modification. Full description of a sea state requires amplitude, frequency, and direction for each component of the wave field. There are myriad observations of amplitude and frequency from numerous field campaigns but very few detailed observations of wave direction. The latter condition represents a distinct and very important void in knowledge required for comprehensive engineering design. The intent of this report is to provide guidance on the directional characteristics of oceanic wind waves in shallow coastal waters based on a dedicated program of field measurements.

2. This report is intended for a readership with somewhat diverse backgrounds. As a result, some of the beginning material is basic and can be skipped (or scanned briefly). In particular, the remainder of Part I discusses importance of directional wave measurements, some past efforts in this regard, and some fundamental differences between low- and high-resolution directional wave gages. Part II is essentially a tutorial on frequency-direction spectra and can be skipped by those familiar with this subject. It also introduces basic notation and some conventional parameters. The reader might wish to scan Part II for these or refer to Appendix B, which lists all notation used in this report. Parameters introduced in Part II are also summarized at the end of Part V. Part III is a description of the measurement scheme, and the remaining parts are discussion and analysis of observations. Starting with Part III, information is germane to the results and so should be consulted.

## Conventional Approach

3. It is important to be able to characterize wave directionality, but the ability to do so has evolved very slowly. Coastal engineers consider wind wave forces in one main sense: how they act at the ocean boundaries. Within this realm, wave forces can be considered in two broad categories: how they act on solid structures and how they induce sediment transport. Solid structures include seawalls, groins, jetties, breakwaters, and the hulls of operating dredges. Sediment transport is important in beach erosion, inlet migration, silting of navigation channels, foundation failure under some solid structures, the fate of disposed dredged material, and the success of beach nourishment projects. In any of these applications, the detailed mechanics is extremely complex. Nonetheless, the gross behavior of wave-boundary interactions can be estimated adequately with simple models which characterize their dominant behavior. Obviously, if wind waves are used as input to a system response model, then the results are, at best, only as good as the wave field description.

4. For computational efficiency, the simplest models are preferred. Where knowledge is lacking, the simplest assumptions are usually made about the behavior of real systems. These two concepts were employed (in the days before computers and advanced gaging techniques) to characterize seas of various complexities as single wave trains. An entire sea would be considered to have a single characteristic height, frequency (monochromatic), and direction (unidirectional), with most natural wave data being estimated from observations. A broad base of engineering design guidance was established by using these three parameters to characterize wind waves as forcing mechanisms. Much of the guidance in the Shore Protection Manual (SPM)(1984) reflects this simple approach to sea state description.

5. With the advent of computers and advanced computation and gaging techniques, it became possible to record and analyze the time series of sea surface displacements at a point in space. Typical wave gages consisted of wave staffs, pressure gages, or heave (vertical displacement) buoys. Analysis of these data showed how wave energy was distributed in frequency; that is, at any given time, a wave field could be considered to contain a number of wave trains, each with its own amplitude and frequency. This type of (real) wave

field is called irregular. Though recognized as important, wave direction could not be determined from these gages.

## Irregular Waves Versus Monochromatic Waves

6. The response of a structure or nearshore bathymetry to attack by irregular waves can be very different from that by monochromatic waves. One difference is that irregular waves can add up their amplitudes (constructive interference) or cancel out their amplitudes (destructive interference) at various places in space. This interference makes such phenomena as wave run up, structural overtopping, and toe scour more or less intense for irregular waves than for monochromatic waves. Furthermore, even though an irregular wave field can be considered (to a first approximation) a linear sum of a number of monochromatic wave trains, sedimentary and structural responses to these waves are nonlinear. Nonlinearity means that estimates of these responses to irregular wave attack cannot be made by simply adding the responses determined from attack by an equivalent number of separate monochromatic waves.

7. The problem of irregular wave attack is more difficult than that of monochromatic waves but is not intractable. Engineering guidance for estimating these responses is derived from (a) gaging and monitoring existing real projects, (b) performing scaled physical model tests of various projects in laboratory wave basins, and (c) constructing mathematical models to represent the processes involved. All of these efforts are currently under way at the US Army Engineer Waterways Experiment Station (WES) Coastal Engineering Research Center (CERC) in Vicksburg, MS.

8. It is extremely useful to be able to characterize an irregular sea as simply as possible. A conventional way is by referring to the wave energy spectrum, which is simply a set of numbers (one for each frequency) proportional to wave energy. The formal name is the *spectrum of wave energy as a function of frequency*, and informally it is usually known as the *frequency spectrum*. If the set of numbers is graphed as a function of frequency, a curve through the plotted points illustrates the shape of the frequency spectrum.

## Models of Frequency Spectra

9. The potential number of frequency spectrum shapes is infinite even within the confines of the simple linear wave theory used to describe a wave field. Fortunately, nature behaves in such a way that the most common shapes of interest can be represented by a rather small class of mathematical functions. These functions are called *models of ocean wave frequency spectra*. Several models have evolved following physical arguments and observations by various investigators.

10. One of the most consistent models for high-frequency wind waves was derived by Phillips (1958). An extension of this model by Pierson and Moscowitz (1964) led to a model for fully developed wind seas in deep water. Observations during the Joint North Sea Wave Project (JONSWAP) (Hasselmann et al. 1973) enabled a further extension of the model for application to developing wind seas in deep water. Transformation of this model to shallow water by Bouws, Günther, and Vincent (1985) has led to what is known as the TMA (TEXEL, MARSEN and ARSLOE) frequency spectrum. Both the JONSWAP and TMA spectral models are being used by CERC for coastal engineering design studies (in the form of physical models). In further developments along this line, the TMA model has recently been modified by Miller and Vincent (1990) to account for nonlinear wave-wave interactions in the middle frequencies as derived by Kitaigorodskii (1983). These models require only a few parameters (usually six or fewer) to describe the whole frequency distribution of wind wave energy.

## Importance of Directionally Distributed Wave Energy

### Heuristic approach

11. Wave energy can be distributed in direction in the same sense that it can be distributed in frequency. That is, at a given frequency, wave energy can be coming from more than one direction. A simple way to visualize this concept is to imagine looking seaward from a beach at two approaching wave trains. The two wave trains have the same period, i.e., the same frequency. However, they are readily distinguishable because they approach the observer from different angles so that the pattern of wave crests for each wave train can be seen. If one train is coming from 45 deg to the observer's

left and the other from 45 deg to the right, the wave crests will intersect at 90 deg. Since the frequency of each wave train is the same, the wavelengths in both wave trains will be the same. The total pattern of wave crests will appear to be a square grid cocked at 45 deg to the beach and moving normally toward the beach.

12. If the two wave trains approach the beach at angles that are not as widely separated, say from 10 deg to the observer's left and from 10 deg to the right, the individual wave train crests will still be distinguishable; but the total crest pattern will be elongated in the longshore direction. Instead of being square, the grid pattern will be a rhombus. It will still move normally toward the beach. As the direction separation becomes yet smaller, the rhombus pattern gets more elongated in the longshore direction. Over most of the wave pattern, an observer with a good means of sensing direction would see an almost unidirectional wave train with crests of alternating waves aimed in slightly different directions.

13. Since wave energy moves in the wave propagation direction, the above examples illustrate wave fields where energy is distributed in direction but not frequency. Harmonic (i.e., frequency spectrum) analysis of the time series of sea surface elevation measured at one point in space would show wave energy at only one frequency for all cases. The wave field is thus monochromatic in that sense. One could add to the picture more waves of the same frequency but different directions. A graph of wave energy as a function of direction for this set of waves would be called the *direction spectrum of wave energy* for that frequency.

14. If the same process is done for waves at all the other frequencies in the wave field, one could construct a three-dimensional diagram of wave energy as a function of both frequency and direction. This type of display is called the *frequency-direction spectrum of wave energy*. If known completely, it constitutes a complete description of sea state insofar as energy available to do work is concerned.

15. In general, it is very important to know the directional characteristics of wave energy. If the energy at all frequencies is confined to a very narrow range of directions, then the engineering guidance based on unidirectional, irregular seas is sufficient for design work. However, if the energy at one or more frequencies is spread over a broad range of directions, then a host of problems can arise if unidirectional guidance is used.

16. For instance, one could imagine a directional distribution wherein the main (or peak) wave energy was shore normal approaching a uniform, plane beach, while a lesser amount of energy was at some angle other than normal. If the peak direction were used in a unidirectional model of shoreline response, the result would be entirely in the form of cross-shore sediment transport. However, if the complete wave field were considered, the smaller waves at an angle to the beach would induce a small, persistent longshore current. The sediment being lifted by the stronger, shore-normal waves would then be transported longshore by the currents induced by the smaller waves. Over time, the net longshore transport could be substantial; that is, unidirectional guidance based on the direction of peak wave energy would give an answer that is incomplete in a potentially important way.

Laboratory studies

17. A well-described quantification of effects of wave directionality at field sites has not been done. Lacking this, perhaps the most profound indications of wave directional effects are the results of two laboratory experiments, one reported by Vincent and Briggs (1989), and the other by Kaihatu and Briggs (in preparation). In the first experiment, wave fields with different distributions of frequency and direction were propagated over a submerged mound in the directional wave basin at CERC. Effects of wave directionality were observed by superposition of many wave trains traveling in a range of directions (a measure of which is called the *directional spread*) which varied from run to run. The ratio of total wave energy in the lee of the mound to that in front of the mound was used as a measure of system response. In all cases, it was observed that the greater the directional spread of the attacking waves, the lower the local relative energy was in the lee of the mound. For wave fields broadening from unidirectional to a 60-deg spread, the relative energy dropped by a factor of about four, a very substantial difference. The results suggest that if this amount of spread is a characteristic of real wave fields, designs based on unidirectional studies could overcorrect for wave attack. While the results are specific to the case tested, it shows the degree of variability of system response in directionally distributed seas. If thought of as an example of wave focusing by a mound of placed, dredged material, these results could influence decisions concerning mound shape, distance offshore of mound placement, and the risk of mitigating beach erosion induced by mound-focused waves.

18. In the second experiment, Kaihatu and Briggs (in preparation) examined the system response (primarily diffraction) in the lee of a (modeled) semi-infinite breakwater subject to various incident wave fields. Different frequency and direction distributions were used, similar to the mound study. Peak wave energy direction was maintained along the normal to the breakwater axis. A reference wave gage was placed near the point of the breakwater. Wave gages to monitor system response were arrayed along straight transects behind and at an angle to the breakwater, with transects originating at the breakwater point. As with the mound study, results varied with incident wave conditions. The dominant variable characterizing system response was directional spread of the incident waves. In contrast to the mound study, it was found that wave heights in the lee of the breakwater increased as spread increased. As much as twice the reference wave height (again, four times the energy) was observed with widespread (about 60-deg) incident waves as compared to unidirectional waves. This occurrence may have been, in part, because of the direct propagation of energy into the lee of the breakwater by waves from high incident directions on one tail of the main directional distribution. Nonetheless, it illustrates the point that peak direction alone is not a sufficient characterization of wave directionality.

19. Collectively, the two experiments indicated that coastal engineering system response can vary dramatically for fixed values of the three conventional wave-field descriptors (characteristic wave height, peak period, and peak direction). At least one measure of the angular spread of energy is required. The experiments suggest strongly that a parameter characterizing directional spread is at least as important as the three conventional parameters.

## Common Directional Wave Gages

20. One can imagine any number of other possibilities for the distribution of wave energy in frequency and direction. For engineering application in real projects, it is necessary to know the energy distribution in real seas rather than in a set of imagined, idealized seas. The present status of guidance in this regard is that while there is a physical wave basin as well as several mathematical theories which can use virtually any sea state description as input for modeling, there is very little detailed knowledge of

the real distribution of wave energy in shallow coastal waters. The primary reasons for this are (a) difficulties in high-resolution directional wave gaging, and (b) difficulties in obtaining observations at any one site over a time span long enough that the statistical character (mean conditions, extreme conditions, conditions during storms, etc.) of natural, shallow-water seas can be identified.

21. There is a variety of gages that sense wave direction, ranging from the human eye to elaborate arrays of sea surface displacement gages and on to satellite imagery. These gages vary markedly in their resolution of directionally distributed seas. The human eye is not well calibrated, gets tired, and gives results that change from human to human. Images from satellite overpasses tend to give data at one point in time (a snapshot) and not the time series required to determine mean properties of the directional distribution. Furthermore, the large extent of their horizontal sampling, often averaging over tens of kilometres, make them inappropriate for detailed (typical scale of a few hundred metres) nearshore studies. Radar devices have potential but have yet to demonstrate that they can yield high-resolution frequency-direction spectra.

22. Some commonly used wave direction sensors which obtain time series at a point in space are of low resolution in that they tend to overestimate directional spread and can only resolve wave trains of the same frequency which are separated by 90 deg or more in direction. They are of three general types:

a. The PUV gage (named for the pressure and two horizontal components of water velocity measured) relies on the unique phase difference between pressure and the horizontal velocity vector in a wave train running at a given direction.

b. The heave-pitch-roll buoy relies on the phase difference between sea surface displacement (the heave axis) and components of sea surface tilt (or slope) determined from pitch-and-roll measurements in a wave train.

c. The Sxy or slope array gage is like the heave-pitch-roll buoy except surface displacement and surface tilt components are found from pressure gages mounted in the water column. Pressure records are converted to surface elevation by way of linear wave theory.

23. Where a directional distribution is well behaved (one main peak direction with lesser energy at nearby directions and very little energy at directions well away from the peak), these gages can do extremely well in estimating peak direction, generally within a few degrees. However, if there are two equal energy wave trains at the same frequency but well separated directions (as in the example given in par. 11), these gages will tend to give an angle somewhere midway between the two peak directions. While such a result gives a kind of mean angle for the wave field as a whole, it does not represent either wave train very well since it attributes the peak wave energy to a direction in which there is no wave energy. Hence, gage output can be quite misleading.

24. With a more advanced analysis algorithm, data from any of the above gages can be processed to detect two separate wave trains at the same frequency, but only if their propagation directions are separated by 70 deg or more (Oltman-Shay and Guza 1984). This algorithm is an improvement, but it still does not give enough information for a complete sea state description.

25. This discussion does not mean that information from any of these gages is of little use. A partial frequency-direction spectrum is immensely preferred over a spectrum with no directional information. Furthermore, these devices are compact and relatively simple to deploy. In complex bathymetry or in highly variable wave fields near solid structures, they are among the most reliable direction-sensing devices in existence.

26. An improvement to these gages, developed by Cartwright and Smith (1964), is an articulated (cloverleaf) buoy which is able to estimate three components of sea surface curvature as well as heave, pitch, and roll. This buoy's directional distribution resolving ability is improved because six properties of the sea surface are measured instead of the three used in the simpler gages. It is able to resolve peak energy directions quite well and angular spreads of about 60 deg. If energy is spread over angles of less than 60 deg, the spread is not well resolved. For example, it could not distinguish very well the different cases in the experiments by Vincent and Briggs (1989), and Kaihatu and Briggs (in preparation). However, resolution of the cloverleaf buoy is better than that of the simpler gages, and it provides a hint of the true spread of a natural sea.

27. This property of the cloverleaf buoy led to a series of measurements reported by Mitsuyasu et al. (1975) at various sites near Japan. From

five observations (only two in shallow water), they estimated the constants related to a series of hypotheses on the directional structure of natural wind-driven seas. Their intent was to provide guidance for using sea state models in engineering design. As a result, their work is among the most frequently referenced in this regard. However, they did not make enough measurements to estimate a wave climate in shallow water; and their conclusions were based on measurements with an intermediate-resolution directional gage. It remains to be seen whether their results are universally applicable, i.e., true at other shallow-water sites, valid in all wave climates, and verified by measurements with a higher resolution directional gage.

## Gage Arrays

28. High-resolution directional gages almost all rely on synoptic observations of sea surface displacement at many points in space. This sampling requirement is analogous to the resolution of frequency spectra by the measurement of sea surface displacement at many points in time (e.g., a time series from a wave staff). Simultaneous observations from a spatial array of sea surface sensors enables the spatial properties (i.e., directionality) of a wave field to be determined from the measured sea surface topography. Note that this method does not require any particular knowledge of a relation between wavelength and wave period. If the time series analog is followed exactly, then one must measure as many points in the wavelength of a wave train as one measures in time divisions of the period of a wave train. For example, if a time series collects 20 samples per period of a given wave, then a spatial array must sample a grid of 20 points on a side (since there are 2 horizontal coordinates) which covers the wavelength of the wave. Requiring a total of 400 gages, this condition is normally beyond practical application.

29. This principle was applied once in an experiment called the Stereo Wave Observation Project (Cote et al. 1960). Stereo photographs of the sea surface were made from low-flying aircraft, and the resulting images were analyzed using topographic techniques. Sea surface elevations were then discretized in a 60- x 90-element grid for an effective 5,400 gage positions. At great expense and effort, one high-resolution directional spectrum was

determined in this way. Though the technique works, it is not practical for daily observations over an extended period.

30. An alternative is to use fewer gages, use what is known of wave behavior, and construct estimation algorithms to compute directional spectra from a (relatively) sparse number of sea surface measurement points. This method uses a practical number of gages (usually around 10 wave staffs or pressure sensors) deployed with intergage spacing tuned to resolve the range of wavelengths expected at a given site. These are called *spatial arrays* (since they are distributed in space), *phased arrays* (since they determine direction by phase differences in passing wave forms), or just *arrays*. Criteria for optimum spacing, layout, and data analysis from gage arrays have been described by Barber (1961); Davis and Regier (1977); Donelan, Hamilton, and Hui (1985); and others. Such arrays can give higher directional resolution than the simpler gages described previously because they measure more properties of the sea surface and their gage elements can be positioned for optimum response to a wave field given the input requirements of the data analysis algorithm used.

31. Array gages cannot be used everywhere. One practical limitation is that a number of gages must be operating simultaneously. The set of gages therefore requires rather constant monitoring and attention. Another is that the wave field must be uniform (i.e., have the same basic statistics) throughout the area covered by the array. This condition is not expected in regions of irregular bathymetry or in regions of high reflectivity (near structures).

32. There is a wealth of literature on the topic of spatial arrays. The bulk of it deals with theoretical considerations of array design, analysis algorithms, and field tests of particular configurations. One of these schemes is described in more detail below. For the purpose of this introduction, the interest is in reports of long-term observations which provide guidance in high-resolution characteristics of nearshore seas.

33. Such observations are scant, especially in inshore waters. Long-term oceanic observations are nonexistent. Donelan, Hamilton, and Hui (1985) performed a 14-month experiment using an array of 14 wave staffs in 10-m water depth at the southern end of Lake Ontario. Their primary interest was in the evolution of wind-generated wave fields, so they collected wave data only when local winds were changing significantly. The resulting set of eighty-four 1-hr observations did not constitute a complete wave climate. Furthermore, the

maximum fetch was 300 km so that wind waves and swell from distant generating areas (as would occur in an oceanic environment) were not present. Thus, while this work is invaluable for studies of local wind wave generation dynamics and for some measure of the climate in a bounded (lake) environment, it does not satisfy the need for oceanic observations.

34. In summary, it is intuitively, theoretically, and experimentally known that detailed directional characteristics of waves incident to shallow, nearshore waters are fundamentally important to coastal processes affecting any engineering endeavor undertaken. Aside from some valuable but shadowy hints of the bulk directional distribution statistics of wind wave energy, there are insufficient direct observations of these distributions to guide an engineer in project design.

## Measurement Program

35. To help alleviate this dearth of knowledge, a program was begun in September 1986 to collect and analyze high-resolution directional wave data at CERC's Field Research Facility (FRF) located near the middle of Currituck Spit, just north of the village of Duck, NC (Figure 1). The intent was to create a long-term database, augmented by the ongoing climatological measurements at the FRF, which would provide a detailed picture of the statistics and dynamics of wave fields incident at that site.

36. The FRF was chosen as the site for several reasons. It is representative of many coastal sites characterized by (a) broad continental shelf, (b) relatively mild bottom slope, and (c) reasonably uniform longshore topography. These properties also make the site ideal for measurements with a high-resolution spatial array gage. The mild sloping bottom substantially dissipates wind waves so that attention can be focused on waves arriving (or attacking) from seaward. The angular viewing window can thus be reduced from the full 360-deg circle required in deep water or near a reflecting structure to the 180-deg half-circle of incoming wave directions. Further, the FRF's permanent staff and computing facilities can be used to monitor, maintain, and error check the directional gage on a day-to-day basis to minimize data losses from the myriad problems that can plague field data collection.

37. The site does not represent all possible coastal sites, so the detailed results are not expected to be universal. Results from this site are

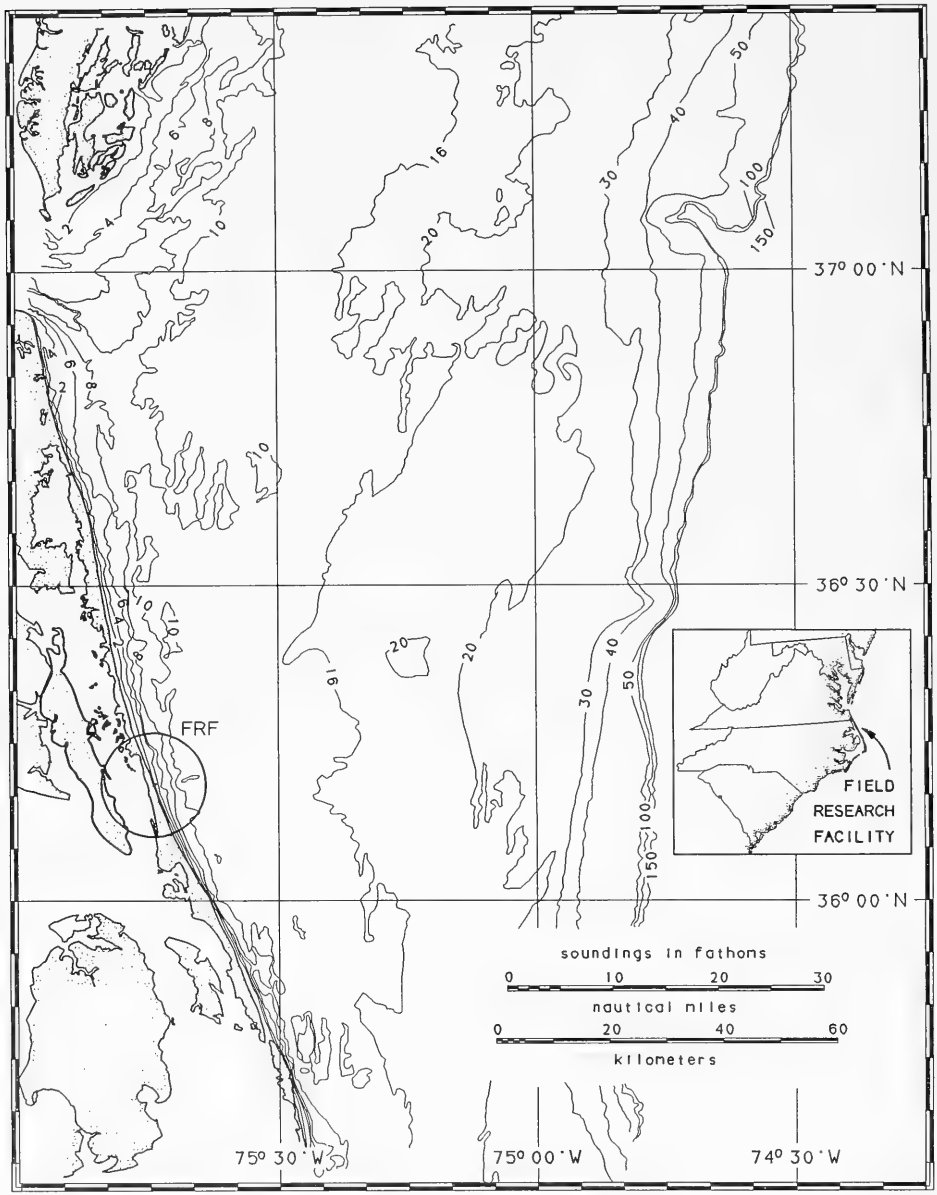


Figure 1. FRF location and offshore bathymetry

expected to be indicative of wave climates inshore of broad, shallow continental shelves. This type of bathymetry is common on the US east coast and in the Gulf of Mexico. It is less common on US coasts of the Pacific Ocean.

38. This report is based on data from the first year of the measurement program. It is a preliminary evaluation of some statistical properties of well-resolved, directionally distributed wave energy. Primary emphasis is on the distribution of bulk or overall directional spread, its relation to conventional sea state parameters, and its use in characterizing detailed wave energy directional distributions. These data have been archived for additional study, and they can be used to upgrade existing numerical and physical models of nearshore processes so that, by higher fidelity representations of natural seas, a truer estimate of structural and nearshore responses will be obtained.

## PART II: NOTATION AND SEMANTICS OF DIRECTIONAL SPECTRA

39. A system of notation is necessary to communicate ideas and organize data for use in mathematical models and computer-controlled physical models. This notation applies to wave energy spectra, corresponding sea surface descriptions, and their interrelationships. Since several types of spectra were mentioned in the introduction, a graphic display is useful so the reader can picture what the notation means. In this section a (conventional) notation is defined, and some pictorial examples of wave spectra are presented.

### Review of Basic Definitions

40. The basis for all analysis used in this report is linear (or Airy) wave theory. Its properties are described and further references given in the SPM (1984). In this theory, a complex wave field is approximated by a number of individual wave components or trains. Each wave train is a simple sinusoidal displacement of the sea surface from a reference (still) water level propagating in one direction along a horizontal plane with a certain speed. If $\eta$ is the water surface,* $x$ and $y$ are horizontal coordinates, and $t$ is time, a single wave train can be represented by

$$\eta(x,y,t) = a \cos(2\pi ft - kx \cos \theta' - ky \sin \theta' + \phi) \qquad (1)$$

where, relative to a straight reference coastline,

$x$ = shore-normal coordinate, originating at sea and increasing toward land

$y$ = longshore coordinate, increasing to the right of an observer looking seaward

$a$ = wave amplitude or half the wave height in linear theory

$f = 1/T$, wave frequency with

---

* For convenience, symbols and abbreviations are listed in the Notation (Appendix B).

$T$ = wave period

$k = 2\pi/L$ , radian wave number with

$L$ = wavelength

$\theta' = 2\pi\theta/360$ , direction (in radians counterclockwise from the negative x-axis) from which waves are coming

$\theta$ = (the same) wave direction in degrees

$\phi$ = initial phase or location in the wave cycle at some fixed point in space and time

41. Wherever possible in this report, wave direction will be given in degrees; therefore, the variable $\theta$ will be used. Conversion to $\theta'$ is only necessary in arguments of trigonometric functions.

42. In linear theory, wave number $k$ is uniquely related to frequency $f$ for a given water depth. The formula is known as the *dispersion relation* and is given by

$$4\pi^2 f^2 = gk \tanh kd \tag{2}$$

where $g$ equals acceleration as a result of gravity, and $d$ equals water depth.

43. Though there are many variables involved in Equations 1 and 2, most are known or can readily be computed. Generally, for a given depth of water, a complete description of the sea surface and all the other properties of a single wave train are known if the variables $a$ , $f$ , $\theta$ , and $\phi$ are specified. In particular, the mean wave energy per unit crestlength $E$ available to do work (on a beach or structure) can be found. It is given by

$$E(f,\theta) = \tfrac{1}{2}\rho g a^2 \tag{3}$$

where $\rho$ equals water density (mass per unit volume). In the ocean, the factors $\rho$ and $g$ vary by less than 3 percent. It is conventional to drop them from expressions which refer to energy (as in spectral formulations) with the understanding that they are to be reintroduced when actual energies are computed. This abbreviated expression for mean wave energy per unit crestlength has units of length squared and is given by

$$E'(f,\theta) = \frac{1}{\rho g} E(f,\theta)$$

$$= \tfrac{1}{2}a^2 \qquad (4)$$

The expression on the right is more formally known as the variance per unit crestlength of the water surface displacement. Thus, Equation 4 is sometimes called the *sea surface variance*. It is still proportional to the energy, as shown.

44. The energy represented by Equation 4 does not expressly depend on frequency, direction, or phase, just amplitude. Frequency and direction are retained (as arguments) on the right side of the equation for two reasons. First, when more than one wave train is present, energy is said to be distributed in the frequency-direction domain. More general expressions of energy will have frequency and direction appear on the left side of the equation. Second, for a numerical or physical model to simulate a sea, the amplitude can be found (if the energy is known) from Equation 4, but frequency and direction must be known for Equation 1 to be complete.

45. Phase $\phi$ does not appear in the energy definition because energy is an average over one wave cycle. Hence, phase information is not usually represented in energy spectral representations. In applied modeling of linear wave fields, phases are typically assigned random values from the range 0 to 360 deg (or 0 to $2\pi$ radians).

46. A real sea, in terms of linear theory, is the sum of many wave components, all having a form like the right side of Equation 1 but with different amplitudes, frequencies, and directions (and phases). It is convenient to consider frequency and direction in discrete terms. For either frequency or direction, one can divide the full range of values into a number of increments (or bands) of finite size and assign any property within a given band to the frequency or direction at the center of the band. This discretization is convenient for bookkeeping (i.e., computer storage or data plotting) and is a consequence of conventional harmonic analysis which forms consistent patterns in the way data are communicated. Since the increments can be made arbitrarily small, this leads to no theoretical loss of

generality. The only restrictions are hardware limitations of measuring and analyzing real data.

47. To discretize frequency, the full range of frequencies of interest (herein those associated with wind waves) is divided into a number $N$ of increments of size $df$. If $f_n$ is the center frequency of the $n^{th}$ increment, any wave having a true frequency in the range $f_n - \frac{1}{2}df < f < f_n + \frac{1}{2}df$ is considered to have the frequency $f_n$ as an approximation. Direction is discretized in the same way. The range of directions of interest (-90 to +90 deg for incident waves near a coast) is divided into a number $M$ of small arcs of size $d\theta$. A wave with a true direction in the range $\theta_m - \frac{1}{2}d\theta < \theta < \theta_m + \frac{1}{2}d\theta$ is assigned the approximate direction $\theta_m$, where $\theta_m$ is the center direction of the $m^{th}$ arc.

48. Within this type of frequency-direction coordinate system, it is relatively simple to write a formula for a complex sea with several contributing wave trains. As an extension of Equation 1, it takes the form

$$\eta(x,y,t) = \sum_{n=1}^{N} \sum_{m=1}^{M} a_{mn} \cos(2\pi f_n t - k_n x \cos \theta_m - k_n y \sin \theta_m + \phi_{mn}) \qquad (5)$$

where

$N$ = number of frequency components

$M$ = number of direction components

$a_{mn}$ = wave amplitude corresponding to frequency $f_n$ and direction $\theta_m$

$f_n$ = center frequency of the $n^{th}$ frequency band and defined by

$f_n = f_1 + (n - 1)df$ for $n = 1,2,\ldots,N$, with

$f_1$ = center frequency of the first frequency band (typically near 0.05 Hz for wind waves)

$f_N$ = center frequency of the last frequency band (typically near 0.3 Hz for wind waves)

$k_n$ = wave number corresponding uniquely with $f_n$ for a given depth $d$ through Equation 2

$\theta_m$ = center direction of the $m^{th}$ direction arc and defined by

$\theta_m = \theta_1 + (m - 1)d\theta$ for $m = 1,2,\ldots,M$, with

$\theta_1$ = center direction of the first direction arc (typically near -90 deg for the coordinate system defined above)

$\theta_M$ = center direction of the last direction arc (typically near +90 deg for the current coordinate system)

$\phi_{mn}$ = initial phase of the wave train associated with the $n^{th}$ frequency and $m^{th}$ direction

49. With this type of bookkeeping, a real sea can be characterized by a finite (but arbitrarily large) number of wave components. With N frequencies and M directions, there is a total of $M \times N$ components. A simple way to archive or plot this information would be to store the two one-dimensional arrays of frequency $f_n$ and direction $\theta_m$ and the two two-dimensional arrays of amplitude $a_{mn}$ and initial phase $\phi_{mn}$. This procedure would completely define the sea surface and all other wave field properties to the accuracy of linear wave theory and to the resolution of the discretized frequencies and directions.

50. However, the interest here is in wave energy. Because of the discretized frequencies and directions, the energy of a wave train at frequency $f_n$ and direction $\theta_m$ is simply proportional to

$$E'(f_n, \theta_m) = \tfrac{1}{2}a_{mn}^2 \tag{6}$$

as in Equation 4 for a single component wave train. When multiplied by (the nearly constant) $\rho g$, Equation 6 gives the (ultimately desired) mean wave energy per unit wave crest for this wave component.

51. Though expressed at a particular frequency and a particular direction, Equation 6 actually represents the energy of all waves that have frequencies in the small frequency band df centered on $f_n$ and directions in the small arc $d\theta$ centered at $\theta_m$. In results from a variety of experiments, the frequencies and directions can be (and usually are) discretized in different-sized frequency bands and direction arcs. If various step sizes are used in data from the same experiment, i.e., from the same wave field, a variety of energies will be obtained by Equation 6 because more or less of the frequency and direction domain is included in each energy estimate. This effect is eliminated if the energy measure of Equation 6 is divided by the product of df and $d\theta$. The result tells how densely energy is concentrated

per unit of frequency and direction and makes it possible to compare results from various experiments. This entity is known as the *frequency-direction spectral density* of wave energy or, more simply, the *frequency-direction (FD) spectrum* denoted by $S(f_n,\theta_m)$ , and defined by

$$S(f_n,\theta_m) = \frac{\frac{1}{2}a_{mn}^2}{df \cdot d\theta} \tag{7}$$

52. The left side of Equation 7 is often abbreviated as $S(f,\theta)$ where the subscripts $m$ and $n$ have been dropped from the arguments, suggesting an approximation of a continuous function.

53. The result expressed by Equation 7 is still proportional to wave energy per unit crestlength for a region of the frequency-direction domain of dimensions $df$ and $d\theta$ from a given experiment since $df$ and $d\theta$ are the same everywhere in the domain. The conversion from spectral density to energy is multiplication of the elements of Equation 7 by $\rho g \cdot df \cdot d\theta$ .

54. Generally, energy is found from larger or smaller areas in the frequency-direction domain by adding (integrating) elements (or partial elements) over the region of interest. In particular, one can obtain the conventional frequency spectrum (resulting from measurements at a single point in space and from which the JONSWAP, TMA, etc., models have been derived) from the frequency-direction spectrum by summing Equation 7 over all direction contributions times the incremental arc $d\theta$ for each frequency. Denoting the frequency spectrum by $S(f_n)$ , the result becomes

$$S(f_n) = \sum_{m=1}^{M} S(f_n,\theta_m)\, d\theta \tag{8}$$

55. This equation gives a measure of the total wave energy in each frequency increment where contributions from all wave directions are included. The frequency spectrum can be considered as a frequency-direction spectrum with the lowest possible directional resolution (none) where the "incremental" arc length is the full 360 deg of possible wave directions. The left side is often abbreviated as $S(f)$ . Since this definition is derived from an integration of $S(f,\theta)$ , it can be called the *integrated frequency spectrum* (IFS).

56. Where the full frequency-direction spectrum is known, one can compute another useful entity known as the direction spectrum. A direction spectrum is a measure of the total wave energy from each direction where the total is found by adding the contributions from each frequency band for a given direction arc. The direction spectrum is denoted by $S(\theta_m)$ and is computed by

$$S(\theta_m) = \sum_{n=1}^{N} S(f_n, \theta_m)\, df \qquad (9)$$

57. The direction spectrum is a relatively new entity, primarily because there are so few observations of the complete frequency-direction spectrum that it has not been computed. It is extremely useful for characterizing the bulk properties of an energy distribution where contributions from all frequencies, not just a particular frequency, are considered. The symbol on the left of Equation 9 is often abbreviated as, simply, $S(\theta)$. Since it is derived from an integration of $S(f,\theta)$, it can be called the *integrated direction spectrum* (IDS).

## Some Fundamental Bulk Parameters

58. Total energy of a wind wave field is proportional (by the factor $\rho g$) to the volume under the frequency-direction spectrum. This is an important parameter with which to characterize any wave field. It is commonly expressed in the form of a characteristic wave height $H_{mo}$. This parameter is derived from the fact that the volume under a frequency-direction spectrum (sometimes called the *zeroth moment*, hence the subscripts "mo") is identically the variance of sea surface displacement, having dimensions of length squared. The square root of this is the standard deviation of sea surface displacement. Under the assumption of a Rayleigh distribution of wave heights, the average height of the highest one-third waves is nearly four times this standard deviation. Whether or not the Rayleigh distribution approximates the wave field everywhere, four times the sea surface standard deviation has come to be regarded as a characteristic parameter of a wave field. Formally, $H_{mo}$ is derived as

$$H_{mo}^2 = 16 \sum_{n=1}^{N} \sum_{m=1}^{M} S(f_n, \theta_m) \, df \, d\theta \tag{10}$$

59. Either of the two sums in Equation 10 can be replaced by the corresponding single sums that define $S(f_n)$ or $S(\theta_m)$. Equivalent alternative definitions for $H_{mo}$ are, therefore,

$$H_{mo}^2 = 16 \sum_{m=1}^{M} S(\theta_m) \, d\theta \tag{11}$$

and

$$H_{mo}^2 = 16 \sum_{n=1}^{N} S(f_n) \, df \tag{12}$$

Equation 12 is the conventional definition, arising from the more commonly observed frequency spectra computed from a time series of observations at a point in space.

60. Two other common parameters are characteristic frequency and characteristic direction for a given sea state. These are typically associated with the frequency and direction at which the most energy is concentrated, corresponding with peaks in the spectra. The symbol $f_p$ is used to denote the frequency at which a spectrum has a maximum in energy density. Both the frequency spectrum $S(f)$ and the frequency-direction spectrum $S(f,\theta)$ usually have peak frequencies, but they may not be the same. If a frequency-direction spectrum has a narrow directional spread at one frequency and a broad spread at a second frequency, the peak of the frequency-direction spectrum would be at the first frequency. When summed over all directions, however, the total energy at the second frequency may be greater. In this case, the integrated frequency spectrum would have a peak at the second frequency. To distinguish the two in notation, additional subscripts are added. Thus, $f_{p,FD}$ equals frequency at the peak of the frequency-direction spectrum $S(f,\theta)$ ; and $f_{p,IFS}$ equals frequency at the peak of the integrated frequency spectrum $S(f)$ . The latter measure is the conventional definition deduced from a time series at one point in space.

61. In the same sense, the symbol $\theta_p$ (peak direction) denotes the direction at which there is a maximum in energy. Conflict can occur here between peaks in the direction spectrum $S(\theta)$ and the frequency-direction spectrum $S(f,\theta)$ . The two peak directions are distinguished by the notation

$\theta_{p,FD}$ equal to direction at the peak of the frequency-direction spectrum $S(f,\theta)$, and $\theta_{p,IDS}$ equal to direction at the peak of the integrated direction spectrum $S(\theta)$.

62. Note that the letter "S" has been used to represent spectral density in general, and the arguments inside the parentheses dictate which spectrum is being referenced. That is, $S(f,\theta)$ denotes the frequency-direction (FD) spectrum, $S(f)$ is the (conventional) integrated frequency spectrum (IFS), and $S(\theta)$ is the integrated direction spectrum (IDS).

## Some Illustrated Examples

63. To form an image of these spectra, Figure 2 shows four examples of wave energy distribution. Three are contrived for illustration purposes, and one is from a real wave field for comparison.

64. Figure 2a illustrates the energy of a single wave train, i.e., a monochromatic, unidirectional sea as might be represented by Equation 1. The picture has three parts, a base, and what appear to be two walls rising perpendicular to the base at its back edges. The base contains a grid which represents the direction (labeled on the front right edge of the base) and frequency (front left edge of the base) coordinates. The grid spacing is $d\theta = 2$ deg along the direction axis and $df = 0.00974$ Hz along the frequency axis. (These numbers were not chosen to confuse the reader but are the resolution direction and frequency increments used in the analysis described later in this report.)

65. Elevations above this base grid form a three-dimensional picture of $S(f,\theta)$. For a single wave train, this appears as a spike at the frequency and direction (roughly, $f = 0.17$ Hz and $\theta = 45$ deg) of the wave train. (Graphics packages notwithstanding, it should formally appear as a rectangular solid with vertical walls and a top and base both of dimensions $df \times d\theta$.) Values of zero exist at all other grid locations. The volume under the spike, $S(0.17 \text{ Hz}, 45 \text{ deg}) \cdot df \cdot d\theta$, is half the squared amplitude of the wave train, following Equation 7, which is proportional to the wave energy, following Equation 3.

66. If the frequency-direction spectrum of Figure 2a is summed over all directions for each frequency, the frequency spectrum is obtained, as in Equation 8. This is shown as the vertical appearing panel at the right rear

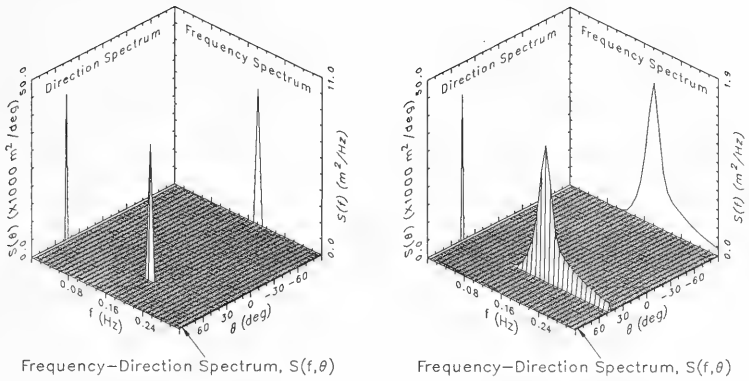


a. Monochromatic, unidirectional

b. Irregular, unidirectional

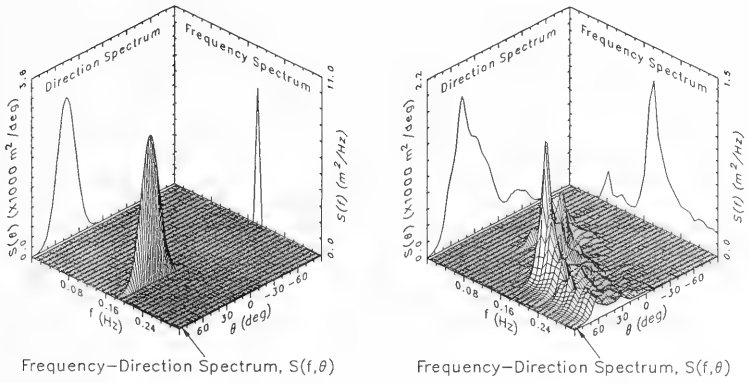


c. Monochromatic, directionally spread

d. Real sea state

Figure 2. Examples of frequency, direction, and frequency-direction spectra

of Figure 2a. Since there is energy at only one frequency in the frequency-direction spectrum, there is energy at only one frequency in the frequency spectrum and the spectrum appears as a spike. (Again, it should be a rectangle of width df .) All direction information is lost, but its cumulative contribution has been accounted for. In this case, the area under the frequency spectrum, $S(0.17\ Hz)\cdot df$, is half the squared amplitude of the wave train.

67. The direction spectrum for this case is shown in the vertical appearing panel at the left rear of Figure 2a. It is found by summing the frequency-direction spectrum over all frequencies for each direction, as in Equation 9. As with the frequency spectrum, there is energy from only one direction, so the direction spectrum is also a spike (i.e., rectangle of width $d\theta$ ). The area under this curve, $S(45\ deg)\cdot d\theta$ , is again half the squared amplitude of the wave train.

68. The unidirectional, monochromatic case is the simplest example of the different spectral types. A more complicated sea can be constructed or represented by simply adding more spikes (rectangular solids) with various amplitudes and at various frequencies and directions to the frequency-direction spectrum.

69. Figure 2b illustrates a case where energy is distributed in frequency but not in direction. This unidirectional, irregular sea is represented by a series of spikes along a line of constant direction (here, again, about 45 deg). The volume under a spike, proportional to the wave energy at the frequency and direction where the spike is located in the grid, can be considered as half the amplitude squared of a wave train having that frequency and that direction. The energy distribution shown in Figure 2b is a JONSWAP (frequency) spectrum as described by Hasselmann et al. (1973) which has been assigned here to a particular direction. When summed over all directions, the result is the frequency spectrum shown in the right rear vertical panel. Since the directional distribution has a width of only one incremental arc, the frequency spectrum is simply a shadow of the frequency-direction distribution. Note that this is not the case in general; the frequency spectrum is the integral with respect to direction of the frequency-direction spectrum.

70. The direction spectrum of Figure 2b, shown in the left rear vertical panel, is simply a spike because all the energy is concentrated in

one direction. The area under this spike is equal to the volume under the frequency-direction spectrum. To add interest, this spectrum has the same $H_{mo}$ , peak frequency, and peak direction of Figure 2a.

71. If the energy is distributed in direction but not in frequency, a shape like Figure 2c results. In this instance, the waves come from several directions, but all wave trains have a frequency falling in the frequency band centered at about 0.17 Hz. Waves with the highest amplitudes (and highest energy) are coming from a direction of about 45 deg, so the peak direction in this case is the same as for the two prior cases. The frequency spectrum is simply a spike centered at about 0.17 Hz since all the energy is concentrated near this frequency. The direction spectrum shows the total energy in the frequency-direction spectrum in each direction arc. It shadows the main distribution because the main distribution is only one frequency band wide. The shape shown is one member of a class of functions used by Mitsuyasu et al. (1975) to characterize their data. Here again the frequency-direction spectrum has the same $H_{mo}$ , peak frequency, and peak direction as the previous two cases.

72. If real seas were as simple as these three cases, it would be straightforward to determine their character. That this is not the case is demonstrated in Figure 2d, which shows a frequency-direction spectrum of a real sea state obtained in the present measurement program. Here, wave energy is distributed in both frequency and direction. The figure shows two distinct groupings of wave energy. In the foreground is a wave field in the early stages of wind generation. It has a distinct peak at frequency 0.17 Hz and direction 45 deg. Energy drops rapidly toward low frequencies and tails off more gradually at high frequencies; a clear directional spread is evident at all frequencies. Behind this primary distribution is another, lesser concentration of energy centered at a frequency of approximately 0.08 Hz and a direction of approximately -30 deg. These low-frequency waves are evidently swell waves from some distant disturbance arriving from a finite range of directions different from the wind sea part of the spectrum.

73. The integrated frequency spectrum of Figure 2d shows the net frequency distribution for both wind sea and swell. The main, wind sea part looks somewhat similar to the JONSWAP curve shown in Figure 2b, indicating that existing models for frequency spectra are capable of approximating real seas reasonably well.

74. The integrated direction spectrum of Figure 2d shows the net directional distribution. Distinct peaks for sea and swell can be seen here as well. The primary wind sea has energy spread over a range of approximately 90 deg with most energy (say, values above about half the primary peak) spread over at least 40 deg. It appears that this can be approximated, more or less, by the distribution model shown in Figure 2c. However, a detailed look at the frequency-direction spectrum shows that the directional distribution is different for each frequency. Distributions at some frequencies have more than one peak. That is, real waves can be attacking a beach or coastal structure simultaneously from many directions and frequencies.

75. All examples shown in Figure 2 have the same $H_{mo}$ , peak frequency, and peak direction. It should be clear that an enormous variety of real sea states is possible for fixed values of these parameters. This means that, while these parameters are important in sea state description, they do not define a sea completely. There are further characteristic properties that must be resolved.

76. The important point here is that the frequency-direction spectrum is a compact form of bookkeeping which illustrates the energy distribution of a wave field. It is a simple extension to one additional dimension of the conventional way in which frequency spectra are considered. The frequency-direction spectrum can be used to reconstruct a realistic sea in numerical and physical models using the equations given; that is, there is an elemental volume of the frequency-direction spectrum for each of the frequency-direction grid intersection points. Using Equation 7, a wave amplitude can then be assigned for each of the discretized frequencies and directions. If an initial phase is chosen at random for each resulting wave train, Equation 5 along with Equation 2 can be used to simulate observed seas in models.

## PART III: MEASUREMENT SCHEME

### Measurement Site

77. For the long-term climatology of directionally distributed waves to be useful, the conditions under which data were collected must be known. This section gives a brief description of the measurement site, the directional gage, and some important aspects of data treatment.

78. As shown in Figure 1, the coastline in the vicinity of the FRF is nearly straight for several tens of kilometres north and south. It is oriented such that the shore-normal direction (facing seaward) is very nearly 70 deg from true north. Waves and onshore winds can approach this site along an easterly 180-deg arc from 340 to 160 deg relative to true north.

79. The adjacent continental shelf is roughly 100 km wide, being narrower to the south where Cape Hatteras, NC, juts eastward. The direction of the nearest approach of the 100-m isobath (roughly, the shelf break) is 10 to 15 deg south of east and is about 80 km distant. A characteristic bottom slope for the shelf is 1 m per kilometre. At a finer scale, the bathymetry is marked by numerous features of 1- to 10-km horizontal scales and 10-m vertical scales scattered in an irregular fashion across the shelf. Waves with periods near 10 sec begin to be influenced by the bottom at depths of 100 m. Considerable refraction of wind waves propagating over this shelf is expected (see, e.g., US Army Engineer District, Wilmington 1980).

80. Within a few kilometres of the FRF, the bathymetry is more regular. A complex bar system exists within about 300 m of the shore (Birkemeier 1984), and waves and currents have created some irregular bathymetry in the immediate vicinity of the pier (Miller, Birkemeier, and DeWall 1983). Away from these regions, isobaths are nearly shore parallel. The bottom slope is nearly uniform at about 1 m per 500 m and is reasonably stable, as indicated by repeated surveys (Howd and Birkemeier 1987). Figure 3 illustrates the bathymetry over a region 600 m north to 600 m south of the pier and extending about 900 m offshore. Figure 3 also shows the coordinate system used to define wave direction and to which Equation 1 applies.

81. The site is subject to a variety of climate which gives rise to a broad diversity in directionally distributed wave energy. Typical wind and wave climate can be roughly classified as four basic types (Leffler et al.

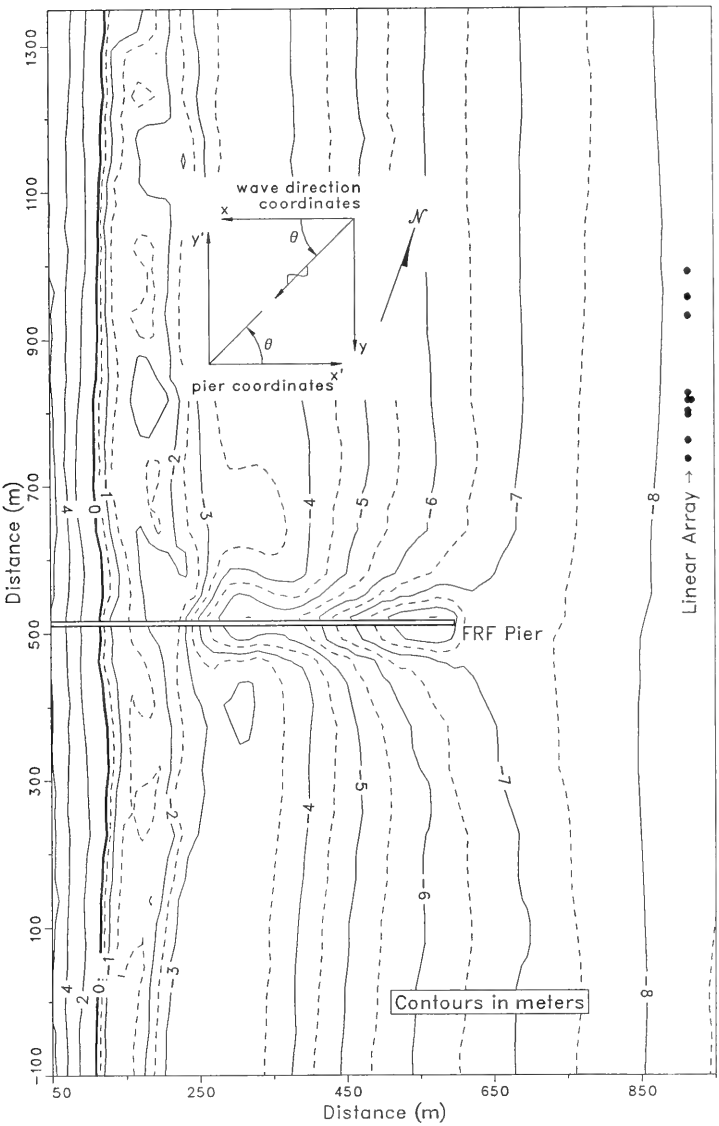


Figure 3. FRF nearshore bathymetry and linear array location

1989). The first is low wind situations, where the wave field is characteristically low-frequency swell propagating in from distant storms in the open Atlantic Ocean. These waves typically arrive from the east to southeast.

82. The most common wave-generating winds are *Northeasters* which arise from either frontal passages or extratropical storms. Frontal systems typically arrive from the west to northwest and have a north-south to northeast-southwest orientation. Winds preceding a frontal passage are typically from the south to southwest. Few nearshore waves are generated because such winds are directed offshore so the regime is fetch limited. Following a frontal passage, winds typically come from the north to northeast. These winds actively generate waves and, if the front stalls near the warm Gulf Stream, considerable nearshore seas can build. Extratropical storms originate as cells of low atmospheric pressure south of the site along the south Atlantic coast. These storms tend to migrate northward along the coast, creating high winds from the east to northeast.

83. Less frequent but more intense wave generators are hurricanes, the fourth type of disturbance. These originate in the equatorial Atlantic, migrate west to northwest, and can make landfall on the Gulf and Atlantic coasts with very destructive winds and waves. Although several hurricanes have passed over or near the FRF since its founding in 1979, none did so during this study.

## Physical Description of the Array

84. The high-resolution directional wave spectra obtained in this investigation are derived from two fundamental parts. The first is an array of sensors which sample sea surface displacement at several points in (horizontal) space. The second is the mathematical treatment of these data to obtain estimates of wave directionality. The two parts are coupled; gage positioning is tuned to optimize the effectiveness of the analysis algorithm.

85. The fundamental principle of operation is based on sampling a moving wavy surface with more than one gage. If a single gage samples this surface, no directional information is obtained; a time series from a single gage will not vary with wave propagation direction. If two, slightly separated gages are used, then a wave crest will generally be detected at one gage before it is detected at the other. The time difference for this wave crest

to move from the first gage to the second gives information about the direction the wave propagates. By harmonic analysis, these time series also give the wave frequency and, by the dispersion relation (Equation 2), an estimate of the wave number, the inverse of which yields the wavelength. The fractional part of the wave period measured by the time difference is proportional to the fractional part of the wavelength by which the crest lags in passing from one gage to the other.

86. With this information it is a matter of simple geometry to estimate wave direction. A crest in a wave train propagating perpendicular to the line between the two gages will reach both gages simultaneously so no time difference is observed. As angle of attack increases, the time difference grows (either positive or negative, depending on the sense of attack angle). Maximum time difference occurs when a wave train propagates along the line between the two gages. In this case the time difference equals the time for the wave to propagate (at its phase speed) the distance between the two gages. A more detailed description of this principle is given in Appendix A.

87. A direct extension of this principle is that, with a very large number of gages, the spatial equivalent of a discrete time series could be obtained. Then, high-resolution directional information could be found from a Fourier wave number transformation, in analogy with frequency transformation. This direct method is highly impractical, requiring hundreds, if not thousands, of gages; consequently, an indirect method has been developed. Theoretical considerations by various investigators, referenced below, indicate that reliable high-resolution directional estimation can also be done with a sparse array of gages, generally 4 to 10, which is much more practical.

88. The FRF array consists of nine pressure gages mounted 0.7 m off the bottom along the 8-m isobath to the north of the pier as shown in Figure 3. A tenth gage, located 5 m seaward of the array, exists to create a colocated Sxy gage. Since the main array is along a straight line, it is called a *linear array*. Its location offshore was determined by satisfying three constraints. First, it had to be outside the surf zone so that linear wave theory would be applicable. Inside the surf zone, bottom-induced steepening and breaking reduce the validity of linear theory. Second, it had to be in water shallow enough that pressure signals could be converted to surface displacement signals without excessive introduction of noise. High-frequency waves are most affected by this. The depth was chosen so that waves with frequency

0.32 Hz or lower could be resolved with reasonable accuracy. This frequency limit serves as a high-frequency cutoff for wind wave analysis. Third, it was necessary that the wave field be statistically uniform over the length of the array. The uniformity requirement meant avoiding any irregular bathymetry or wave reflectors that might focus wave energy selectively at one part of the array. This constraint was satisfied by placing the array well outside the nearshore bar system and also seaward and updrift (for the most common high energy waves) of the pier.

89. Within the array, each gage is powered by a 28-V power supply (grounds are common) located at the seaward end of the pier. Combined power and signal cables run from the pier to the array, with one cable serving two gages. Each pressure transducer is a Senso-Metric Model SP973(C), which has a pressure-sensitive diaphragm referenced to an evacuated cavity. Diaphragm displacement is sensed with a piezoelectric strain gage. Strain gage output is amplified so that 5-V analog output corresponds to full-scale pressure, which is 25 psi* relative to an internal, thermally compensated, electronically preset reference pressure of 14.70 psi. The internal diaphragm is coupled to environmental pressure through a silicon oil chamber behind a second, exposed diaphragm. A perforated copper cap containing copper wool protects the outer diaphragm from physical damage and inhibits biofouling. Signal wires lead back to the seaward end of the pier, to the landward end of the pier, and into the FRF computer room. Signals are electronically filtered with a 10-Hz, fourth-order, Butterworth filter, primarily to eliminate 60-Hz noise. Filtered signals are then passed through an analog-to-digital signal converter having 11-bit accuracy to a Digital Equipment Corporation VAX 11/750 computer for data acquisition and storage.

90. The manufacturer's stated accuracy for the pressure transducers is ±0.25 percent of full scale which corresponds to an accuracy of ±0.043 m of water in a static water column. Site calibrations, performed annually as well as before and after deployment, indicate a stable field accuracy of ±0.006 m for wave-induced fluctuations about a mean stataic water column height of 8 m, the nominal operating depth of these gages. The digitization step has a

---

* To convert pounds per square inch to Newtons per square metre, multiply by a factor of 175.1268.

similar value, being equivalent to 0.007 m of water for an 11-bit binary discretization of the full-scale signal.

91. Spacing between the gages along the linear array appears irregular in Figure 3 but is, in fact, distinctly specified by analysis requirements. Minimum gage spacing is 5 m, and maximum spacing (the length of the array) is 255 m . These distances are associated with directional resolving ability for waves with the shortest wavelength (highest frequency) and longest wavelength (lowest frequency) of interest. The remaining gages are spaced more or less so that unique multiples of the minimum spacing are distributed evenly up to the length of the array (which is about 51 multiples of the minimum spacing). With nine gages, there are 36 possible unique spacings. In this array, there are some redundant spacings left intentionally for checking spatial homogeneity of the wave field, but well over half of the 51 spacing increments are present. These are distributed for optimum resolution of wind wave directions in the frequency range 0.05 to 0.32 Hz.

92. It is not critical that the spaces are exact multiples of the minimum spacing, but it is critical that gage locations are well measured. Measuring was done by surveying the gage mounts (using a range pole which protruded through the water surface and was held by an operator on the FRF's Coastal Research Amphibious Buggy (CRAB)) with a Zeiss Elta-2 total station referenced to the FRF coordinate system (see Birkemeier and Mason 1984). Accuracy of the total station and CRAB combination is ±0.03 m. Accuracy of pole positioning is estimated to be ±0.15 m. The maximum directional error of this array is ±3 deg, which occurs only if two minimum-spaced gages are used. In normal analysis, a minimum of five gages is used. Spacing is such that positioning errors result in a wave direction error of ±0.3 deg.

## Data Collection

93. Data from the 10 pressure gages were sampled in groups called *collections*. Each collection consisted of sequentially sampling the digitized analog voltage from each gage every 0.5 sec (2 Hz). The A/D sampling sweep rate was 10 kHz, so it took 0.001 sec to sample 10 channels. This introduced a negligible phase shift between channel samples; i.e., the sampling was almost instantaneous for the 10 channels. Time series length for each channel was 16,384 points. At 2 Hz, this is a duration of 2 hr 16 min 32 sec. Raw

voltages were stored for each gage as four records of 4,096 points (34 min 8 sec). This record division was used later in data quality control.

94. A time line of satisfactory data collection start times is shown in Figure 4. Most of the first year's data collection coincided with routine daily FRF observations (Birkemeier et al. 1985) at 0100, 0700, 1300, and 1900 Eastern Standard Time (EST) under low-energy conditions. Additional daily collections at 0400, 1000, 1600, and 2200 EST occurred under high-energy conditions, defined as times when $H_{mo}$ at a reference gage exceeded a predefined level or when specifically prescribed by an investigator.

95. At the beginning of the collection year, during September and October 1986, the SUPERDUCK experiment (Crowson et al. 1988) was conducted. During this period, collections were timed with tidal extremes, and data were gathered for seven records of 4,096 points for each gage. These collections were processed by considering records 1 to 4 as one sample and records 4 to 7 as a second sample, even though the two samples overlapped by one record. This gave a closely spaced sampling of almost independent observations during SUPERDUCK.

96. Gaps in the data stream in Figure 4 are the result of several causes. Short gaps were caused mostly by computer downtime or gage wiring problems such as ground loops or loose connections. Longer gaps during SUPERDUCK were caused by problems associated with installing a new gage. Serious long-term data collection for this report did not begin until late in January 1987, so there is a 3-month gap following SUPERDUCK. For the remainder of the year, data coverage was good. A total of 1,046 frequency-direction spectra were measured.

## Error Checking

97. Conversion of observed data to frequency-direction spectral estimates requires computing products of frequency spectra from the nine gages in the array. This means that data quality must be exceptionally high so that spiky or drifty data from one gage do not contaminate results in spectral multiplication with results from the other eight gages. Additionally, the linear array analysis programs are based on the hypotheses that the wave field is homogeneous along the array (i.e., the same wave trains occur at all gages) and stationary in time (e.g., does not go from a flat sea to a full-blown


Figure 4. Time line of satisfactory data collections

storm during a 2-hr collection interval). If these assumptions are violated, results are suspect. Hence, there are three measurement problems for which to check: malfunctioning gages, temporal non-stationarity, and spatial inhomogeneity.

98. A spatially inhomogeneous wave field is one where properties change substantially over some region of interest, in the present case over the length of the linear array. If wave direction differs from one end of the array to the other, the cross-spectra of signals between pairs of equally separated gages will be different. This condition arises because the time difference of wave forms passing one relative to the second of a pair of gages is directly related to wave direction. A preliminary examination of cross-spectral densities at redundant gage spacings under a variety of wave fields measured with the FRF linear array indicated no significant errors due to spatial inhomogeneity. Hence, it has been assumed in all subsequent analysis that wave conditions are homogeneous.

99. Of the remaining problems of malfunctioning gages and temporal non-stationarity, the former has been found to be the most severe. An error-checking computer program has been written to identify failed gages so they could be eliminated from further analysis. The error-checking principle employed is quite simple. Since multiple gages were deployed in an (assumed) homogeneous sea, certain statistical properties of data from each gage should be identical. Intercomparison of data from all gages can then reveal inoperative gages. Two types of properties were used. One was *integral properties*, requiring the summing of data values; the other was *point properties*, which examined extreme points in a set of time series.

100. Integral properties were mean value, standard deviation, skewness, kurtosis, and trend. The first four of these are conventional time-series parameters, defined in any statistics text. Trend is the difference of the end values of a straight line fitted through the data. It gives a measure of the bulk (low-frequency) rate of change of a measured property.

101. The procedure was to compute each of the integral properties for each of the four, sequential 4,096-point records for each gage in a collection. All 10 gages were used since the tenth gage was sensing virtually the same environment. Division into four records provided a sequence in time of these statistical properties. For each of the four records and for each property there were then 10 estimates of that property, one for each gage.

The median of the 10 estimates was used as a reference (except for skewness and kurtosis, for which the reference values were zero). Any estimate that deviated from the reference value by a preset amount was flagged by the computer on a printed output summary. The preset deviation comparators were found empirically by examining time-series records of malfunctioning gages for comparison with records from functioning gages. The comparators are not listed here because they apply to the set of gages used in this experimental setting and so are somewhat unique (however, the principle can be applied elsewhere).

102. To test for temporal stationarity, the standard deviations were used. The square of the standard deviation is the variance (pressure variance is related to sea surface variance) which is proportional to wave energy. So, if the pressure standard deviations were stationary, wave energy was expected to be likewise. To check for stationarity, the median standard deviations of the four records were intercompared. The median of these was used as reference in this test and as a scale of the collection as a whole. The criterion for stationarity was that no median standard deviation depart from this reference by more than 15 percent.

103. The integral parameters are good for information about a record or collection as a whole. However, if the data have a few isolated spikes or short duration offsets, these properties may not be obvious because of the smoothing effect of integration. Sharp changes in time-series data result in increased variances over broad regions in frequency spectra and so must be avoided if not real. To check for sudden changes at any point in collected data, the maximum and minimum values, maximum and minimum first derivatives, and maximum and minimum second derivatives were isolated from the full 16,384-point time series for each gage. Both dimensional and nondimensional forms were computed. Normalizing parameters were the time-step (0.5 sec in all cases) and the reference standard deviation from the stationarity check above. The medians of these point parameters were found from the set of 10 gages, and deviations were flagged as for the integral parameters above, also using empirically determined comparison criteria.

104. If one or more properties of a gage were flagged, that gage was not used in analysis. The analysis programs were written so that data from a subset of gages could be analyzed. The trade-off for fewer gages is a loss of directional resolution. Loss of some gages is more critical than others. For

instance, if either of the two gages with the smallest spacing is lost, results for high-frequency waves are severely compromised. In this case, no analysis was performed. If these two are not lost, then considerable directional information can be obtained with as few as five gages.

105. For the data set discussed in this report, there were never fewer than six functioning gages; most of the time there were eight. To estimate the effects of this, tests were performed with subsets of gages in two collections where all gages were operational. The tests indicated that the general features of the frequency-direction spectra were reasonably well represented by all the gage subsets used in the first year of collection. Some of the finer details of the spectra were changed in amplitude or in directional position so that, in refined studies of spectral structure, the pattern of operating gages needs to be considered.

106. To keep track of the set of operating gages, a parameter called the *gage pattern* was created for each collection. It is a nine-place character string which represents the linear array gages in order of placement. In each place in the string is an identifying number if the gage is functioning or a minus (-) sign if the gage was not used in analysis. This parameter is archived along with analysis results for future reference. In this report, all results are used where six or more gages were functioning, making optimum use of data obtained and providing a reasonably faithful first look at directional spectral structure.

## Directional Spectral Estimation

107. For the gages in a collection that are retained for analysis after error checking, the next step is estimation of the directional distribution of energy. The computation is done in four parts: (a) Fourier transformation of time series to the frequency domain, (b) conversion of pressure spectra to sea surface variance spectra, (c) computation of cross spectra between all gage pairs for each frequency, and (d) estimation of a directional distribution that corresponds to the spatial variation in cross-spectral density for each frequency.

### Fourier transformation

108. Fourier transformation is done by conventional methods. The 16,384-point time series for each gage is divided into 15 half-overlapping

segments of 2,048 points. Each segment is tapered with a Kaiser-Bessel window (a modified Bessel function of the first kind, compensated uniformly for loss of variance because of windowing) to reduce leakage. The segments are then fast Fourier transformed to the frequency domain. An intermediate-resolution transform is found by averaging the 15 transformed segments, frequency by frequency. Final resolution transforms are found by averaging results over 10 adjacent frequency bands. The final resolution bandwidth is 0.00976 Hz. Transform estimates are retained for 28 frequency bands ranging from band-center frequency 0.054 to 0.318 Hz, i.e., the wind wave frequencies of interest. Resulting degrees of freedom are at least 150 (assuming 8 contiguous segments and ignoring any gain from lapped segments) for which the Chi-square confidence limits are nearly Gaussian. They equal approximately ±19 percent at the 95-percent level and ±15 percent at the 90-percent level.

Conversion of pressure signals

109. Conversion of pressure signals measured near the ocean bottom to water surface displacement is done through the linear wave theory pressure response factor as described in the SPM (1984). It is a frequency-dependent function of water depth and gage elevation which provides the amplification necessary to compensate for attenuation of wave properties with depth. It is larger for high-frequency waves since the pressure signal of these waves attenuates more rapidly with depth. In 8 m of water, the factor ranges from about 1.05 for 0.054-Hz signals to about 13.1 for 0.318-Hz signals. Note that any noise in the higher frequency signals is also amplified by the larger factor. If the signal-to-noise ratio drops at these frequencies (as it does in low-wind conditions when the wave field is mostly relict swell), noise can become important and can contaminate the high-frequency parts of the spectra. This possibility needs to be considered in interpretation of results.

Computing cross spectra

110. Cross spectra are computed from products at corresponding frequencies of Fourier transforms of data from two different gages. They have two parts, called *coincident* and *quadrature* spectra. The two parts contain information about the products of the amplitudes of the Fourier transforms and the phase difference of a signal at one gage relative to a signal at the other. This phase difference contains wave directional information. At a given frequency, the cross spectra can be computed for all gage pairs. As mentioned above, there are 36 pairs possible with 9 gages. When the

cross-spectral values (at a given frequency) are ordered in terms of gage separation distance (called *lag space*), a pattern emerges that is interpreted for the directional distribution of all the waves at a given frequency. Since there are 28 frequencies (in this analysis), there are 28 sets of cross-spectral patterns to interpret. The pattern for any one frequency is considered independent of the pattern at any other frequency.

Estimation of directional spectra

111. Conversion of cross-spectral patterns in lag space to directional spectra is done with a statistical method known as Iterative Maximum Likelihood Estimation (IMLE) The IMLE method is a more accurate adaptation of a simpler method called Maximum Likelihood Estimation (MLE). Both methods are alternatives to the more conventional Fourier transformation of directional spectral wave numbers (the spatial equivalent of frequency transformation). Either MLE or IMLE is necessary because the gage array cannot be made long enough to sample adequately the longer wind waves.

112. In the MLE method, an empirical function is found to represent a directional spectrum that is nearly consistent with the observed cross-spectral patterns. The empirical function is found from a weighted sum of the cross-spectral estimates. The weights are required to minimize the effects of noise in cross spectra and give an optimum response in the vicinity of each discrete set of viewing directions. This scheme was first proposed by Capon, Greenfield, and Kolker (1967) for the analysis of seismic data. Davis and Regier (1977) describe the theory and application of the method to ocean wave data obtained from spatial arrays. A further application of the method to data from heave-pitch-roll buoys is derived by Oltman-Shay and Guza (1984). Details of the computational algorithms are given in these references.

113. The MLE method has two properties that make it less than optimum. One is that directional spectra from the MLE algorithm frequently do not recover observed cross spectra upon inversion of the algorithm. The other is that formal estimates of error (confidence intervals) for MLE spectral estimates are computationally prohibitive for routine use and not necessarily reliable.

114. In the first problem, Davis and Regier (1977) noted that if the MLE directional spectral estimate is inverted to obtain the cross spectrum, the observed cross-spectral matrix is not recovered exactly. They performed tests with simulated data in a six-gage array. They found that energy

estimates from the MLE estimate differed from the true spectrum by about 20 to 40 percent at high-energy directions in the true spectrum when the true spectrum had a finite spread (the method was nearly perfect for unidirectional waves). An improvement for this problem was proposed by Pawka (1982, 1983), who argued that a correction term could be added to an MLE estimate for each viewing direction. The magnitude of the correction term was determined from the difference between the observed cross spectrum and the cross spectrum resulting from inversion of the MLE estimate. Adding the correction term to the existing result provides a new MLE estimate of the directional spectrum. Since this system is transcendental, a further correction can be found by inverting the new MLE estimate and comparing the result to the observed cross spectrum. This process is repeated until the differences are minimized. Since it is iterative, this method is known as Iterative Maximum Likelihood Estimation (IMLE). Details of IMLE are described by Pawka (1982, 1983) and summarized by Oltman-Shay and Guza (1984). This algorithm was used to process the data described in this report.

115. The problem remains of confidence intervals for final frequency-direction spectra. In contrast to the MLE method, there is no formal estimate of error for the IMLE method. One might use a formal error computation from the MLE method as a crude estimate of error in the IMLE method. However, such error estimates are only measures of statistical noise and, while of value, are not complete. Errors also occur because of interrelationships imposed by the IMLE algorithm between a true directional distribution and a specific array geometry. This algorithm is nonlinear, so it is difficult to compute a general error estimate from any type of linear analysis; each true directional distribution can have its own unique error distribution.

116. Perhaps the best approach to this problem is to conduct a series of tests using simulated, but realistic, directionally distributed wave energy. The assumption is made that real directional distributions close in shape to the simulated cases have similar error distributions and so give an indication of the verity of the IMLE method. Results of such tests are reported by Pawka (1983). Several hundred spectra, having one or two directional peaks of varying widths, were employed in this test. A five-gage array was used. Typical results were that errors using the IMLE method were about 13 percent of the errors from the MLE method for unimodal (single peaked) directional distributions and about 1 percent for bimodal distributions. This

error reduction indicates a substantial advantage of the IMLE method. When ensembles of 16 artificial cross spectra with random noise (to simulate field data) were tested, the IMLE method was typically 4 to 20 times more accurate than the MLE method. In no case were the general features of the true spectrum misrepresented using the IMLE method.

117. This is not formal proof that IMLE works in all possible cases, but the tests lend substantial confidence that the estimates obtained do represent underlying true spectra faithfully. Since the FRF array has nine gages (instead of five used in Pawka's tests) and measured spectra have more than 150 deg of freedom (compared to 32 in the tests), it is expected that the quality of results reported here are better than the test results.

118. One important property of IMLE is that results for spectra with broad spreading are characterized by obvious but relatively minor fluctuations about the true spectral distribution. This behavior means that all maxima and minima in a measured directional spectrum are not meaningful separators of individual wave trains. A deep minimum between two adjacent maxima is more meaningful. This distinction is important in interpreting observations, especially in analysis of modes (multiple peaks in directional distributions) as discussed in Parts V and VI.

## Working Data Base

119. Computational output from the IMLE algorithm is a discrete directional spectrum of wave energy (sea surface variance) for each of the 28 frequencies in the cross-spectral estimates. The direction increments vary between frequencies because directional resolution is frequency dependent. The higher frequency (shorter wavelength) waves are better resolved because more of these wavelengths are represented by the length of the linear array. Output direction increments vary from about 0.5 deg for 0.318-Hz waves to about 3.5 deg for 0.054-Hz waves.

120. It is convenient to have direction increments the same for all frequencies so that a regular array can be used to represent the full frequency-direction spectrum. As a trade-off between the two resolution extremes, directional results were integrated over 2-deg arcs and renormalized with this direction increment to create evenly spaced directional spectra at all frequencies. This computation resulted in 90 direction arcs (91 arc center

directions) to represent the full 180-deg looking window of the linear array. The frequency-direction spectrum $S(f_n,\theta_m)$ is then a matrix of 28 ( = N, the number of frequencies) x 91 ( = M, the number of directions) elements.

121. This matrix is the final discretized representation of a given observed sea state. It can contain up to 2,548 (28 × 91) wave trains. Along with the date, start time, gage pattern, and mean depth, this is a complete set of information to characterize the desired energy distribution properties, including the integrated frequency spectrum $S(f_n)$ from Equation 8 and the integrated direction spectrum $S(\theta_m)$ from Equation 9.

## PART IV: EXAMPLES OF OBSERVED FREQUENCY-DIRECTION SPECTRA

122. In this section results from three typical nearshore wind wave regimes are shown. It should be remembered that sea state in any given observation depends on both history of generating winds (including variability in speed and direction) and spatial distribution of generating winds. The latter property is important because waves at a site can result from both local generation and propagation from distant generating areas. Results shown here are taken out of context of the complete generation history and may have detailed structure different from other cases. Nonetheless, the general structure is sufficiently representative for purposes of illustration.

### Low-Wind, Low-Energy Regime

123. Figure 5 represents the most common sea state, which is persistent low-energy swell found in day-to-day observations along most coasts. Figure 5a shows the frequency-direction spectrum in three dimensions with the integrated frequency spectrum on the right rear panel and the integrated direction spectrum on the left rear panel, similar to the pattern used in Figure 2. Figure 5b is a contour plot of the frequency-direction spectrum normalized by its own maximum value, making the normalized spectral density range between 0 to 1. Contours are drawn at 10-percent intervals. Directions are as defined in Figure 3.

124. The general features of this case are associated with a primary mode (or lump) of energy with peak frequency and direction of about 0.09 Hz and about -30 deg, respectively. Total energy is characterized by a representative wave height $H_{mo}$ of about 0.5 m. There is very little energy at the higher frequencies which suggests that there is little active wind generation. The integrated frequency spectrum is shaped qualitatively like common models of frequency spectra, having a steep low-frequency side and a high-frequency side that decays more gradually.

125. Of interest is the extent to which the energy is spread in direction. In Figure 5a, the integrated direction spectrum indicates energy is almost uniformly distributed from about 0 to -40 deg with a slightly enhanced peak at about -30 deg. For a given energy density, the contour plot in Figure 5b indicates that the greatest spread is near the spectral peak

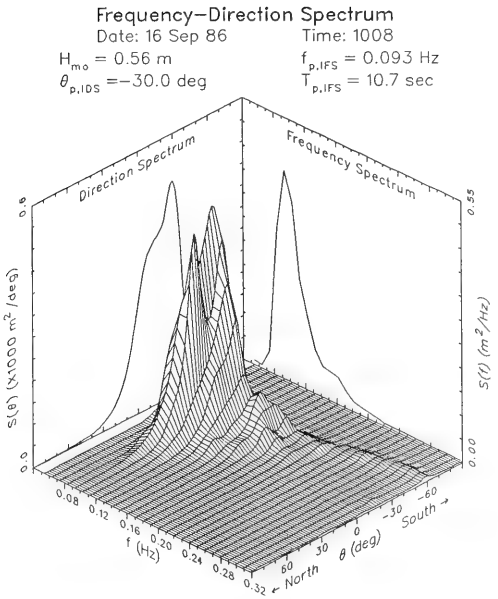


a. Perspective plot

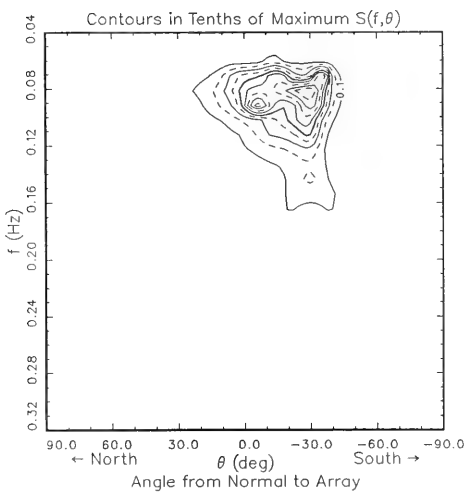


b. Contour plot

Figure 5. Spectra from a typical low-energy case

frequency and less spread is at higher frequencies. This pattern is very different from the commonly assumed unidirectional distribution of energy. It initiates questions as to whether or not this is a common occurrence and, if so, how it may depend on other sea state descriptors. These and other questions are addressed below.

## Early Storm Example

126. Figure 6 shows a frequency-direction spectrum in the early stages of a storm. Two distinct groupings of energy are apparent in the figure. One group, located on the negative-angle side of the graph, has little high-frequency energy and is likely the remnants of the prestorm sea state. The other group is characterized by sharp peaks at the higher frequencies. These are centered at directions in the range 40 to 50 deg. The contour plot, Figure 6b, indicates that the high-energy part of this group is spread over about 10 to 20 deg in direction. This is narrower than the low-energy swell shown in Figure 5 but is still very different from unidirectional.

127. The integrated frequency spectrum in Figure 6a shows an almost uniform distribution of energy with frequency for frequencies less than about 0.22 Hz. This is the contribution from the low-energy waves coming from the negative-angle directions. The peak in the frequency spectrum is near the high-frequency end of the analysis band. This structure is consistent qualitatively with wind wave growth models in which wind forcing acts first to build high-frequency waves and, in time, results in migration of the spectral peak frequency to lower values. The total energy in this case is relatively low, as indicated by the $H_{mo}$ value of about 0.6 m, again suggesting a young sea.

128. The integrated direction spectrum in Figure 6a shows the low background energy spread from about -60 to 40 deg (an arc of about 100 deg). The young part of the sea state has a peak direction of about 50 deg and is concentrated in the direction range from about 35 to 60 deg (an arc of about 25 deg). This suggests that directional spread may be small in the early stages of wind generation, another question for later analysis.

129. An interesting property of Figure 6a is that there appears to be two clear groupings of energy, each of which resides in a distinct region of the frequency-direction domain. Such a condition is not always expected. A

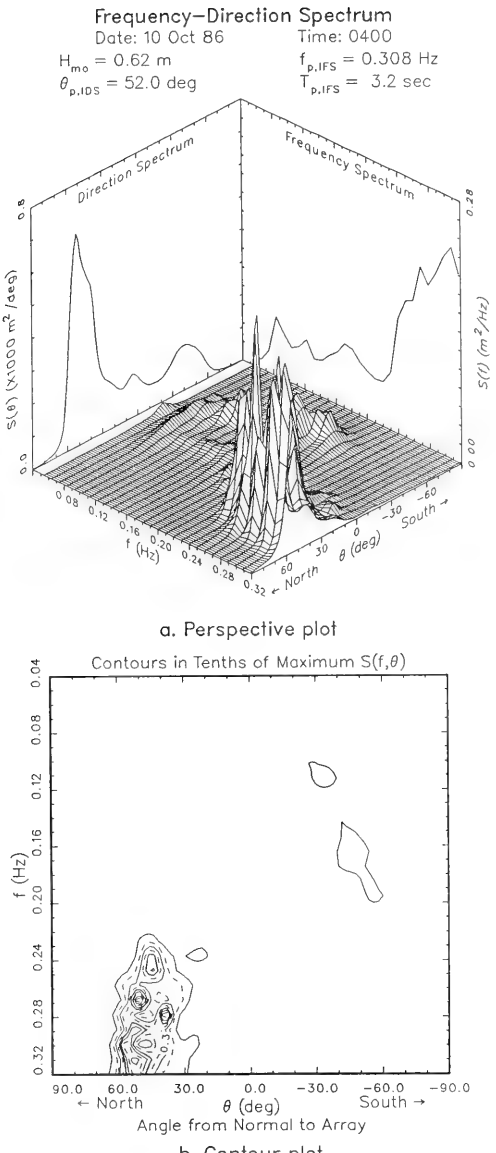


Figure 6. Spectra from an early storm case

local wind-driven sea could occur from the same arc of direction as the background swell such that there would exist a strong multimodal variation with frequency in that range of directions. Low-frequency waves at later stages of a locally wind-driven sea could occur at the same frequencies as part of the background swell, creating multimodal directional distributions of energy at these frequencies. Questions then arise as to (a) how often there are distinct groupings of wave energy; (b) where groupings merge, how well the complete spectrum can be related to the generation and radiation processes that govern the wave field; (c) how important multiple peaks are to the overall energy distribution; and (d) whether or not there is similarity in energy distribution shapes.

## A Well-Developed Sea State

130. Figure 7 shows the frequency-direction spectrum 21 hr after the time of the spectrum shown in Figure 6. Considerable energy is present as indicated by the $H_{mo}$ of about 3.1 m. The peak frequency in the frequency spectrum has evolved from about 0.31 Hz in Figure 6 to 0.11 Hz in Figure 7. Both the frequency-direction spectrum of Figure 7a and the contour plot of Figure 7b show the peak direction to be near -20 deg. The integrated direction spectrum shows a maximum in total energy at about 10 deg. In all distributions the total energy spread is rather large. Energy is spread over a range of about 60 deg based on the 50-percent contour line in Figure 7b. In the integrated direction spectrum of Figure 7a, the spread is nearer to 90 deg based on the arc subtended by the energy distribution at half the spectral peak.

131. This example has several interesting features. One is a suggestion of refraction. Low-frequency waves in Figure 7 are more nearly shore-normal (i.e., near 0 deg) than are high-frequency waves. Compared to high-frequency waves, low-frequency waves require a rather significant horizontal space to evolve by wind forces. A wave train with a 10-sec period has a phase speed of order 10 to 20 m/sec in water depths greater than 8 m. At these speeds, a wave could cross the continental shelf (see Figure 1) in about 1 to 2 hr, a time scale comparable to the duration of one data collection in the present experiment. Long waves also are affected by the bottom at greater depths than are high-frequency waves and so would tend to be steered more by

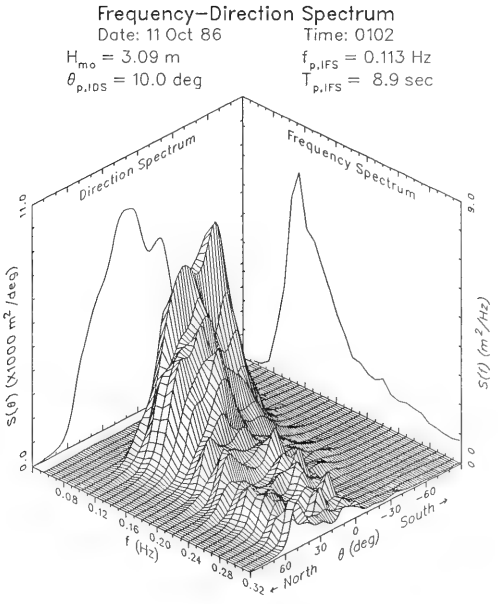


a. Perspective plot

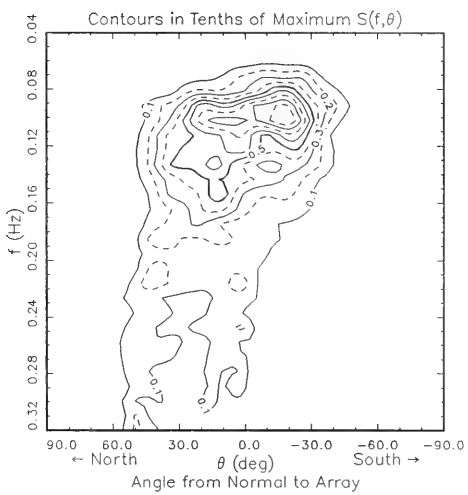


b. Contour plot

Figure 7. Spectra from a well-developed sea

the bathymetry of the continental shelf than the shorter waves. Though the above argument is largely hypothetical, it seems quite reasonable to expect a refraction-induced concentration of low-frequency energy near the shore-normal direction and a lesser effect on high-frequency waves. This effect is also suggested, but less dramatically, by Figures 5 and 6.

132. Refraction would have the effect of spreading the total energy (integrated with respect to frequency) over a greater arc in direction. At any given frequency in the contour plot of Figure 7b, the total directional spread, as indicated by the 10-percent contour line, is about the same, roughly 60 deg, being just slightly greater at the lower frequencies. The integrated direction spectrum, which adds contributions from all frequencies for each direction, shows the total energy spread over an arc of about 100 deg, based on the arc for which the curve exceeds 10 percent of the spectral maximum. It will be necessary to keep this effect in mind when considering parametric representations of directional spread.

133. Another feature in this example is that most of the high-frequency components appear to have two peaks (or modes) in direction. This is seen in both plots of Figure 7. Since the peaks are well separated in direction and the distributions drop to rather low values between the peaks, this suggests that there may be superimposed wave fields from two separate processes or sources. Another possibility is that wave energy has been reduced in certain directions and frequencies from a more complete, single mode distribution. Whatever the cause, the bimodal distributions are evident. These features are examined in more detail below.

134. It should also be noted that, with all the directional structure just discussed, the integrated frequency spectrum of Figure 7a is not particularly distinguished. It appears like many other observed frequency spectra but gives no obvious clue as to the directional structure of the spectrum.

## PART V: DATA REDUCTION/PARAMETERIZATION

135. Directional properties of the observed frequency-direction spectra are found from a set of parameters which reduce the volume of data from the entire spectrum (2,548 numbers in the analysis used here) to just a few representative numbers for each case. Observed data are a signature of the physical processes (local distribution of wave energy in frequency and direction) represented by a geometric figure (the frequency-direction spectrum). Characteristics of the physical processes are deduced from the shape or shapes of all or part of the observed spectra.

136. A conventional parameter (one that can be estimated reasonably well with a low-resolution directional measurement system) is peak direction, of which there are several measures. These were defined in Part II for the full frequency-direction spectrum and for the integrated direction spectrum. A peak direction can also be assigned for the distribution at each frequency in a frequency-direction spectrum.

137. If the full frequency-direction spectrum is known, there are several other important characteristics that can be determined. A primary parameter of interest is one that characterizes directional spread. This is broadly defined as an arc of directions containing a significant amount of wave energy. A second parameter is directional asymmetry. This indicates how evenly energy is distributed on either side of a peak in a directional distribution. Depending on the level of detail desired, these two parameters can be determined from the frequency-direction spectrum as a whole (bulk characterization), from distributions at individual frequencies (frequency characterization), or from individual modes (well-separated peaks) within the distribution at a given frequency (modal characterization). Once computed, these parameters can be ordered and correlated with other parameters to characterize the variety and variability of observed sea states.

### Frequency Characterization of Spread, Asymmetry, and Position

138. A conventional treatment of directional distributions of wave energy (see, e.g., texts by Goda 1985 or Horikawa 1988) is to consider a slice through the frequency-direction spectrum $S(f_n, \theta_m)$ along a line of constant frequency (e.g., $f = f_n$, one of the frequencies from discrete Fourier

analysis) and to normalize it with the frequency spectral density at that frequency $S(f_n)$ . The result, given the symbol $D(f_n,\theta_m)$ , is called the directional distribution function. It is defined by

$$D(f_n,\theta_m) = \frac{S(f_n,\theta_m)}{S(f_n)} \tag{13}$$

where the $\theta_m$ are the discrete directions from the directional analysis. The units of the directional distribution function are $deg^{-1}$ . It is useful because it has unit area, i.e.,

$$\sum_{m=1}^{M} D(f_n,\theta_m)\, d\theta = 1 \tag{14}$$

by virtue of Equation 8 when Equation 13 is inserted in Equation 14. The normalization of Equation 13 makes it possible to intercompare the directional distributions from spectra with various frequency spectral densities $S(f_n)$ .

139. Peak direction is a fundamental parameter in any directional distribution. In addition to the bulk peak directions $\theta_{p,FD}$ and $\theta_{p,IDS}$ defined in Part II, a peak direction denoted as $\theta_{p,n}$ can be found from the directional distribution at each frequency. It is equal to the direction of the maximum of $D(f_n,\theta_m)$ [or $S(f_n,\theta_m)$ ] at frequency $f_n$ . There will be a peak direction for each of the $N$ frequencies in a discrete frequency-direction spectrum.

140. Several alternatives were considered for defining directional spread. A common one is called the *full width at half power*, defined as the arc subtended by points on the shoulders of a directional distribution function which have values of one-half the maximum of $D(f_n,\theta_m)$ for a given $f_n$ . This definition of spread has been used by many authors because it is a simple, meaningful parameter for unimodal distributions. However, its assignment and meaning become somewhat complicated when the distribution has more than one main mode, especially if the modes have comparable areas. Another method is to define spread indirectly through a parameter of an analytic function fitted to the data. This method was used by both Mitsuyasu et al. (1975) and Donelan, Hamilton and Hui (1985) and works well if the

observed directional distributions are near in shape to the analytic models. However, there is no particular assurance that observations in a given experiment will conform to proposed analytic models, and strong biases may occur in parameterization if model and data do not conform well.

141. Used here is a third alternative which is simple, meaningful, easy to compute, and can be defined for distributions with any number of modes. If the sum in Equation 14 is not taken over all directions but is truncated at a particular direction $\theta_j$ , the result is the cumulative area under the distribution function from $\theta_1$ (= 90 deg, one of the shore-parallel limits of wave direction) to the arbitrary direction $\theta_j$ . If this computation is done for all values of $j$ from 1 to $M$ , the result is a cumulative distribution function with values ranging from 0 to 1, with the $j^{th}$ value indicating what fraction of the total energy (at frequency $f_n$ ) is included between angles $\theta_1$ and $\theta_j$ . In this sense, the directional distribution function can be treated just like any statistical distribution function. One constraint on this method is that wave energy must be bounded in direction. If the energy is distributed over a full 360 deg (as is possible in the deep ocean), there is no meaningful starting point for the integration. In the present study, the waves are assumed to arrive from a maximum range of 180 deg so that integration can start from either of the two shore-parallel azimuths.

142. The directions for which the cumulative energy is 25 percent, 50 percent, and 75 percent of the total have been chosen as characteristic directions. Since these directions divide the energy into quarters, they can be called the *quartile directions*. A mathematical expression for the (discrete) cumulative distribution function is

$$I(f_n,\theta_j) = \sum_{m=1}^{j} D(f_n,\theta_m)\, d\theta \tag{15}$$

and the three characteristic directions, called $\theta_{25\%,n}$ , $\theta_{50\%,n}$ and $\theta_{75\%,n}$ , respectively, satisfy the equations

$$I(f_n,\theta_{25\%,n}) = 0.25 \tag{16a}$$

$$I(f_n,\theta_{50\%,n}) = 0.50 \tag{16b}$$

$$I(f_n,\theta_{75\%,n}) = 0.75 \tag{16c}$$

143. Subscripts for the representative directions carry the frequency index $n$ since they are associated with the directional distribution at a particular frequency. The function $I(f_n,\theta_j)$ is interpolated where necessary to satisfy Equations 16(a-c) since it is defined only at discrete angles.

144. Figure 8 illustrates the relationships between the directional distribution function, the cumulative distribution function, and the representative directions. Figure 8a shows $D(f_n,\theta_m)$ for $f_n = 0.083$ Hz and for the particular date and time shown in the figure. Points at discrete directions have been connected by straight lines to simulate a continuous distribution. Figure 8b shows the corresponding cumulative distribution function from Equation 15. The horizontal dashed lines in Figure 8b show the 25 percent, 50 percent, and 75 percent values of $I(f_n,\theta_j)$. Their intersections with the solid curve define the corresponding characteristic angles. These are shown as vertical dashed lines in both parts of Figure 8.

145. There are three useful parameters that can be determined from these three characteristic angles. One is a directional spreading parameter $\Delta\theta_n$ which is identified as the arc which encompasses the central 50 percent of the energy at frequency $f_n$. Mathematically, it has the definition

$$\Delta\theta_n = \theta_{25\%,n} - \theta_{75\%,n} \tag{17}$$

where it should be noted that the definition is consistent with the direction axis shown in Figure 8, with angle decreasing from left to right. The spread angle is shown in Figure 8 as the horizontal, double-ended arrow. It includes the central 50 percent of the energy because 25 percent of the energy is to the left of $\theta_{25\%,n}$ and 25 percent is to the right of $\theta_{75\%,n}$.

146. This parameter can represent directional spread for all distributions. If the directional distribution is a spike (unidirectional waves), the integral is a step function and $\Delta\theta \rightarrow 0$ deg. If the directional distribution is white (the same energy in all directions), then $\Delta\theta \rightarrow 90$ deg, a meaningful representation of the central 50 percent of the energy. If the spectrum is multimodal at frequency $f_n$, the central 50 percent of energy is still characterized. Note that the summation of Equation 15 could be reversed, starting at the other longshore azimuth to obtain the same essential result.

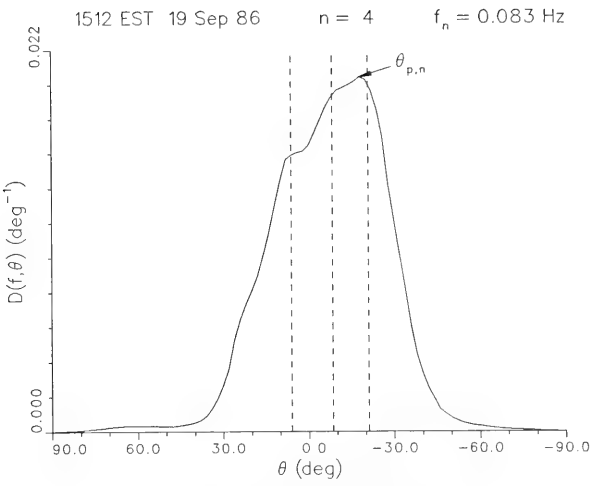


Figure 8. Schematic of distribution functions illustrating directional parameter definitions

The 25 percent and 75 percent angles would switch places, but the magnitude of their difference would be unchanged.

147. A second useful parameter gives a measure of the degree of symmetry in a directional distribution. Almost all models of directional distribution assume that the energy is symmetrically distributed about some peak direction. If so, the peak direction $\theta_{p,n}$ would correspond to $\theta_{50\%,n}$. There is no assurance that this is necessarily so in shallow seas, where processes such as bathymetrically induced scattering, nonlinear interactions among shoaling waves, and generation by irregular winds could induce significant asymmetry in directional distributions of incoming waves. In the simplest asymmetric distribution, the curve will be steeper on one shoulder than on the other. The integrated cumulative distribution will rise rapidly on this shoulder with the effect that the 50-percent angle will be nearer the quartile angle on the steep side. A simple way to characterize this is to define an asymmetry parameter $A_n$ as

$$A_n = \ln \left( \frac{\theta_{25\%,n} - \theta_{50\%,n}}{\theta_{50\%,n} - \theta_{75\%,n}} \right) \tag{18}$$

which is unique to a particular frequency $f_n$ within a given frequency-direction spectrum.

148. This parameter simply compares the spreads of the two halves of the central 50 percent of the energy at this frequency. If $\theta_{50\%,n}$ is halfway between $\theta_{25\%,n}$ and $\theta_{75\%,n}$, it means the two halves have roughly equal spreads as measured by the difference angles. The ratio of the differences, in this case, is unity. The natural logarithm of one is zero so there is zero asymmetry (by this definition). If $\theta_{50\%,n}$ is closer to $\theta_{25\%,n}$ than to $\theta_{75\%,n}$, the ratio is less than one and its logarithm will be negative. In this case, the distribution rises more rapidly on the 25-percent side so that a negative $A_n$ indicates a rapidly rising left side and a more gradually decaying right side for the angular coordinate system shown in Figure 8. A positive $A_n$ indicates a gradually rising left side and a steeper right side. Use of the logarithm makes it possible to compare distributions which are asymmetric but mirror images of each other. Both will have the same magnitude of $A_n$, but one will be negative and the other positive.

149. The asymmetry parameter is most meaningful in unimodal directional distributions or in isolated modes of multimodal distributions (described below). In this report, $A_n$ is used to group directional distributions with similar shapes, as discussed in Part IX.

150. A third parameter, also used in geometric comparisons, is a positioning parameter determined from the mean of $\theta_{25\%,n}$ and $\theta_{75\%,n}$. Called $\overline{\theta}_n$, it is given by

$$\overline{\theta}_n = \tfrac{1}{2}(\theta_{25\%,n} + \theta_{75\%,n}) \tag{19}$$

This parameter is used in Part IX to translate distributions along the direction axis so that composite distributions can be constructed. For distributions with the same spread parameter, it ensures that 25- and 75-percent angles will align for all members of a composite and consequently allows intercomparison of directional distribution shapes having constant spread. Note that $\overline{\theta}_n$ is used as a characteristic direction for repositioning data on the direction axis. It is not the same as peak direction $\theta_{p,n}$, which is the direction of the maximum of a distribution function.

## Some Bulk Spreading Parameters

151. The parameters given by Equations 17, 18, and 19 are all specific to distributions at a given frequency within a frequency-direction spectrum. To characterize an entire frequency-direction spectrum, some measure of the bulk or overall properties of the spectrum must be used. In this report, two bulk spreading parameters are considered. One is deduced from the integrated direction spectrum $S(\theta_m)$ in the same way that $\Delta\theta_n$ was found from $S(f_n,\theta_m)$. The other is a spectrally weighted sum of the set of $\Delta\theta_n$ found from a given frequency-direction spectrum.

152. A spread parameter based on $S(\theta_m)$ is considered first. The IDS is given by Equation 9. The area under this curve is, from Equation 12, one-sixteenth $H_{mo}^2$. A cumulative distribution can be constructed from $S(\theta_m)$ by the expression

$$I(\theta_j) = \sum_{m=1}^{j} \frac{S(\theta_m)}{(\frac{1}{4}H_{mo})^2}\, d\theta \tag{20}$$

which varies from 0 to 1 like the expression given in Equation 15. Angles representing the 25-, 50-, and 75-percent directions, named $\theta_{25\%,IDS}$, $\theta_{50\%,IDS}$, and $\theta_{75\%,IDS}$, respectively, satisfy the relations

$$I(\theta_{25\%,IDS}) = 0.25 \tag{21a}$$

$$I(\theta_{50\%,IDS}) = 0.50 \tag{21b}$$

$$I(\theta_{75\%,IDS}) = 0.75 \tag{21c}$$

in analogy with Equations 16(a-c). A bulk spreading parameter derived from these angles is

$$\Delta\theta_{IDS} = \theta_{25\%,IDS} - \theta_{75\%,IDS} \tag{22}$$

and represents the angle subtending the central 50 percent of the total energy in a wave field.

153. The parameter given by Equation 22 includes the effects of any frequency-dependent scattering mechanisms in that energy is summed across all frequencies to get $S(\theta_m)$. If low-frequency waves have more shore-normal directions than high-frequency waves, the total energy can be smeared across the direction axis. The proper total width is given by Equation 22 if one is not concerned with the detailed frequency distribution of energy. If this is of concern, a second definition of bulk spreading may be more appropriate.

154. In the second definition, the spread parameters for each frequency $\Delta\theta_n$ are multiplied by the corresponding frequency spectral densities $S(f_n)$ and summed. The result is normalized by the total energy to obtain a spectrally weighted mean directional spread $\Delta\theta_{SW}$. The mathematical expression for this is

$$\Delta\theta_{SW} = \frac{1}{(\frac{1}{4}H_{mo})^2} \sum_{n=1}^{N} S(f_n)\ \Delta\theta_n \tag{23}$$

155. This definition is introduced in analogy with the spectrally weighted peak direction parameter proposed by The IAHR Working Group on Wave Generation and Analysis (1989). Here, the bulk spread obtains most of its value from regions of high energy in the frequency spectrum. Furthermore, the effect of refraction from frequency to frequency is less pronounced. In particular, if the general spread for all frequencies is about the same (see Figure 7b), the result of Equation 23 will be close to this spread estimate. It will generally be less than the estimate of Equation 22 because the smearing effect (see Figure 7a, direction spectrum panel) is reduced.

156. Other parameters of the bulk frequency-direction spectrum can be computed from the characteristic directions given by Equations 21(a-c). For instance, asymmetry and positioning parameters can be assigned like the individual frequency parameters given in Equations 18 and 19, respectively. These have not been used in this report and are not explicitly defined.

## Parameters for Modal Analysis

157. An important property of directional distributions is the number of distinct peaks or modes that occur. These can suggest the existence of various sources or sinks of wave energy (e.g., island sheltering, see Pawka 1983 and Pawka, Inman, and Guza 1984) or may be a signature of nonlinear interactions among wave trains (Elgar and Guza 1985a, 1985b). All of these mechanisms act to distribute wave energy in direction and need to be considered. In this report, a simple modal analysis is conducted wherein the number and relative strengths of modes are computed from the directional distributions at each frequency. This is intended to determine the frequency of occurrence of multimodal distributions, to compute their relative importance, and to indicate if further research is required.

158. The first requirement is a definition of a mode. As mentioned in Part III, IMLE results can have maxima and minima that are simply deviate approximations to a true unimodal directional distribution and not truly distinct modes. To ensure that a minimum of $D(f_n,\theta_m)$ between two maxima is more likely a true modal separation and not just an artifact of analysis, the following is used as a definition: a distinct mode occurs when a minimum in a directional distribution is less than half of the smaller of the two surrounding maxima.

159. Figure 9a illustrates one such case. In that figure there are three maxima: (a) a small one at about 50 deg azimuth, (b) a main one at about -10 deg azimuth, and (c) an intermediate one at about -60 deg azimuth. By the definition given above, only the minimum marked $\theta_{min}$ between the last two maxima is considered significant. The distribution to the left of $\theta_{min}$ is considered one mode, and the distribution to the right of $\theta_{min}$ is considered another mode. The directional bounds on the first mode are 90 deg on the left and $\theta_{min}$ on the right. The second mode begins at $\theta_{min}$ and extends to -90 deg on its right. The number of modes in this case is two.

160. A measure of the relative importance of each mode is the fraction of total area (or energy) under the directional distribution contained in each mode. To do this, it is necessary to integrate $D(f_n,\theta_m)$ over the parts of the distribution associated with each mode. Since $D(f_n,\theta_m)$ integrates to unity over its full 180-deg range, the partial areas under the modes automatically give the fractional part of the total energy. If the distribution does not go to zero in the gap between the modes, the tails of the modes overlap and some assumptions must be made about their treatment. In this crude first approach, the assumption is that overlapping tails have no area so that integration over the limits of a mode distribution gives an estimate of the (normalized) energy in the mode. At a mode boundary (i.e., $\theta = \theta_{min}$), half the area in the direction bin (of width $d\theta$) is assigned to each mode. At the alongshore azimuths (+90 and -90 deg), the energy is very small; therefore, the same boundary rule can apply there without loss of generality.

161. The symbol $P_n^{(k)}$ is used to represent the fractional area in the $k$ mode (counting, arbitrarily, from the left) of a directional distribution at frequency $f_n$. Clearly, two parameters of a mode definition are the directions that bound a mode. If the indices of the discrete directions bounding a mode are $r$ and $s$, the notation for these directions is $\theta_{r,n}^{(k)}$, the direction boundary on one side of mode $k$ at frequency $f_n$, and $\theta_{s,n}^{(k)}$, the direction boundary on the other side of mode $k$. The boundary directions are either an alongshore azimuth or $\theta_{min}$ as shown in Figure 9. Note that at $\theta_{min}$ in multimodal distributions, $\theta_{s,n}^{(k)} = \theta_{r,n}^{(k+1)}$, i.e., the right bound for one mode is the left bound for the next mode.

162. With these definitions, an expression for the fractional area (energy) in mode $k$ is given by

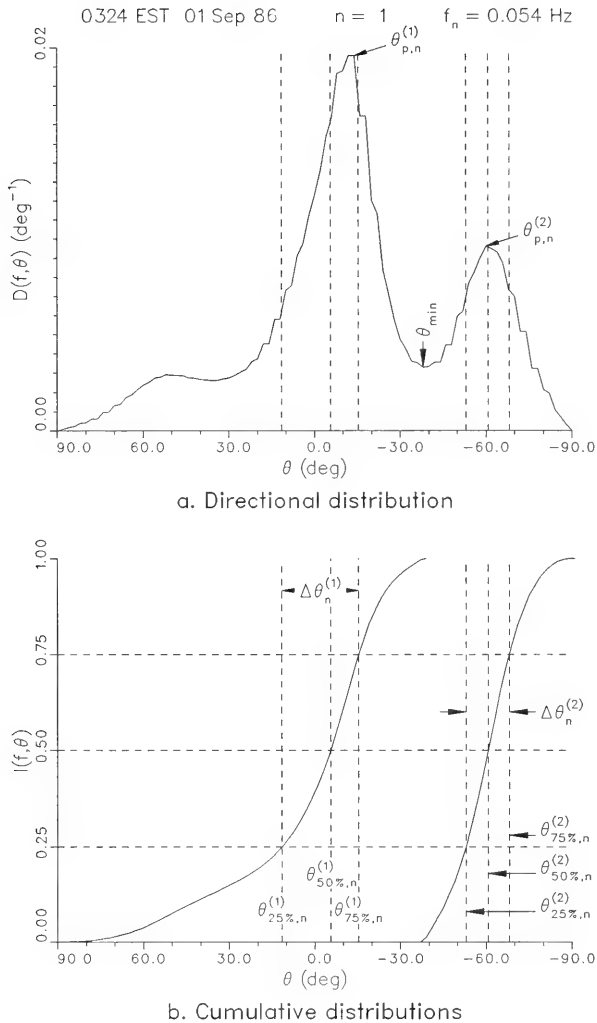


Figure 9. Schematic of distribution functions showing parameter definitions for multimodal shapes

$$P_n^{(k)} = \tfrac{1}{2} D(f_n,\theta_{r,n}^{(k)})\ d\theta + \sum_{i=r+1}^{s-1} D(f_n,\theta_i)\ d\theta + \tfrac{1}{2} D(f_n,\theta_{s,n}^{(k)})\ d\theta \qquad (24)$$

where this must be applied to each of a total of $K$ modes. If there is only one mode, then $K = 1$ and $P_n^{(1)} = 1$, since this case makes Equation 24 virtually identical to Equation 14. In all cases,

$$\sum_{k=1}^{K} P_n^{(k)} = 1 \qquad (25)$$

for each $f_n$ to satisfy Equation 14, i.e., that the sum of all the parts is unity.

163. To be consistent with parameterizations of the bulk and frequency distributions of directional energy, there must be a set of characteristic directions which indicate the peak and quartile directions in a mode, as well as the mode bounding directions. A modal peak direction, given the symbol $\theta_{p,n}^{(k)}$, is defined as the direction of the peak in $D(f_n,\theta_m)$ [or $S(f_n,\theta_m)$] for mode $k$ at frequency $f_n$, where the search is conducted between the bounding directions $\theta_{r,n}^{(k)}$ and $\theta_{s,n}^{(k)}$. Examples of modal peak directions are illustrated in Figure 9a.

164. Within a mode, characteristic directions can be defined at which the cumulative distribution has values of 25, 50, and 75 percent of the total area, just as was done for the whole distribution at each frequency and which led to Equations 15 and 16. Here, the directional distribution $D(f_n,\theta_m)$ must be normalized by $P_n^{(k)}$ so that the integral between the mode bounding directions will equal unity. The cumulative distribution function for mode $k$ is defined by

$$I^{(k)}(f_n,\theta_j) = \frac{1}{P_n^{(k)}} \left[ \tfrac{1}{2} D(f_n,\theta_{r,n}^{(k)})\ d\theta + \sum_{i=r+1}^{j} D(f_n,\theta_i)\ d\theta \right] \qquad (26)$$

165. Figure 9b illustrates two cumulative distribution functions resulting from Equation 26 for a bimodal ($K = 2$) directional distribution. The modal quartile directions, symbolized by $\theta_{25\%,n}^{(k)}$, $\theta_{50\%,n}^{(k)}$, and $\theta_{75\%,n}^{(k)}$, respectively, satisfy the relations

$$I^{(k)}(f_n, \theta^{(k)}_{25\%,n}) = 0.25 \tag{27a}$$

$$I^{(k)}(f_n, \theta^{(k)}_{50\%,n}) = 0.50 \tag{27b}$$

$$I^{(k)}(f_n, \theta^{(k)}_{75\%,n}) = 0.75 \tag{27c}$$

166. These quartile directions are illustrated as vertical dashed lines in Figure 9b for each of the two modes shown. The object in this definition is to have a nearly exact analogy with the parameterization shown in Figure 8. In this way, the shapes of individual modes in a multimodal distribution can be compared with the shapes of unimodal distributions having similar parameters.

167. Characteristic spread, asymmetry, and positioning parameters for individual modes are derived from the representative directions in the same way that Equations 17, 18, and 19 are defined. Directional spread for frequency $f_n$ and mode $k$ is given by

$$\Delta\theta^{(k)}_n = \theta^{(k)}_{25\%,n} - \theta^{(k)}_{75\%,n} \tag{28}$$

Figure 9b illustrates these as double arrows between the 25- and 75-percent vertical dashed lines for each of the two modes shown.

168. An asymmetry parameter for mode $k$ and frequency $f_n$ is given by

$$A^{(k)}_n = \ln \left\{ \frac{\theta^{(k)}_{25\%,n} - \theta^{(k)}_{50\%,n}}{\theta^{(k)}_{50\%,n} - \theta^{(k)}_{75\%,n}} \right\} \tag{29}$$

and a positioning parameter is given by

$$\overline{\theta}^{(k)}_n = \tfrac{1}{2} \left( \theta^{(k)}_{25\%,n} + \theta^{(k)}_{75\%,n} \right) \tag{30}$$

169. One set of these three parameters (or, equivalently, the three characteristic angles) can be found for each of $K$ modes for a directional distribution along frequency line $n$. If the distribution is unimodal, $K = 1$ and Equations 28, 29, and 30 become identical with Equations 17, 18, and 19, respectively.

## Parameter Data Base

170. A set of all the parameters described above has been computed for each frequency-direction spectrum thereby forming a parameter data base with which to characterize the observations. Parameters are grouped by analysis objectives. This section defines the groups and summarizes the set of parameters.

171. The first group contains properties associated with a collection. They are:

| Parameter | Definition |
|---|---|
| Date/Time | Collection date and start time |
| Gage Pattern | List of checked, operating gages |
| Depth | Mean water depth during the collection |

172. The second group contains integral parameters of and properties uniquely determined from the frequency-direction spectrum as a whole. They are:

| Parameter | Definition |
|---|---|
| $H_{mo}$ | Characteristic wave height, four times the square root of the volume under the frequency-direction spectrum |
| $f_{p,FD}$ | Peak frequency from the maximum of $S(f_n, \theta_m)$ |
| $\theta_{p,FD}$ | Peak direction from the maximum of $S(f_n, \theta_m)$ |
| $\Delta\theta_{SW}$ | Spectrally weighted directional spread from Equation 23 |

173. The third group is simply the peak frequency and its inverse, the peak period, from the integrated frequency spectrum. Peak frequency and peak period are two of the conventional parameters of sea state characterization. They are:

| Parameter | Definition |
|---|---|
| $f_{p,IFS}$ | Peak frequency from the maximum of $S(f_n)$ |
| $T_{p,IFS}$ | (= $1/f_{p,IFS}$) peak period from the maximum of $S(f_n)$ |

174. The fourth group contains the characteristic directions of the integrated direction spectrum. These and their derivatives (spread, asymmetry, and position) characterize the bulk directional properties of a wave field. They are:

| Parameter | Definition |
|---|---|
| $\theta_{p,IDS}$ | Peak direction from the maximum of $S(\theta_m)$ |
| $\theta_{25\%,IDS}$ | Direction at which 25 percent of total energy is to the left (or counterclockwise) and 75 percent is to the right (clockwise) |
| $\theta_{50\%,IDS}$ | Direction at which 50 percent of total energy is on each side |
| $\theta_{75\%,IDS}$ | Direction at which 75 percent of total energy is to the left and 25 percent is to the right |

175. The fifth group contains the parameters of the directional distribution function for each frequency in the frequency-direction spectrum. The number of parameters at each frequency is conditional on the number of modes found in the distribution. Basic parameters and characteristic directions are always computed for the whole (180-deg) distribution, independent of any modal definition. They are:

| Parameter | Definition |
|---|---|
| $f_n$ | Frequency at discrete index n |
| $S(f_n)$ | Integrated frequency spectral density at $f_n$ |
| $\theta_{p,n}$ | Peak direction at frequency $f_n$ |
| $\theta_{25\%,n}$ | Direction at which 25 percent of $S(f_n)$ is to the left |
| $\theta_{50\%,n}$ | Direction which evenly divides $S(f_n)$ |

| | |
|---|---|
| $\theta_{75\%,n}$ | Direction at which 75 percent of $S(f_n)$ is to the left |
| K | Number of modes found at this frequency |

176. If K is greater than one, the distribution at frequency $f_n$ is multimodal. In this case, an additional set of parameters is computed for each of the K modes. They are:

| Parameter | Definition |
|---|---|
| k | Index (count relative to K ) of this mode |
| $P_n^{(k)}$ | Fraction of $S(f_n)$ contained in mode k |
| $\theta_{p,n}^{(k)}$ | Peak direction within mode k |
| $\theta_{r,n}^{(k)}$ | Direction which bounds mode k on the left (counterclockwise) side |
| $\theta_{25\%,n}^{(k)}$ | Direction at which 25 percent of energy in mode k is to the left |
| $\theta_{50\%,n}^{(k)}$ | Direction which evenly divides the energy in mode k |
| $\theta_{75\%,n}^{(k)}$ | Direction at which 75 percent of energy in mode k is to the left |
| $\theta_{s,n}^{(k)}$ | Direction which bounds mode k on the right (clockwise) side |

177. Note that it is the set of quartile angles (25-, 50-, and 75-percent points in the integrated distributions) that is saved rather than the derived parameters (spread $\Delta\theta$ , asymmetry A , and position $\overline{\theta}$ ). This is because the derived parameters are easily computed from the quartile angles and because the quartile angles are more fundamental properties of a distribution.

178. Once compiled, this rather lengthy collection of parameters can elucidate the directional properties of a set of wave field observations at several levels of detail. The set is not exhaustive but is rather a collection of some obvious properties which are of interest in directional characterization.

## PART VI: BULK DIRECTIONAL CHARACTERISTICS

179. The most important objective of the present study is to characterize the directional properties of the total energy in the set of observations that has been made. This characterization is done with the bulk parameters defined above in two ways: (a) the distribution of a property which indicates its range and most probable values; and (b) correlations between parameters to see how they relate as well as intercomparisons between parameters for the same property where two definitions have been given (e.g., peak direction and directional spread).

### Peak Direction

180. Two parameters were isolated to obtain a general concept of the range and probability of occurrence of the direction of wave approach: (a) $\theta_{p,FD}$ , the direction of the maximum spectral density in the frequency-direction spectrum, $S(f,\theta)$ ; and (b) $\theta_{p,IDS}$ , the direction of maximum energy in the integrated direction spectrum, $S(\theta)$ . The two parameters are distinct in that the former indicates the direction of the most energetic peak of all frequencies and directions, whereas the latter indicates the direction of dominant overall wind wave energy.

181. Figure 10 shows the distribution of $\theta_{p,FD}$ , computed by summing the number of cases where peak direction fell within discrete direction arcs and normalizing the result by the total number of cases to find the percent of cases in each arc. The directional spectra were already discretized into $d\theta$ = 2-deg arcs, and this made a convenient division for the distribution calculation. All 1,046 cases from the first year's collection were considered. At this stage, no distinction was made as to other parameters of the wave field (energy level, spread, etc.)

182. Figure 10 indicates that peak direction ranges generally across a 120-deg arc from 60 to -60 deg. The main peak in the distribution is in the direction range of 6 to -20 deg, i.e., from roughly shore normal to slightly south of shore normal. This range is consistent with the fact that the observation set is dominated by low-energy, day-to-day sea states. These consist primarily of low-frequency waves which have likely propagated across the continental shelf from the open, deep Atlantic. The shelf break, which is

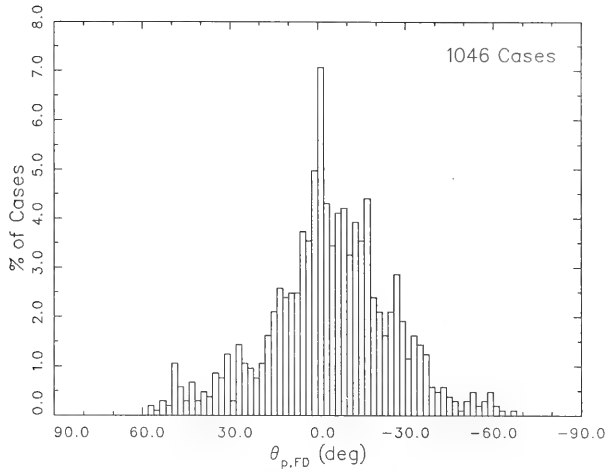


Figure 10. Distribution of peak directions, $\theta_{p,FD}$, derived from frequency-direction spectra

roughly aligned with true north (see Figure 1), would tend to refract the waves to slightly south of shore normal.

183. The same general trend is shown in Figure 11, which is the distribution of peak directions from the integrated direction spectra. Here, the peak of the distribution is more nearly centered on shore normal. This

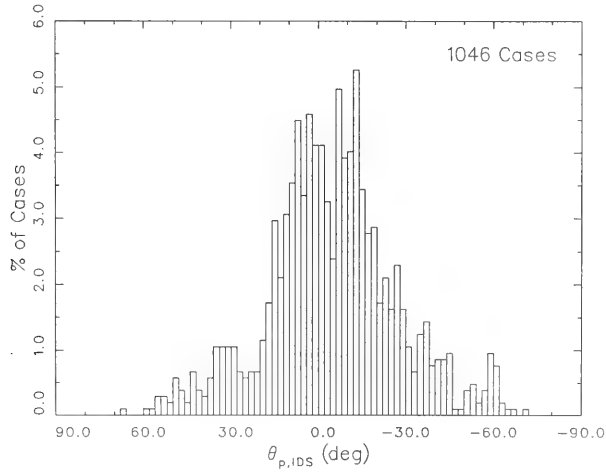


Figure 11. Distribution of peak directions, $\theta_{p,IDS}$, derived from integrated direction spectra

may be attributed to the fact that the integrated direction spectrum includes contributions from waves at all frequencies, including those at high frequencies. High-frequency waves tend to be less influenced by refraction for a given shoaling propagation path. The effect is to add enough high-frequency energy to the integrated direction spectrum to shift its peak relative to the singular peak of the frequency-direction spectrum. Figure 7 is a good example of this. In Figure 7, the peak of the frequency-direction spectrum is at a low-frequency lobe centered near -30 deg. However, because there is a lot of high-frequency energy at positive angles, the integrated direction spectrum (left rear vertical panel) has a peak near 10 deg. This creates a 40-deg difference in the two measures of peak direction.

184. The scatter resulting from this type of difference is shown in Figure 12 which is a correlogram of the two measures of peak direction. The diagonal line is the perfect correlation reference. Fewer than 1,046 symbols are visible because both measures of peak direction are discrete. Hence, one symbol location may represent several observations. The figure shows a gross

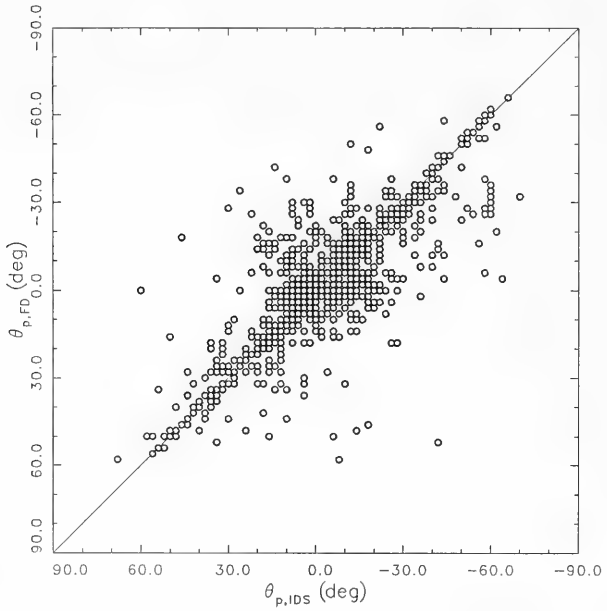


Figure 12. Correlation of peak directions from integrated direction spectrum and frequency-direction spectrum

correlation trend but much scatter, especially near shore-normal. Refraction may be partly responsible for the scatter, but another reason is that the directional distributions in well-developed sea states tend to be broad and, to some extent, rather flat. Figures 5 and 7 both show this in their integrated direction spectra. Peak direction can be the result of a slight elevation in spectral density above a broad level of nearly constant values. In statistical fairness, confidence intervals on each estimate can allow the true peak to lie anywhere on the broad distribution maximum. In conditions where peak direction is well away from shore normal, there is better correlation between $\theta_{p,FD}$ and $\theta_{p,IDS}$. These cases tend to be young, narrow seas (see, e.g., Figure 6) which align well with the wind, and are mostly high-frequency waves which are not strongly refracted. Hence, much scatter is expected in estimates of peak direction for aged or well-developed wave conditions. As a result, peak direction may not be the best parameter with which to characterize a sea state with large directional spread.

185. Peak direction is one of the conventional sea state descriptors, however, so it is retained in this analysis. Since the interest here is in directional properties of the total energy, the parameter $\theta_{p,IDS}$ is considered most representative. Its correlations with characteristic wave height $H_{mo}$ and peak period $T_{p,IFS}$ ( $= 1/f_{p,IFS}$, where the peak frequency of the conventional frequency spectrum is used) are shown in Figures 13 and 14, respectively. These parameters are two other conventional sea state descriptors.

186. In Figure 13, the range of peak directions is generally large for low $H_{mo}$ and narrows toward the shore-normal direction at larger $H_{mo}$. At low $H_{mo}$, the largest concentration of points is near the shore-normal direction and tends toward the negative directions, consistent with the argument for low-energy, long-period swell. The more extreme values at low $H_{mo}$ are likely from the early stages of locally wind-generated seas. These are typically short-period waves which align with wind direction. They have less tendency to be steered by bathymetric effects. At high $H_{mo}$, the wave field tends to be in a well-developed state with significant low-frequency energy arriving from deeper water.

187. In terms of peak period (Figure 14), the short-period waves have a tendency to be from positive directions. This is consistent with the propensity for local, wave-generating winds to be from the northeast quadrant. At

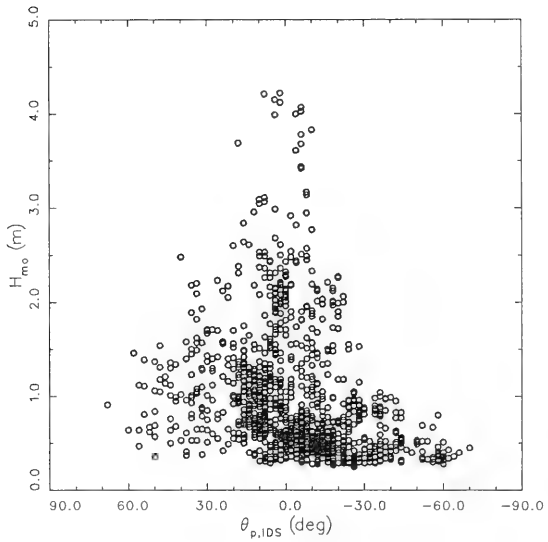


Figure 13. Correlation of peak direction with characteristic wave height

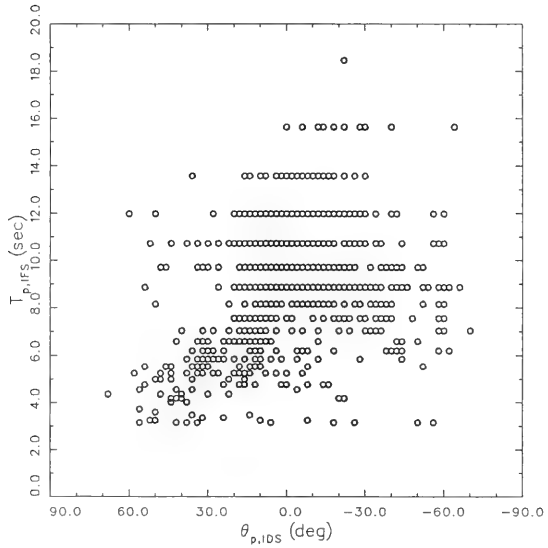


Figure 14. Correlation of peak direction with peak period

longer periods, the tendency is for the directions to scatter about shore normal. Periods of swell and well-developed wind seas overlap in this region. In this figure, both period and direction are discretely defined so that one symbol may represent more than one observation. This makes the distribution appear more uniform than indicated by Figure 11, which shows the true distribution.

188. The parameters $H_{mo}$ and $T_{p,IFS}$ can be combined indirectly to make a dimensionless parameter known as bulk wave steepness. Using $f_{p,IFS}$ from the frequency spectrum in Equation 2 yields the corresponding wavelength $L_{p,IFS}$. The ratio $H_{mo}/L_{p,IFS}$ defines bulk wave steepness. The correlation of this with peak direction $\theta_{p,IDS}$ is shown in Figure 15. Though there is significant scatter, the climatology is consistent with previous discussion. Long, low waves (low steepness) tend to center on shore-normal with some contributions from the southeast quadrant (negative angles). High-steepness waves, associated with energetic seas, tend to be distributed through the northeast quadrant (positive angles).

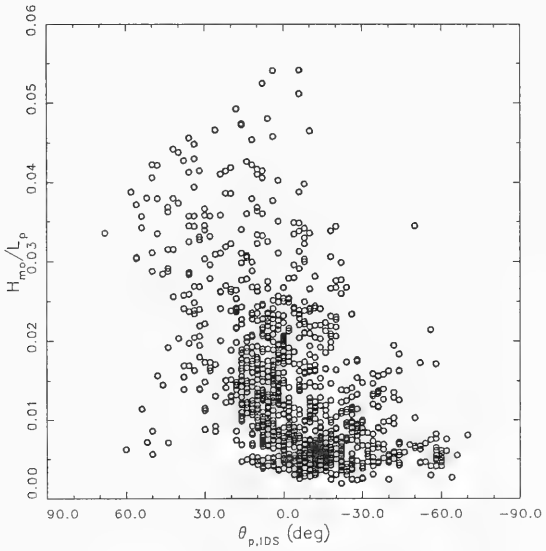


Figure 15. Correlation of peak direction with bulk steepness

189. The point of this section is that the observed wave climate is consistent with existing knowledge of wave behavior as defined by the conventional parameters of characteristic height, period, and direction. It is noted that bulk peak direction $\theta_{p,IDS}$ in cases of large directional spread may have a large uncertainty of estimation, as mentioned above. The range of observed peak directions is from 60 to -60 deg in azimuth relative to shore normal. Most of the observations cluster around the shore-normal direction because all observations were used in the analysis and the sampling is naturally biased toward the longer waves of low-energy, nonstorm conditions.

## Directional Spread

190. A primary objective in the present study is to characterize directional spread. Two measures of bulk directional spread were introduced above: (a) the arc containing the central half of total energy in the integrated direction spectrum $\Delta\theta_{IDS}$, and (b) the spectrally weighted sum of the arcs containing the central half of the energy at each frequency $\Delta\theta_{SW}$. The distributions of these parameters, their correlation with each other, and their correlation with height, period, and direction parameters are considered here.

191. Figure 16 shows the distribution of directional spreads determined from the integrated direction spectrum. The distribution is rather smooth and distinctly unimodal indicating that wave-field energy (in this data set) always has a finite directional spread. There are very few cases with a spread of less than 20 deg and very few with a spread greater than 60 deg. The bulk of cases lies in the range 35 to 45 deg.

192. What is striking about this result is that there is no indication of a unidirectional wave field. Such a field would appear in Figure 16 at 0 deg on the abscissa. There are none. In light of the experiments by Vincent and Briggs (1989) and Kaihatu and Briggs (in preparation), mentioned previously, the most probable spread from Figure 16 is nearer the high-spread end of their range of cases. For purposes of guidance for model studies in engineering design, this result suggests strongly that finite directional spread be included as a test parameter. The range indicated in Figure 16 can be considered representative of sites adjacent to broad, shallow continental shelves.

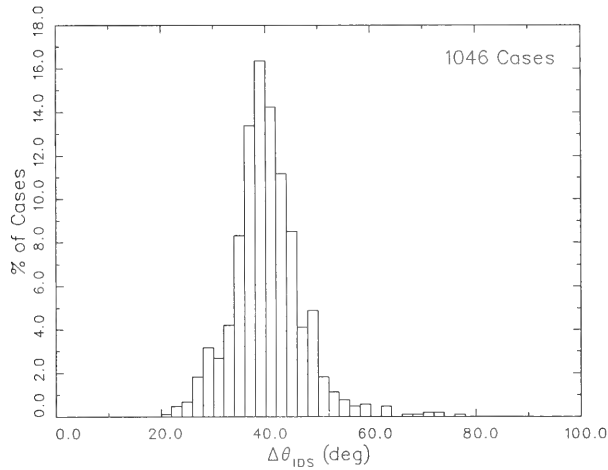


Figure 16. Distribution of directional spread parameter derived from integrated direction spectra

193. This result is supported by the distribution of spectrally weighted directional spread estimates shown in Figure 17. Here, the range is similar, being from about 15 to 50 deg. Most probable values are in the range from about 34 to 42 deg. These numbers are all slightly less than

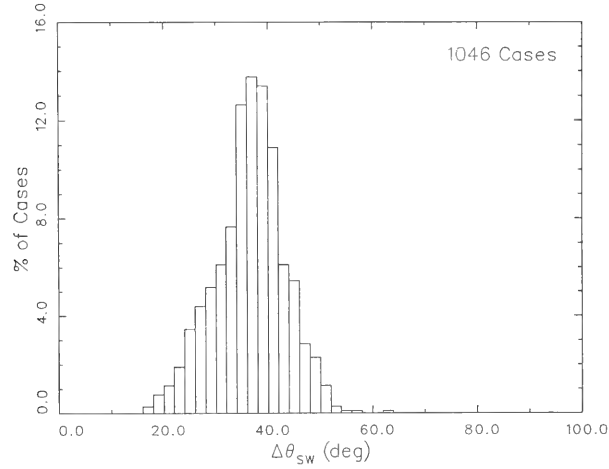


Figure 17. Distribution of spectrally weighted directional spread parameter

corresponding numbers from Figure 16 because $\Delta\theta_{SW}$ reduces the effect of frequency-dependent broadening of the overall energy which is included in $\Delta\theta_{IDS}$ .

194. This condition is illustrated by Figure 18, which is a correlation plot of the two directional spread parameters. Figure 18 shows that $\Delta\theta_{IDS}$ is almost always greater than or equal to $\Delta\theta_{SW}$ . A likely mechanism is refraction which varies from frequency to frequency in some wave fields (see

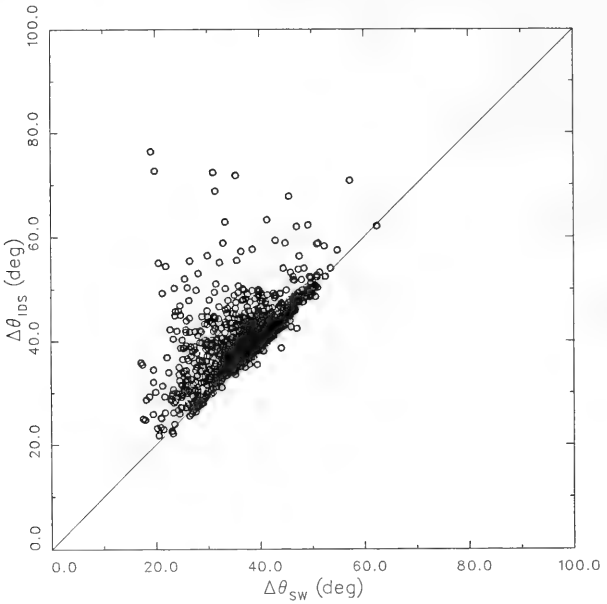


Figure 18. Correlation of spectrally weighted directional spread parameter with spread parameter of integrated direction spectra

Figure 7) and which smears the directional distribution of the integrated direction spectrum along the direction axis. If the directional spread at each frequency had a constant value, the spectrally weighted spread would have that value since the contribution from each frequency would be the same. If the distributions were offset slightly from frequency to frequency, as happens under refraction, the summing of energy across all frequencies would make the

net result wider than the spread at any given frequency. Hence, $\Delta\theta_{IDS}$ would tend to be greater than $\Delta\theta_{SW}$ .

195. For a bulk characterization, the parameter $\Delta\theta_{IDS}$ will be used from here on. It characterizes directional spread of the true (uniformly integrated) total energy at the observation site. Since $\Delta\theta_{SW}$ is less influenced by variations from frequency to frequency, it tends to miss the full range of directions at which there is significant energy. This property defeats the immediate purpose of characterizing overall directional spread.

196. Correlations of $\Delta\theta_{IDS}$ with the conventional height, period, and direction parameters are shown in Figures 19, 20, and 21, respectively. In the height relationship (Figure 19), directional spread has its greatest range at small $H_{mo}$ . Smaller spreads tend to occur in the early stages of wind-generated growth (see Figure 6) and in some cases of swell. Large spreads may be caused by rapidly veering winds or when swell and wind-sea waves coexist but from widely separated directions. These cases are the extremes and generally occur at low energy. An interesting feature of Figure 19 is that

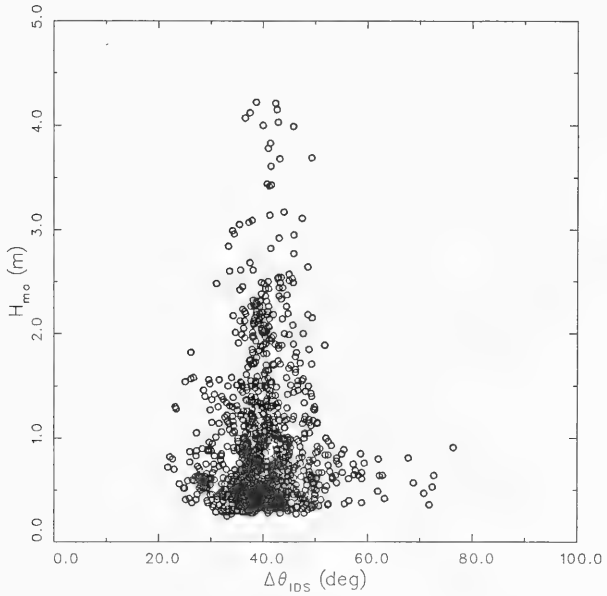


Figure 19. Correlation of directional spread with characteristic wave height

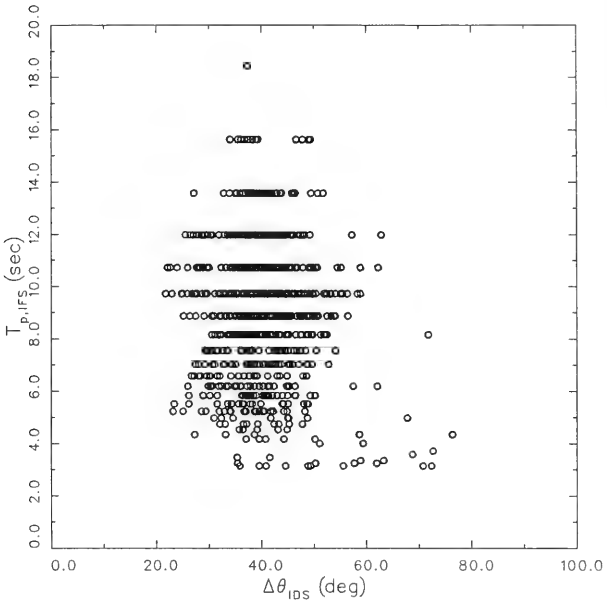


Figure 20. Correlation of directional spread with peak period

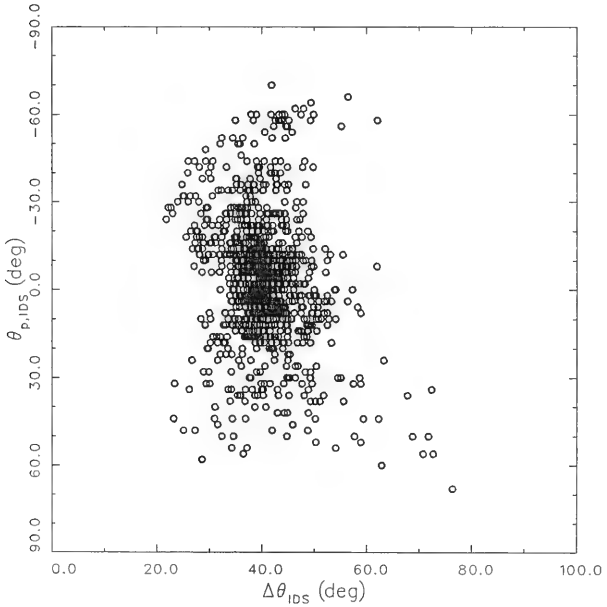


Figure 21. Correlation of directional spread with peak direction

the central tendency of the directional spread parameter appears to be about the same for all energy levels. Though there are not many high-energy cases, the few existing points are scattered, rather narrowly, about a spread of 40 deg. The same clustering is seen at the lowest energies.

197. This behavior is also seen in the correlation of $\Delta\theta_{IDS}$ with $T_{p,IFS}$ (Figure 20). Excepting a few outliers, directional spread characteristics appear to be roughly the same for all values of peak period. The large spreads at low $T_{p,IFS}$ are likely the result of waves from light, irregular winds and coexisting swell. These correspond to the large spreads at low energy shown in Figure 19.

198. The same tendency is shown in Figure 21 where directional spread is correlated with peak direction $\theta_{p,IDS}$. Though the overall scatter in spread values is slightly lower for shore-normal peak directions (0 deg), the most common spread tends to be around 40 deg for all peak directions.

199. Figure 22 shows directional spread correlated with bulk steepness. Here, again, the characteristic directional spread appears relatively

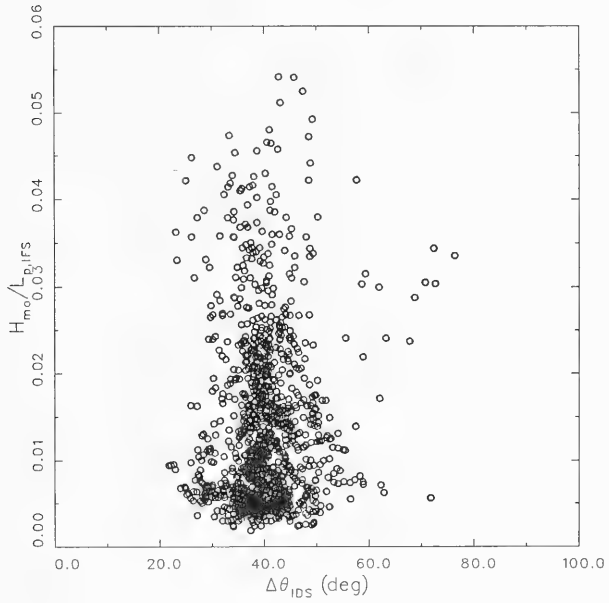


Figure 22. Correlation of directional spread with bulk steepness

insensitive to variations in this parameter. The same central values and roughly the same scatter occur for low-steepness (mostly swell) and high-steepness (active wind sea) conditions.

200. There are several important conclusions from this analysis. One is that there never appears to be a wave field which is unidirectional. Another is that directional spread (as defined here) appears to exist in the range 20 to 60 deg with a most common value near 40 deg. This distribution appears roughly to be independent of the three bulk parameters (height, period, and direction) conventionally used to characterize sea state. This suggests that the distribution of directional spreads shown in Figure 16 is a reasonable characterization for most sea states which occur at this and similar sites.

## PART VII: MODAL ANALYSIS

201. The results of the last section were based on bulk properties of frequency-direction spectra. While meaningful, they do not give much information about the more detailed structure of the spectra. Knowledge of spectral structure is necessary for understanding physical processes associated with wind waves and for incorporating observations into physical and numerical models of those processes, including wave generation, refraction, shoaling, transformation, and nonlinear interactions. An important property of wave directionality is the extent to which there is more than one peak, or mode, in directional distributions of wave energy. Multimodal distributions can arise from any of the processes mentioned, and all of the processes can be active at the present experiment site. In this section, a simple evaluation of the number and relative strengths of modes is conducted as an indication of the necessity for further study.

202. This type of analysis is different from the bulk analysis of the last section because characteristics at one frequency are considered independent of characteristics at other frequencies. Any coherence in spectral shape from frequency to frequency is therefore lost. The bulk parameters treated each spectrum as a unit and inherently included shape effects, though in a smoothed, integral fashion. The advantage of frequency-by-frequency analysis is that structural similarities and differences between distributions at different frequencies can be isolated. In this way, it may be possible to define a set of basic modal shapes from which a spectrum or a set of spectra can be constructed.

203. A simple initial approach is to examine slices through the frequency-direction spectrum along lines of constant frequency and to evaluate the number, strengths, and shapes of the resulting directional modal structure. The simplest result that could be expected from this is that distributions at all frequencies and for all spectra are unimodal, consisting of one primary maximum of energy. However, it can be seen in the high-frequency part of Figure 7 and in the sample distribution of Figure 9 that at least some of the distributions are multimodal. Hence, it is necessary to count them.

204. Part of the frequency-by-frequency parameter set defined in Part V is the number $K$ of modes found for each frequency in a frequency-direction spectrum. It should be remembered that the mode separation definition used

here is a valley in a directional distribution where the energy density is less than half that at the lesser of the two adjacent distribution peaks. This definition is subjective, and analysis results will change if the definition is changed. For all 1,046 cases in the present data set, the parameter K was scanned and the number of unimodal (K = 1), bimodal (K = 2), trimodal (K = 3), etc., cases were counted for each frequency. These numbers were then converted to percentages of total cases.

205. Results of this computation are shown in Figure 23. Along the frequency axis the center of each bar is at the representative frequency $f_n$, and the bar width is the resolution bandwidth df. For a given frequency, the length of each shading pattern represents the percent of cases having the number of modes associated with the shading pattern.

206. Figure 23 indicates that virtually all of the directional distributions at 0.09 to 0.10 Hz (the tallest, black bar) are unimodal. The percent of unimodal cases drops off on either side of this. At the highest

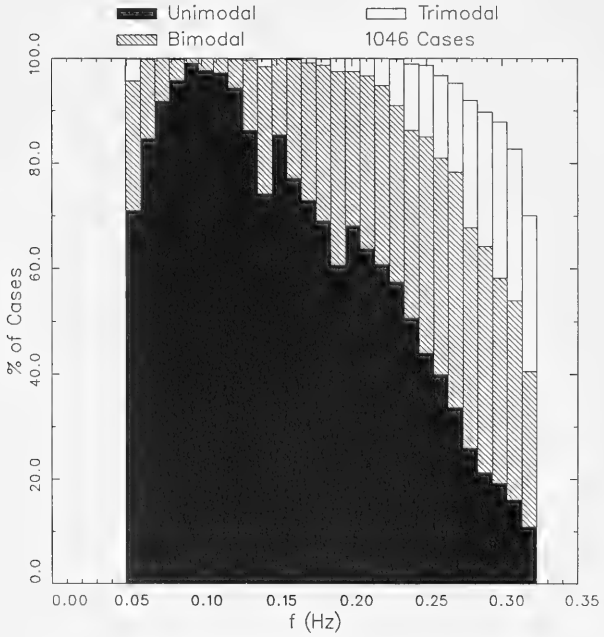


Figure 23. Frequency-by-frequency distributions of numbers of modes

frequency (about 0.32 Hz), only about 10 percent of the cases are unimodal, about 30 percent are bimodal (diagonal shading), about 30 percent are trimodal (white shading), and the remaining 30 percent (blank space above the white-shaded bar) has more than three modes. At the lowest frequency (about 0.05 Hz), roughly 70 percent of the cases are unimodal, another 25 percent are bimodal, and the rest are trimodal.

207. Taken as a whole, the figure indicates that well over half of all single-frequency directional distributions are unimodal. This is deduced from the figure by the ratio of total black-shaded area to total area for all frequencies. Roughly another 20 percent are bimodal (ratio of diagonal-shaded area to total area) and the rest have more than two modes. The large percentage of multimodal distributions indicates that this is an important feature of natural, shallow-water, wave fields.

208. The computation that led to Figure 23 only counted the number of modes and not their relative strength (the extent to which energy is distributed among the modes). For instance, a bimodal distribution could have 90 percent of its energy in one mode and only 10 percent in the other. In this case, the second mode is of little importance from an energy standpoint because it contains very little energy. However, if each mode in a bimodal distribution has half the energy of the distribution, then both modes are of equal importance, and neither can be neglected.

209. To examine this effect, a computation was done with the modal fractional energy parameter $P_n^{(k)}$ defined by Equation 24 and listed with the individual mode parameters in Part V. For each directional distribution (including the unimodal ones), the mode with the maximum energy, i.e., having the maximum fraction $P_n^{(k)}$ of total energy, was isolated and identified as the primary mode. For unimodal cases this was the only mode, and its fraction of total energy was identically one (100 percent). Primary mode energy fractions were then grouped into 10-percent-wide bands and counted; that is, a certain number of distributions had 90 to 100 percent of their energy in the primary mode (maximum $P_n^{(k)}$ in the range 0.9 to 1.0), others had 80 to 90 percent in the primary mode, yet others had 70 to 80 percent in the primary mode, and so on. The number of cases in each group was divided by the total number (1,046) of cases in the data set and multiplied by 100 percent. The result was the percent of all cases having a given fractional range of energy in the primary mode. For example, Figure 9a shows a bimodal distribution with

roughly 70 to 80 percent of its total area in its primary mode (to the left of $\theta_{min}$ ) and the remaining 20 to 30 percent in the lesser mode to the right of $\theta_{min}$ . This case is one of the number (for this frequency) of cases having 70 to 80 percent of its energy in the primary mode.

210. Results of this computation are shown in Figure 24, which is a cumulative bar chart like Figure 23. This figure indicates that in a band of low frequencies from about 0.06 to 0.13 Hz, 95 to 99 percent of all cases (read from the %-of-cases axis) have 90 to 100 percent (black-shaded bars) of total energy in the primary mode. Note that this includes the unimodal cases, which identically have 100 percent of energy in the primary (only) mode. At the highest frequency, fewer than 20 percent of all cases have 90 to 100 percent of energy in the primary mode. At this same frequency, an additional 5 percent (or so) of all cases have 80 to 90 percent of energy in the primary mode, a further 7 percent (or so) of all cases have 70 to 80 percent

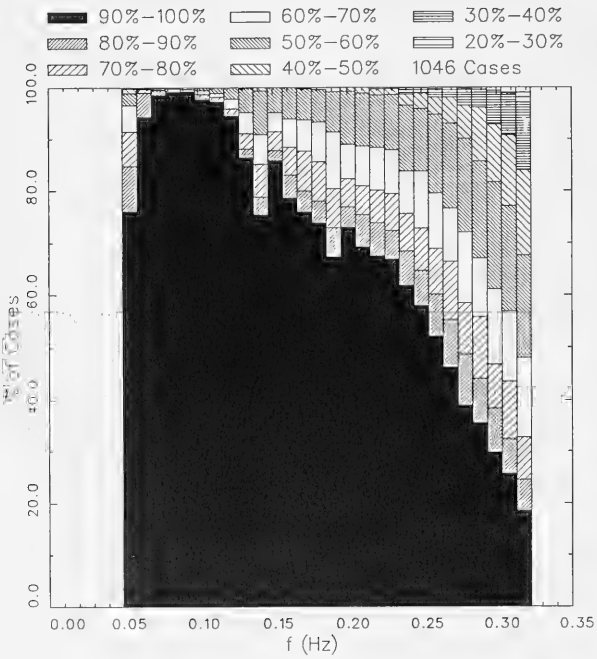


Figure 24. Frequency-by-frequency distribution of percent of energy contained in primary mode

of energy in the primary mode. The distribution is cumulative so that, for the highest frequency, one can see that about 32 percent of all cases (the top of bar with the broad diagonal shading which slopes upward from left to right) have between 70 and 100 percent of total energy in the primary mode.

211. Overall, it appears that roughly two-thirds of all directional distributions have 90 to 100 percent of energy (the ratio of black-shaded area to total area in Figure 24 as a whole) in the primary mode. This means that the remaining one-third of cases, primarily at the higher frequencies, have significant energy in secondary modes. In response to the question initiated by the results given in Figure 23, the answer is that a significant fraction of distributions are multimodal and that secondary modes are commonly as energetic as primary modes. Hence, modal structure must be considered important in natural directional distributions (at this site, at least).

212. Some of the multimodality can be discounted as being caused by low signal-to-noise ratio and large pressure response function. These conditions occur most often at the higher frequencies. Energy at these frequencies is typically low relative to the spectral peak (e.g., the frequency spectra in Figures 5 and 7) so that, if there is roughly the same amount of noise at all frequencies in the system, the signal-to-noise ratio will be low at the higher frequencies. The pressure response function (which converts pressure to sea-surface displacement via linear wave theory) for a frequency of 0.32 Hz in 8 m of water is about 13. Any noise at this frequency also is amplified by a factor of 13. These effects can degrade the cross-spectral estimates from which the directional distributions are computed. The results can be noisy distributions which might be interpreted as multimodal when, in fact, they are just not known very well.

213. However, at intermediate frequencies (0.15 to 0.20 Hz, say) there is typically greater energy (see the frequency spectra in Figures 5, 6, and 7), and the pressure response function is only about 2 for 8 m of water. In this case, the effects of noise should be far less. Figure 23 indicates that there is still significant bimodality (20 to 40 percent) at these frequencies, and Figure 24 shows that more than 20 percent of all cases at these frequencies have at least 30 percent of total energy in the secondary mode. Hence, the conclusion remains that multimodal distributions are an important feature of wave directionality at the present experiment site.

## PART VIII: PEAK DIRECTION AND SPREAD AT THE FREQUENCY LEVEL

214. Of interest in directional analysis at the frequency-by-frequency level are the peak direction and directional spread. This section considers the distributions of peak direction $\theta_{p,n}$ and directional spread $\Delta\theta_n$ (from Equation 17) for each of the 28 frequencies $f_n$ in the observed frequency-direction spectra. In light of the modality discussion above, the distributions are done both for all (1,046) cases and for just unimodal cases (number varies with frequency). The distinction is made to see if multimodality has any effect on distributions of these parameters. Of particular interest is directional spread which, at the frequency level, is based on an integral across all modes in a directional distribution.

### Peak Direction

215. Figure 25 contains distributions of peak direction $\theta_{p,n}$ for the case where all data are considered, and one distribution is computed for each frequency. In Figure 25, frequency and number of cases are noted in the upper right corner of each subplot. The lowest frequency is in the upper left subplot. Frequency increases across, then down the page. Note that the scale for the percent of cases is different for the top row of subplots.

216. Figure 25 shows that the low-frequency distributions (top row) all have peak directions ranging from about shore-normal (0 deg) to slightly south of shore-normal (about -20 deg), consistent with the refraction arguments given earlier for long waves originating in the open, deep Atlantic. As frequency increases, the distributions become wider, suggesting a reduced effect of refraction and an increase in dominance of other wave processes and local wind as wave generating and transforming mechanisms. At high frequencies (bottom row), peak directions range from about 70 to -80 deg, almost across the whole horizon.

217. When directional distributions identified as multimodal are removed, the set of distributions of peak direction become those shown in Figure 26. Since most of the low-frequency distributions are unimodal (from Figure 23), the results are little changed from Figure 25 for these frequencies. In fact, little significant change is seen at all except at the highest frequencies (bottom row). In these cases, the number of samples has dropped

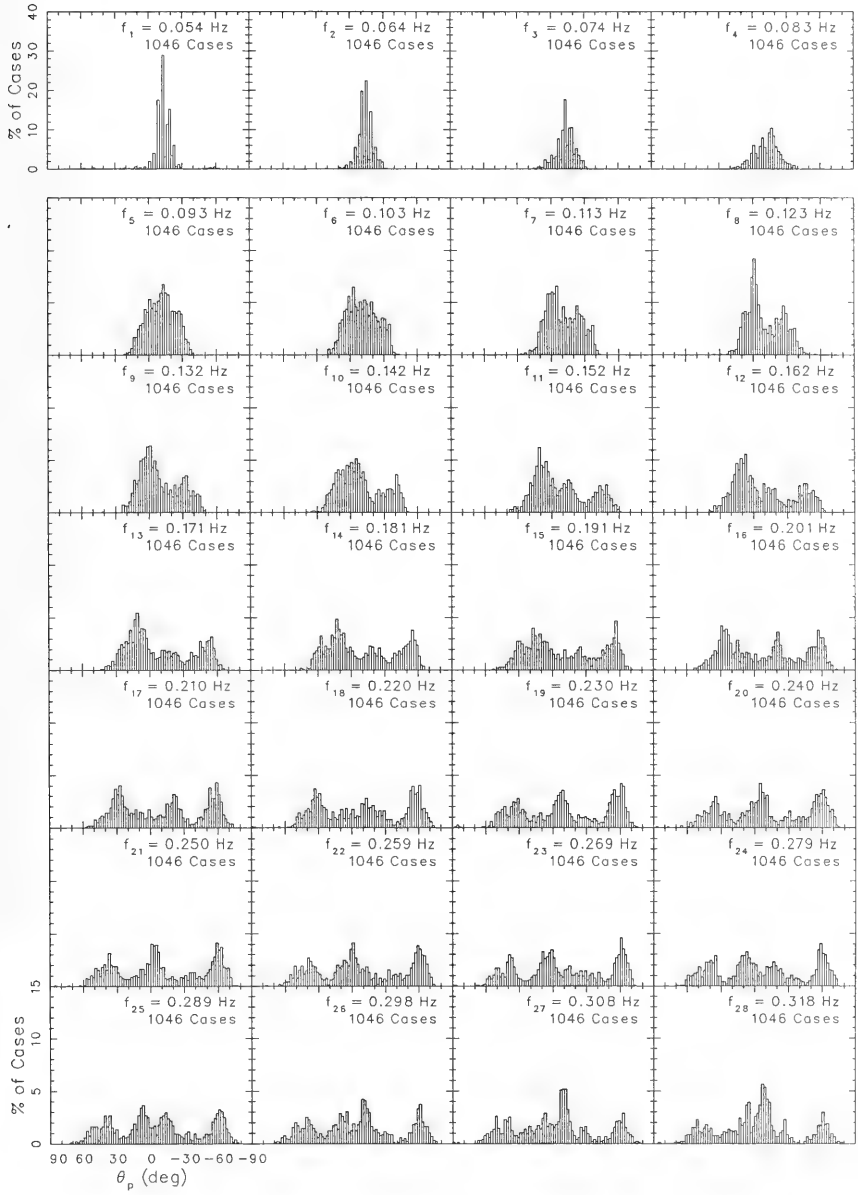


Figure 25. Frequency-by-frequency distributions of peak direction using all data

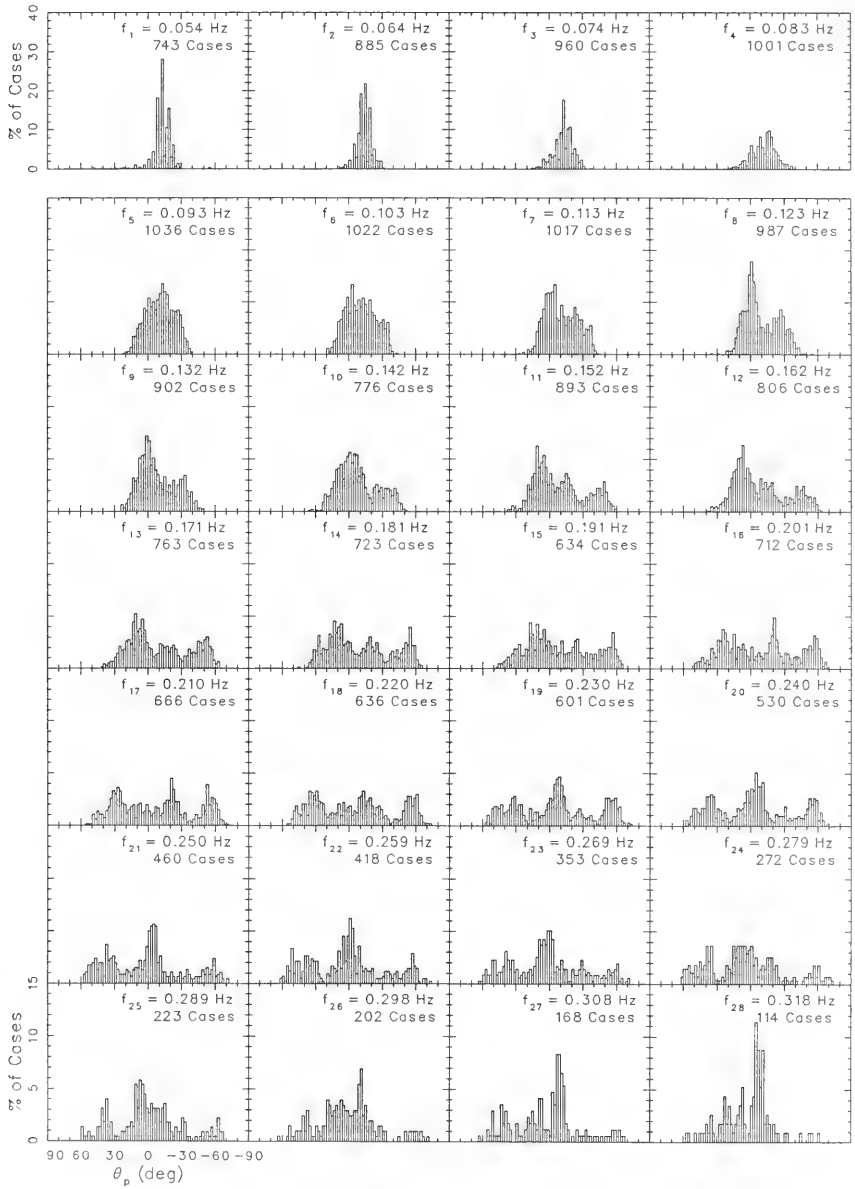


Figure 26. Frequency-by-frequency distributions of peak direction using only unimodal data

significantly since there are few unimodal directional distributions at high frequencies (see Figure 23). Compared to Figure 25, it appears that the tendency is for unimodal, high-frequency directional distributions to have peaks more nearly around the shore-normal direction. Overall, however, the differences between Figures 25 and 26 are slight.

## Directional Spread

218. Figure 27 shows the distribution of directional spreads $\Delta\theta_n$ where all data are considered. A distribution of $\Delta\theta$ is given for each frequency which is identified through the subscript n . The interest here is how these distributions compare to each other and to the distribution of bulk spread parameter shown in Figure 16. At the low frequencies (except the lowest) in Figure 27, the range of spreads is from about 15 to 50 deg. The peaks of the spread distributions at low frequencies is in the range 25 to 30 deg. As frequency increases, the range of spreads increases and the peaks in the distributions shift to greater values. At the highest frequencies (bottom row), spreads range from about 5 deg to 90 deg and peaks in the distributions are in the region 40 to 45 deg.

219. Compared to the bulk results of Figure 16, where the range was 20 to 60 deg and the peak was at 40 deg, it is seen that low frequencies have a narrower range with lower peak values. Higher frequencies have a wider range with slightly higher peak values. In composite, which results in the bulk spread estimates, the ranges and peaks are averaged (by integrating the frequency-direction spectrum with respect to frequency) so that the net result falls between the extremes. At none of the frequencies are the distributions exceptionally different from the bulk result; that is, all spread distributions are single-peaked, most of the cases fall in the range 20 to 60 deg, and most probable spread angles are in the range 25 to 45 deg.

220. It is noted that here, again, there are very few cases with very small directional spreads. Thus, these wave fields are far from unidirectional, a result consistent with the bulk representation. In the high frequencies at the bottom part of Figure 27, there is a tendency for an increase in the incidence of very broad spreads, with a significant number exceeding 60 deg at the highest frequencies. These large spreads are likely

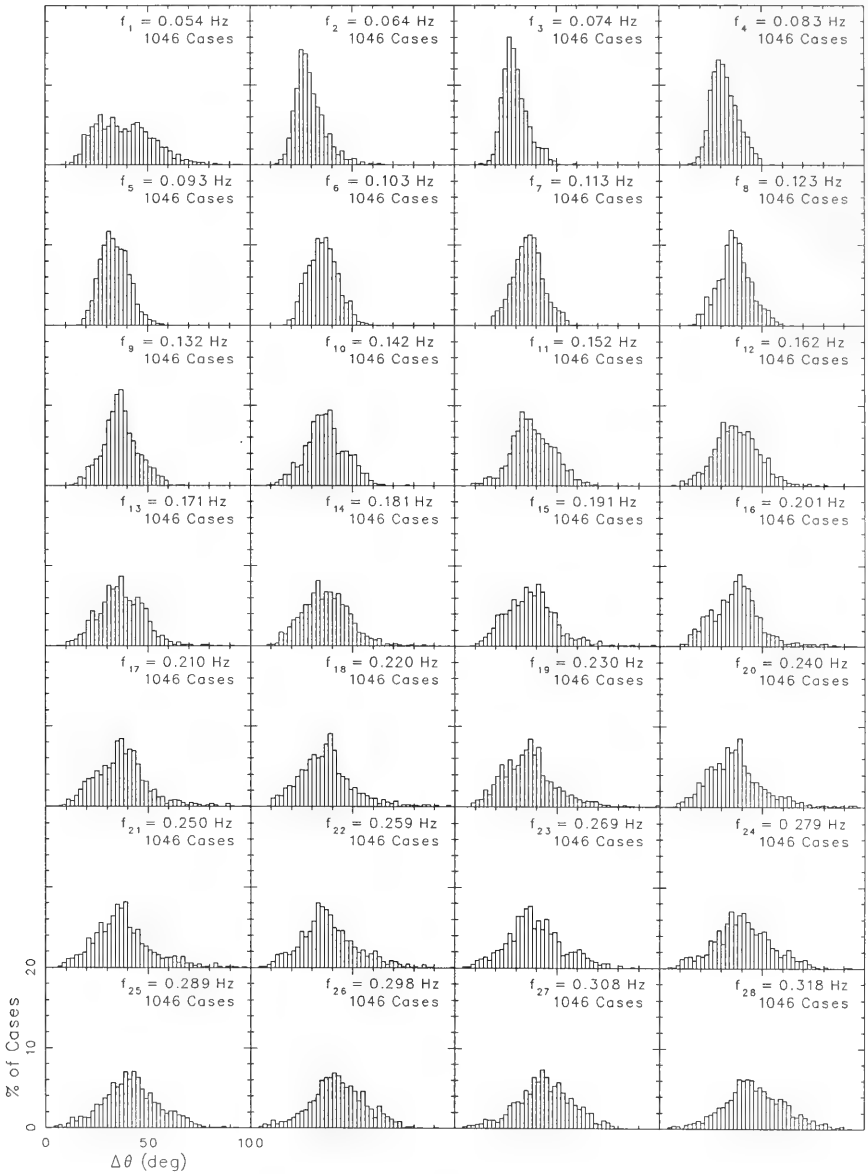


Figure 27. Frequency-by-frequency distributions of directional spread using all data

due to multimodal directional distributions where modes are widely separated. This condition causes $\Delta\theta_n$ to become quite large.

221. If the data are restricted to unimodal cases, the incidence of broad spreads is reduced, as evidenced in Figure 28. Most of the directional distributions are unimodal at the low frequencies (Figure 23) so the spread distributions are little changed. At high frequencies, however, the effect of eliminating multimodal distributions is to cause spread distributions to become more like those at middle frequencies. The range of spreads is from about 10 to 60 deg, and peaks in the distributions are in the range from about 35 to 40 deg.

222. In summary, Figures 25 to 28 indicate that low-frequency wind waves tend to arrive from the shore normal to slightly south of shore-normal directions, and their directional distributions tend to be slightly narrower than the bulk results of Figure 16. Ranges of peak direction and directional spread tend to increase with increasing frequency. High-frequency wind waves tend to arrive from anywhere on the (180-deg) horizon and, for full 180-deg directional distributions, can have a characteristic spread of energy up to 90 deg. Wave fields with unimodal directional distributions tend to display a similar behavior in peak direction but a more uniform behavior of directional spreads from frequency to frequency. Unidirectional wave fields are extremely rare (in this data set) at any wind wave frequency. Overall, the directional spread properties at each frequency, especially in the unimodal cases, is not very different from the bulk properties shown in Figure 16.

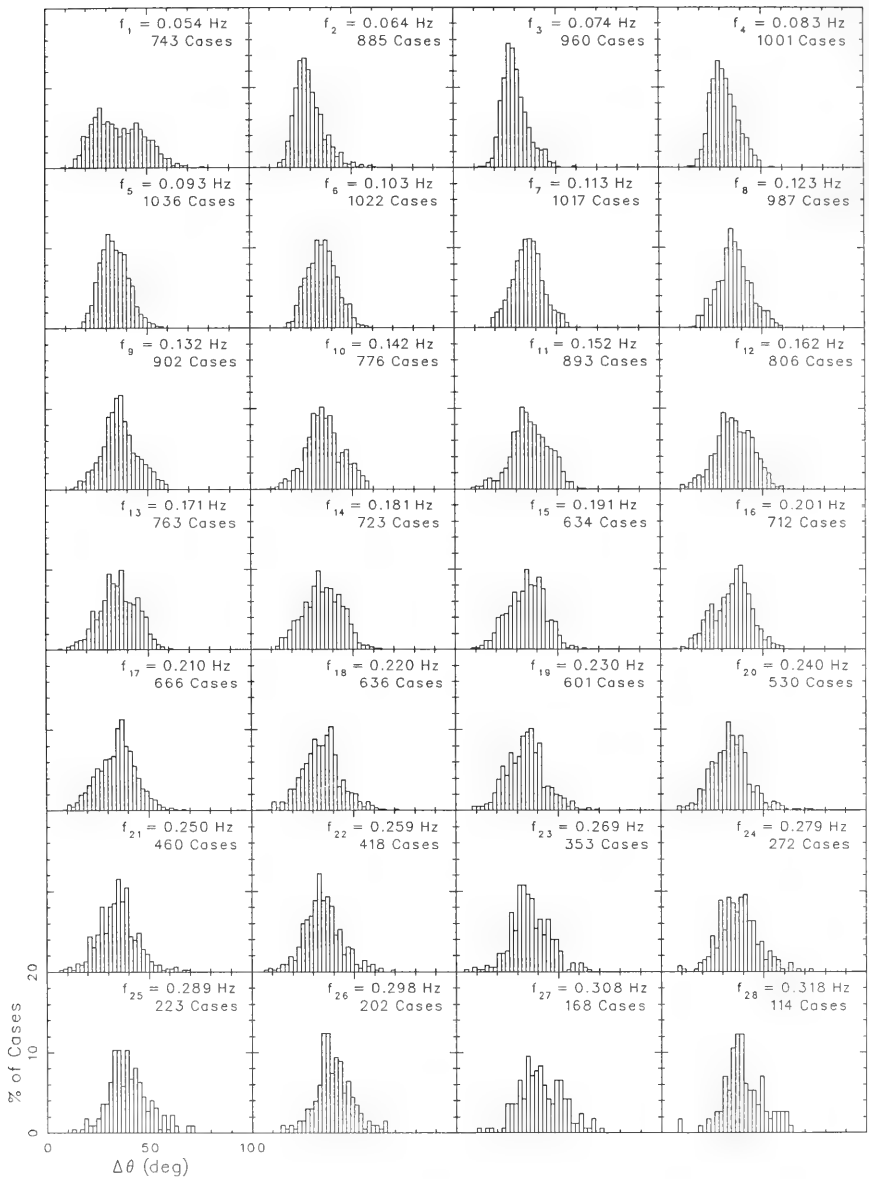


Figure 28. Frequency-by-frequency distributions of directional spread using only unimodal data

## PART IX: SHAPES OF DIRECTIONAL DISTRIBUTIONS

223. Up to this point, the directional characteristics of the present observation set have been described with parameters derived from the frequency-direction energy distributions. Of paramount importance are the shapes of the distributions themselves. These are required for accurate definitions in physical and numerical models. They are also critical for the advancement of wave theory, which must account for observed distribution shapes if such shapes are different from what has been proposed in the past. Furthermore, if observed frequency-direction spectra can be characterized by a simple class of functions, then these functions can be used as elementary building blocks to construct or characterize any, even the most complex, observed sea states.

### Data Reduction

224. This section describes a basic first examination of the shapes of naturally occurring directional distribution functions. A rational first assumption is that the observed distributions identified as unimodal represent the most basic units of directional structure. It can be assumed, then, that multimodal distributions are simply a collection of superimposed unimodal distributions having different energy level and directional positioning parameters. Hence, attention is focused on the shapes of unimodal distributions.

225. The data examined are the set of directional distribution functions $D(f_n,\theta_m)$ defined by Equation 13. Since these are the frequency-direction spectral densities $S(f_n,\theta_m)$ divided by the frequency spectral densities $S(f_n)$, the first step in data reduction has taken place. That is, the effect of variable total energy has been removed. Since the normalization is unique at each frequency, the resulting distributions must be considered on a frequency-by-frequency basis, at least initially. The potential data set consists of 1,046 directional distributions for each of 28 frequencies.

226. The number of cases is reduced by requiring acceptable distributions to be unimodal. This results in a different number of samples at each frequency, as indicated in Figure 23. For instance, almost all the

distributions at frequencies near 0.10 Hz survive this decimation, but only about 10 percent of the highest frequency cases are retained.

227. In an initial attempt to classify the distributions, the directional spread parameter $\Delta\theta_n$ alone was used. Classification was done for each frequency $f_n$ separately. This approach would result in the simplest possible classification in that the directional distributions could all be defined by specifying a single parameter, directional spread. Determining the adequacy of this approach is important because at least two investigations of directional distribution have characterized results with a single parameter. Mitsuyasu et al. (1975) used the function proposed by Longuet-Higgins, Cartwright, and Smith (1963) of the form

$$D(f,\theta) = G(s)\ |\cos\tfrac{1}{2}(\theta - \theta_o)|^{2s} \tag{31}$$

where $s$ is the single parameter (which can vary with $f$), $\theta_o$ is the distribution peak direction, and $G(s)$ is a coefficient given by

$$G(s) = \frac{2^{2s}}{360\ \text{deg}}\ \frac{\Gamma^2(s+1)}{\Gamma(2s+1)} \tag{32}$$

where $\Gamma$ is the gamma function (see Abramowitz and Stegun 1970). The coefficient $G(s)$ satisfies requirement of unit area under $D(f,\theta)$. The definition given here differs slightly from that given by Mitsuyasu et al. (1975) in that it has been converted to units of $\text{deg}^{-1}$ to conform to the system of units used in this report. Their definition is in units of $\text{radians}^{-1}$. Donelan, Hamilton, and Hui (1985) proposed a function of the form

$$D(f,\theta) \propto \text{sech}^2[\beta(\theta - \theta_o)] \tag{33}$$

The free parameter in this function is $\beta$ which may depend on frequency. A coefficient is needed on the right side of Equation 33 to give unit area under $D(f,\theta)$. Each of these models is a function, symmetric about $\theta_o$, which depends on a single parameter. It would be most fortunate if the data in the present set fit one of these models.

228. To test this hypothesis, data were grouped by 2-deg increments of $\Delta\theta_n$, shifted along the direction axis by the angle $\bar{\theta}_n$, and averaged.

This provided a composite mean (and standard deviation) distribution for the spread class and frequency considered. The angle $\overline{\theta}_n$ is defined by Equation 19. It has the important property that it aligns the directions bounding the central half of the energy in each distribution rather than the distribution peaks. Since it is an integral property (relying on all data in a distribution), it is more stable than a single point (the peak value) in a distribution. Variations of the peaks or tails of the distributions will become obvious in the composite distribution, the test of adequacy of the classification scheme.

229. For distributions with small spreads, the scheme works reasonably well, as illustrated in Figure 29, which represents a composition of data with frequency 0.054 Hz and directional spread in the range 20 to 22 deg. Figure 29a shows the mean (solid line) plus and minus one standard deviation (dashed lines) of the set of 29 cases with distributions shown in the spaghetti plot of Figure 29b. The composite is well defined, is reasonably symmetric, has no severe outlier points in Figure 29b; and the standard deviation varies, at most, by about 10 percent of the distribution maximum.

230. However, with intermediate and high directional spreads, it becomes evident that the distributions do not collapse well to a single representative composite. This is illustrated in Figure 30, which shows the data from 80 cases at frequency 0.103 Hz and directional spread in the range 40 to 42 deg. Mean and standard deviation curves are shown in Figure 30a. Here, the standard deviation shows significant fluctuations in the vicinity of the composite peak. The most obvious discrepancy is that the distribution peaks in Figure 30b do not coincide but rather scatter as much as 30 deg on either side of the central direction (0 deg). Since all samples have been aligned at the directional spread boundaries, the differences must be that the distributions are asymmetric.

231. This result suggests that a more refined classification of the distributions is necessary. The additional parameter chosen for this was the asymmetry parameter $A_n$ defined by Equation 18. It gives an indication of how rapidly a distribution rises on one side relative to the other. The data were regrouped within classes of directional spread $\Delta\theta_n$, asymmetry $A_n$, and averaged as before. This was done separately for data from each frequency $f_n$.

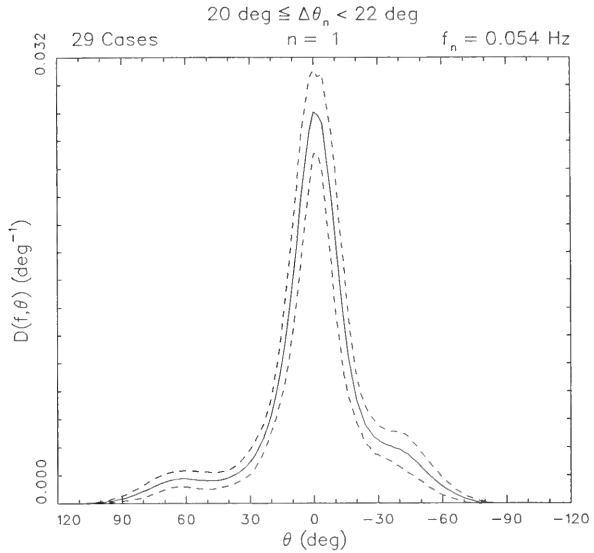


a. Mean (solid line) plus and minus one standard deviation (dashed lines)

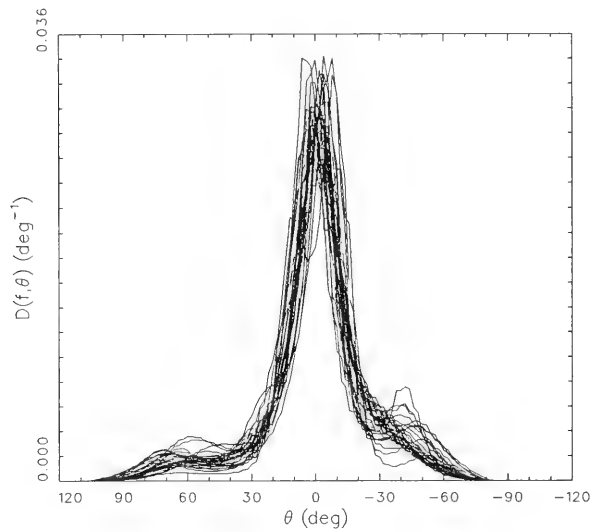


b. Contributing curves

Figure 29. Composite directional distribution for a case with narrow spread

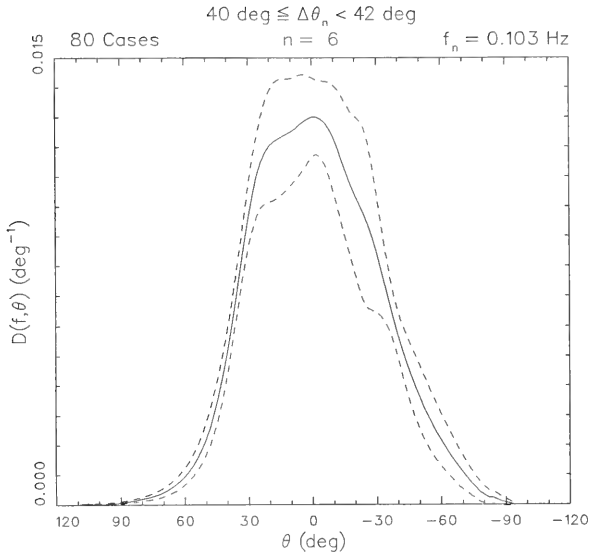


a. Mean (solid line) plus and minus one standard deviation (dashed lines)

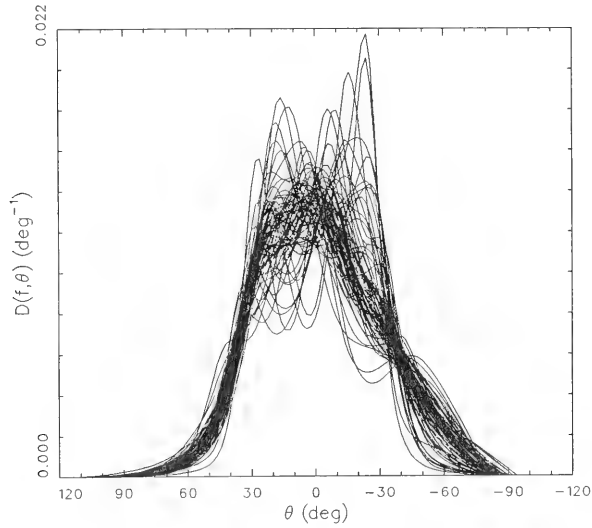


b. Contributing curves

Figure 30. Composite directional distribution for a case with intermediate spread

232. A typical $\Delta\theta_n$ , $A_n$ grouping is shown in Figure 31, which shows the composition means (solid lines) plus and minus one standard deviation (dashed lines) for data with $\Delta\theta_n$ in the range 38 to 42 deg and $A_n$ in the range −0.69 to −0.36 for each of the 28 frequencies. To obtain more samples in each class, the width of the directional-spread classes was increased from 2 to 4 deg. The odd limits on the asymmetry class arise because data were grouped in even increments of the exponent function of $A_n$ . In this case, $0.5 < \exp(A_n) < 0.7$ . Frequency and number of cases in each composite are shown in the upper-right corner of each subplot. Subplots with no curves have fewer than two cases (for which no standard deviation could be computed).

233. The most interesting aspect of Figure 31 is that the distributions appear to be about the same for all frequencies when classified by just the two parameters $\Delta\theta_n$ and $A_n$ . All rise sharply on the left and decay slowly with a minor lobe of energy on the right. This result suggests that directional distributions can occur with similar shapes at all frequencies. The same behavior was observed in graphs (not shown here) of composite distributions for all classes of directional spread and asymmetry. This means that composite shapes can be constructed using data from all frequencies. Classification is then only by directional spread and asymmetry (two parameters), and not by frequency.

234. Figure 31 also shows that there is more scatter (larger standard deviations) in the results for the highest frequencies, partly because there are fewer cases at these frequencies. The scatter may also be due to noise which becomes important at low wave energy. As discussed in Part VII, low signal-to-noise ratios lead to a degradation of directional spectral estimates. To ensure that reasonably large-signal data were used in subsequent composites, the set of distributions was further decimated by requiring frequency spectral density to be well above signals associated with limits of instrument accuracy and signal discretization. Both of these were approximately the equivalent of 0.005 m of water in a static water column. A value of twice this, 0.01 m, was used to distinguish low-energy signals. This cutoff squared times the frequency-dependent pressure response function and divided by the resolution bandwidth df (= 0.00977 Hz) provided the value of $S(f_n)$ below which data were excluded. At the lowest frequency, data with $S(f_1) < 0.01$ $m^2/Hz$ were excluded. At the highest frequency, this increased to the exclusion of data with $S(f_{28}) < 1.73$ $m^2/Hz$. Of the total 29,288

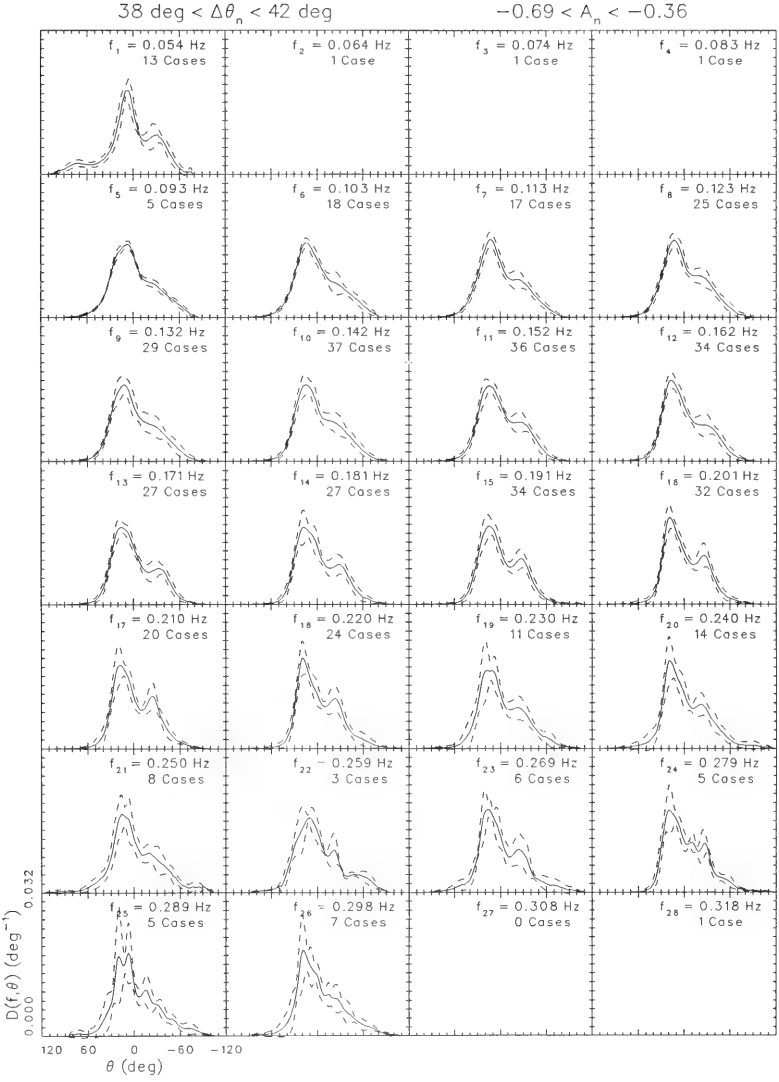


Figure 31. Frequency-by-frequency composite distributions showing mean (solid line) plus and minus one standard deviation (dashed lines) for given ranges of spread and asymmetry

directional distributions available (1,046 frequency-direction spectra multiplied by 28 frequencies per spectrum), only about half (14,218 distributions) remained after this discrimination procedure. However, some assurance was obtained that noisy (low-resolution) data were eliminated, and some compensation was gained by being able to group data from all frequencies.

235. Directional distributions were grouped a third time and composite curves constructed. Thirteen classes of directional spread parameter $\Delta\theta$ were used, ranging from 10 to 62 deg in 4-deg arcs. The frequency subscript n is dropped because samples from all frequencies are grouped together. Twelve classes of asymmetry were used. Because of the way asymmetry is defined in Equation 18, a distribution with one value of asymmetry which is positive should be the mirror image of a distribution with the same magnitude of asymmetry but which is negative. Hence, the 12 asymmetry classes were in terms of the magnitude of asymmetry $|A|$, ranging from 0.0 to 1.2 in bands of 0.1. A distribution with negative asymmetry was reversed about the central (0-deg) direction after being shifted by the centering angle $\overline{\theta}$ and before being summed in the composite. All composite curves are thus computed as if they had positive asymmetry, but a count is kept of the number of positive and negative contributions.

## Resulting Shapes

236. Results are illustrated in Figures 32 to 44. One figure is shown for each of the 13 classes of directional spread. The total number of cases is 14,218. The largest number of cases contributing to any one class is 708 (in Figure 37, 30 deg $< \Delta\theta <$ 34 deg, for the class with lowest asymmetry, $0.0 < |A| < 0.1$). Classes with fewer than two cases are not graphed, as no standard deviation could be computed.

237. All classes are shown to illustrate the range of shapes discovered, the transition of shapes between spread and asymmetry classes, the nature of the structure which gives rise to asymmetric distributions, and, through the case counts, the relative importance of each class. Classes with the smallest asymmetries ($0.0 < |A| < 0.1$, in the upper-left subplot of each figure) have shapes most nearly like the symmetric models. This special subgroup is called the *symmetric class* of distributions. Asymmetry occurs in the remaining distributions as the result of a lobe of energy which appears to

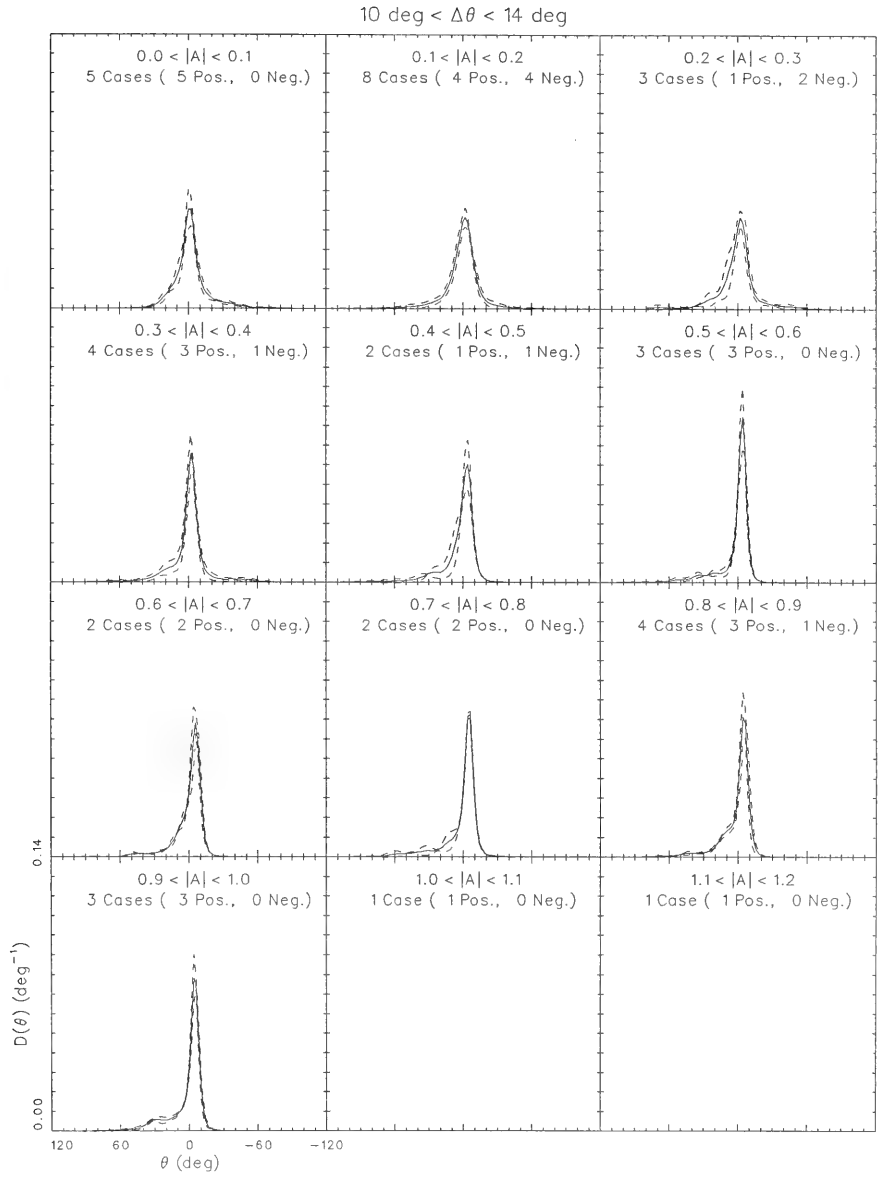


Figure 32. Composite directional distribution functions for spread parameter in the range 10 to 14 deg and for all asymmetry classes

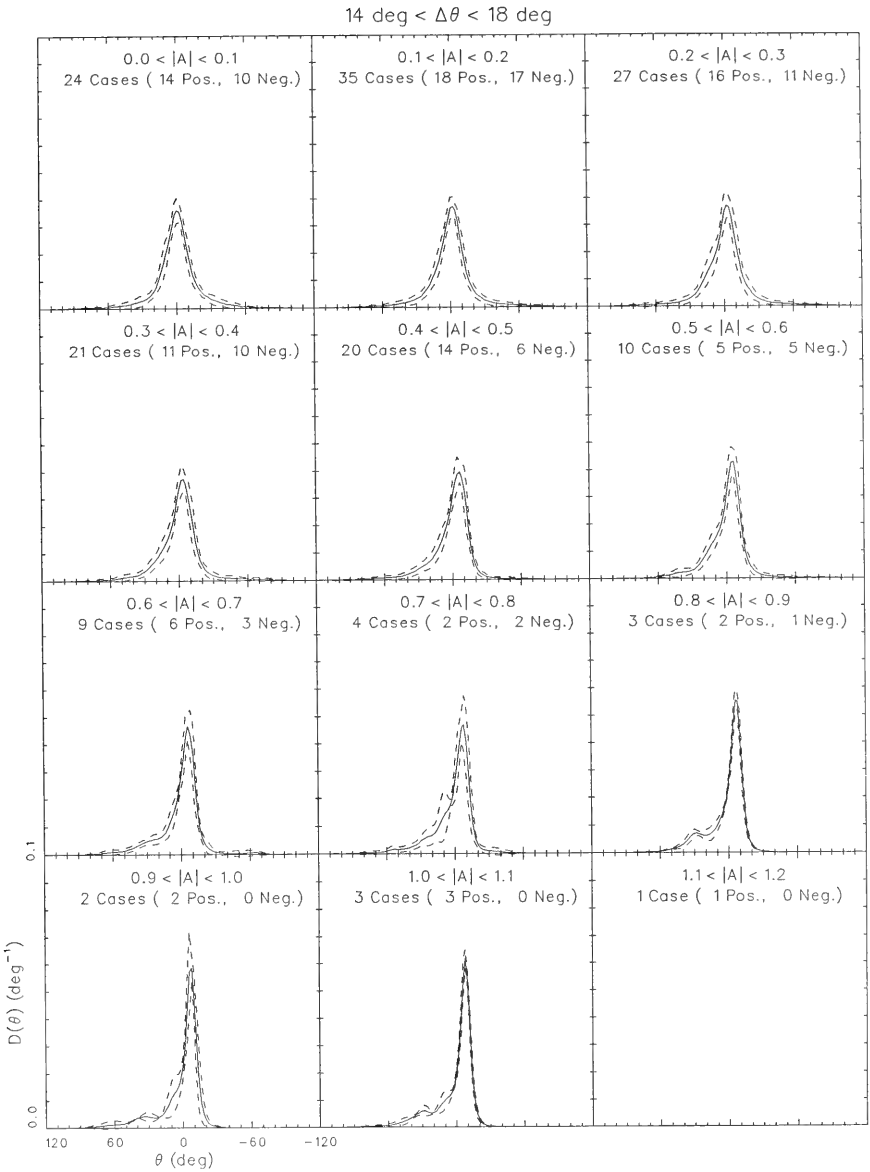


Figure 33. Composite directional distribution functions for spread parameter in the range 14 to 18 deg and for all asymmetry classes

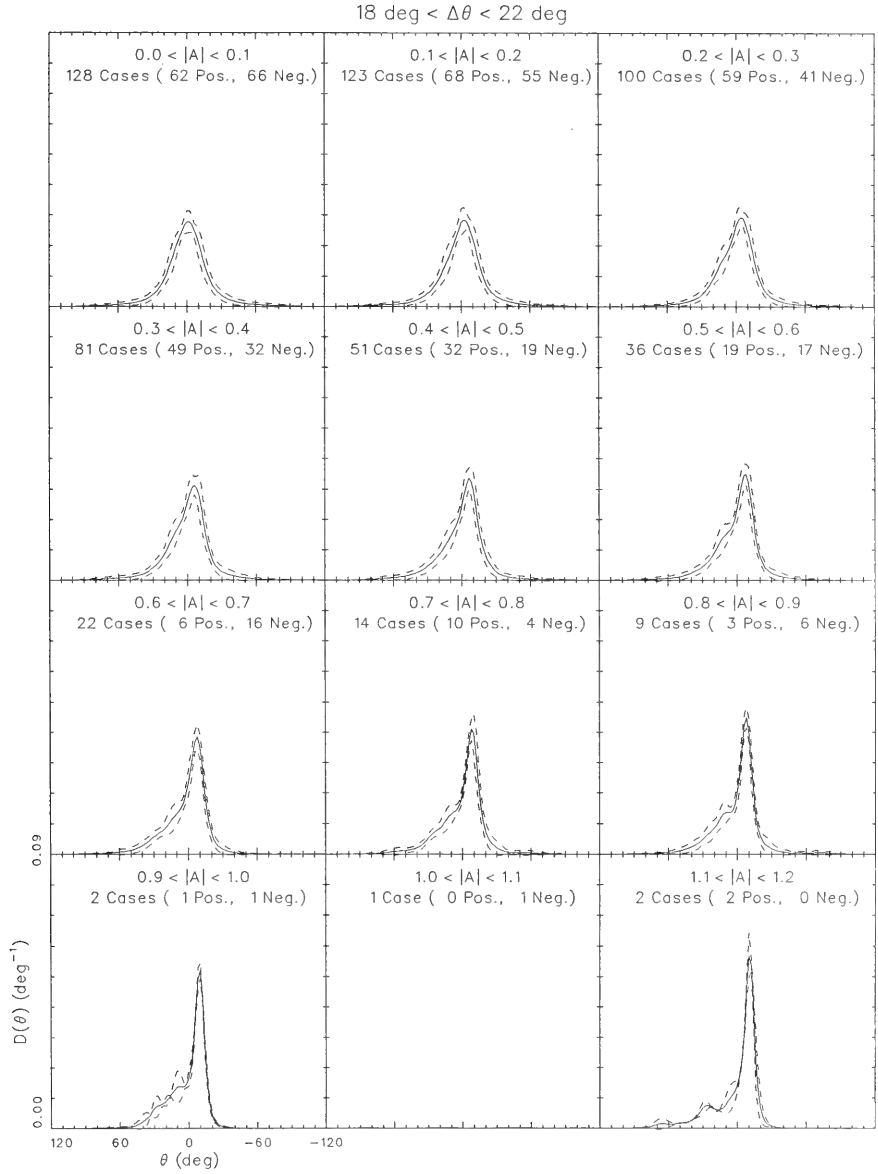


Figure 34. Composite directional distribution functions for spread parameter in the range 18 to 22 deg and for all asymmetry classes

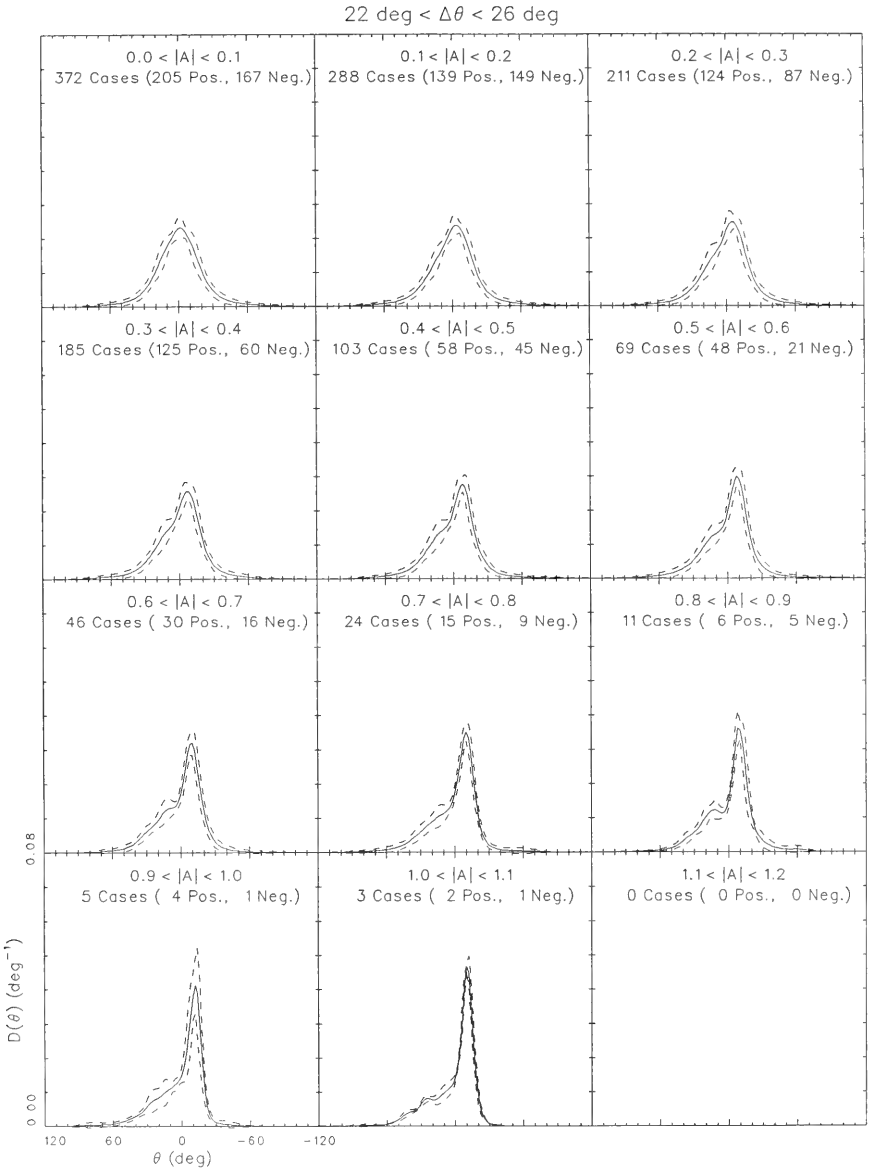


Figure 35. Composite directional distribution functions for spread parameter in the range 22 to 26 deg and for all asymmetry classes

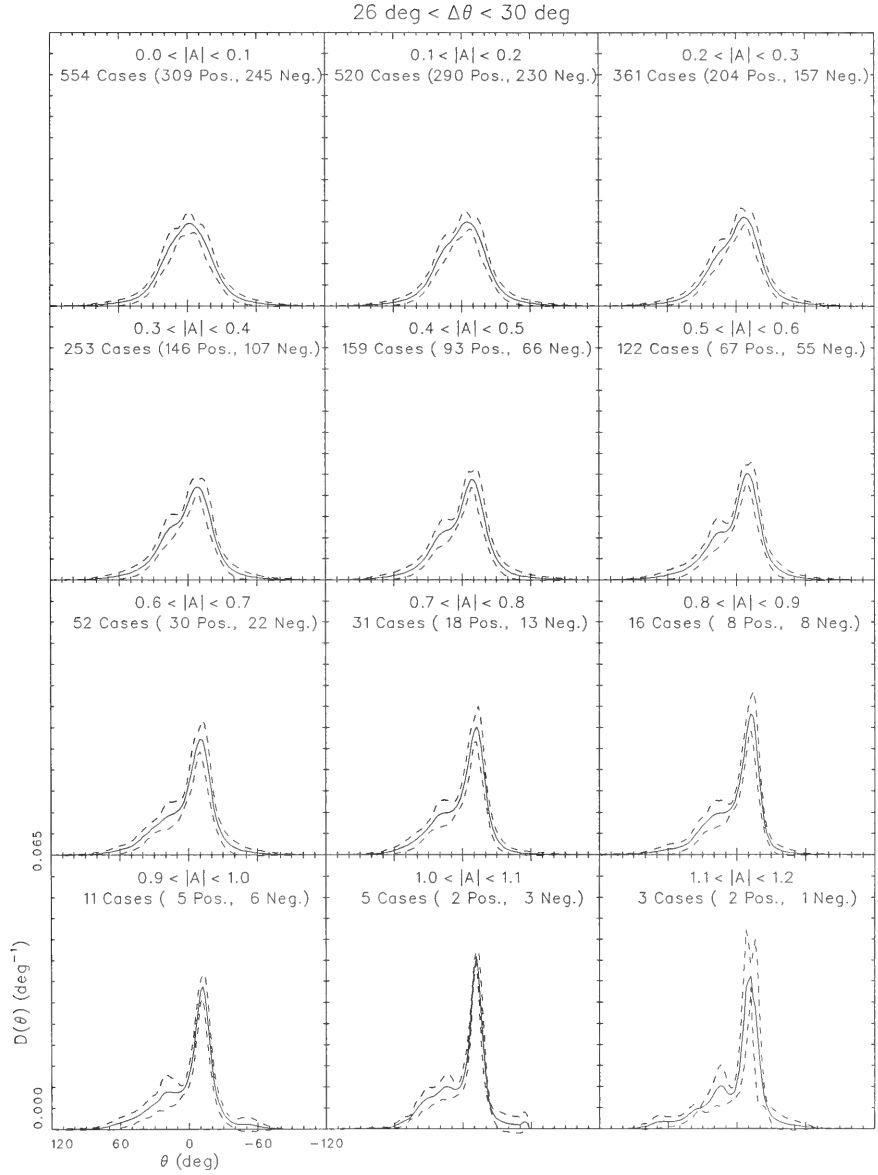


Figure 36. Composite directional distribution functions for spread parameter in the range 26 to 30 deg and for all asymmetry classes

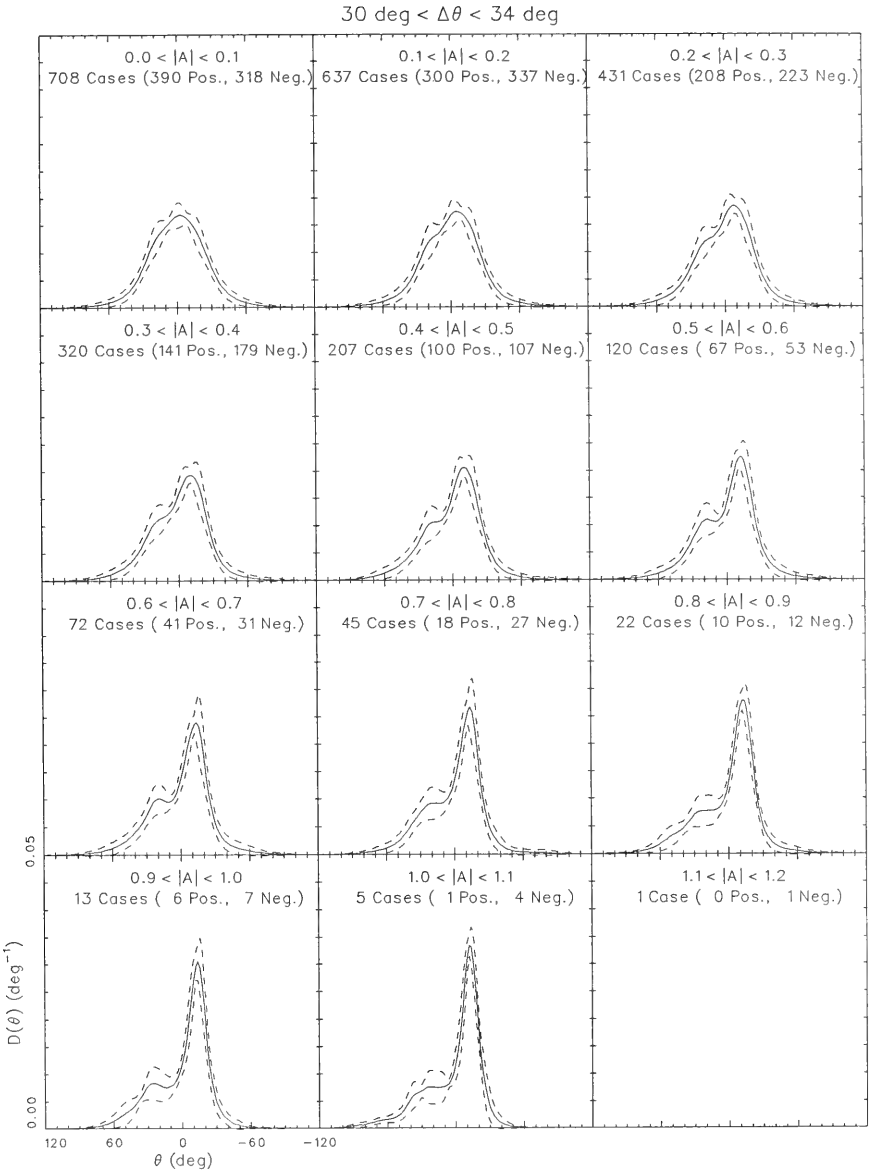


Figure 37. Composite directional distribution functions for spread parameter in the range 30 to 34 deg and for all asymmetry classes

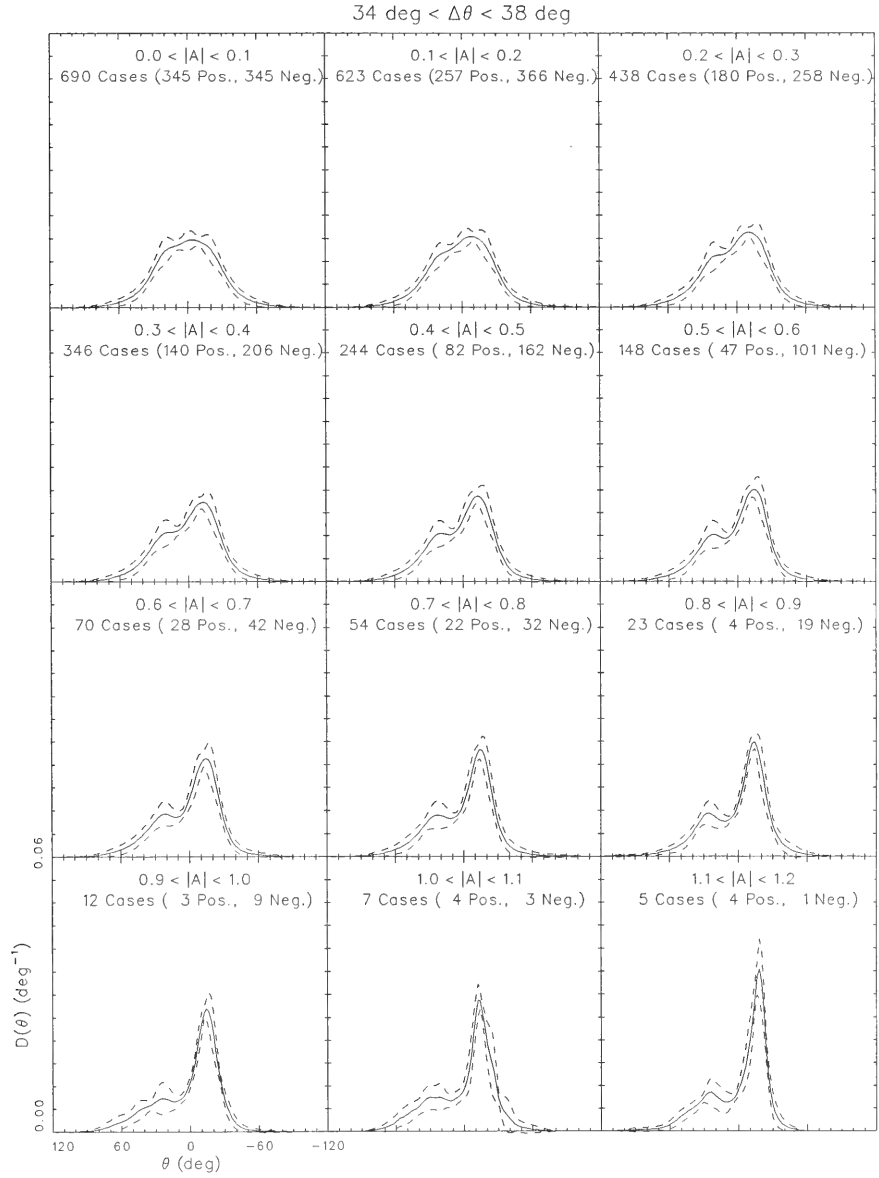


Figure 38. Composite directional distribution functions for spread parameter in the range 34 to 38 deg and for all asymmetry classes

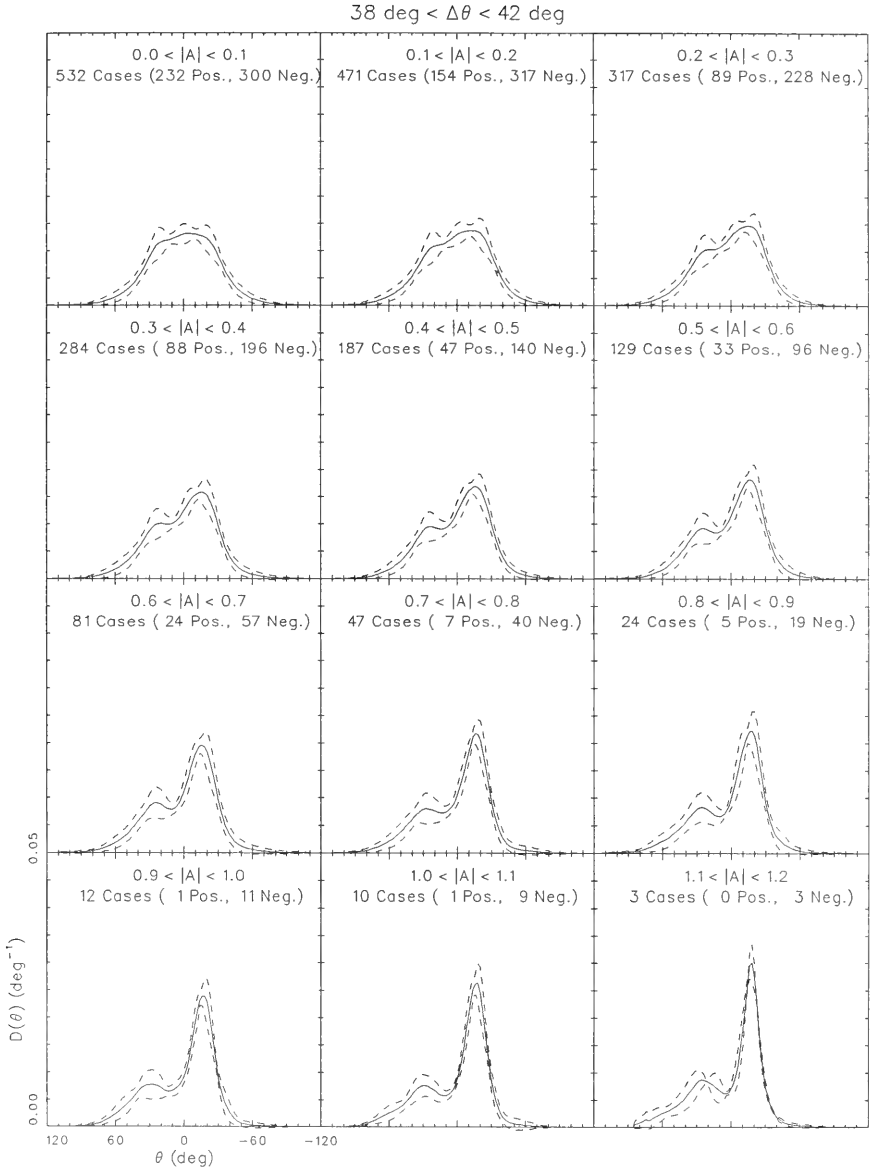


Figure 39. Composite directional distribution functions for spread parameter in the range 38 to 42 deg and for all asymmetry classes

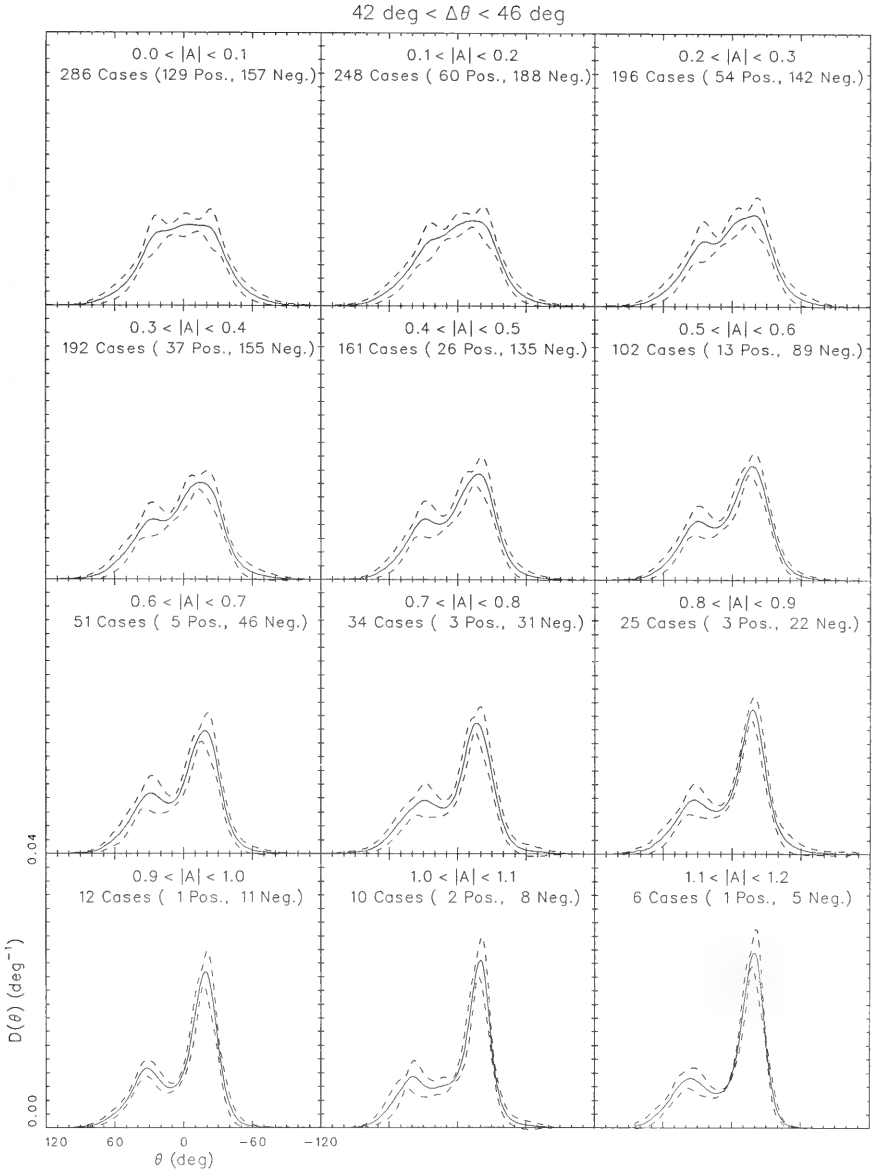


Figure 40. Composite directional distribution functions for spread parameter in the range 42 to 46 deg and for all asymmetry classes

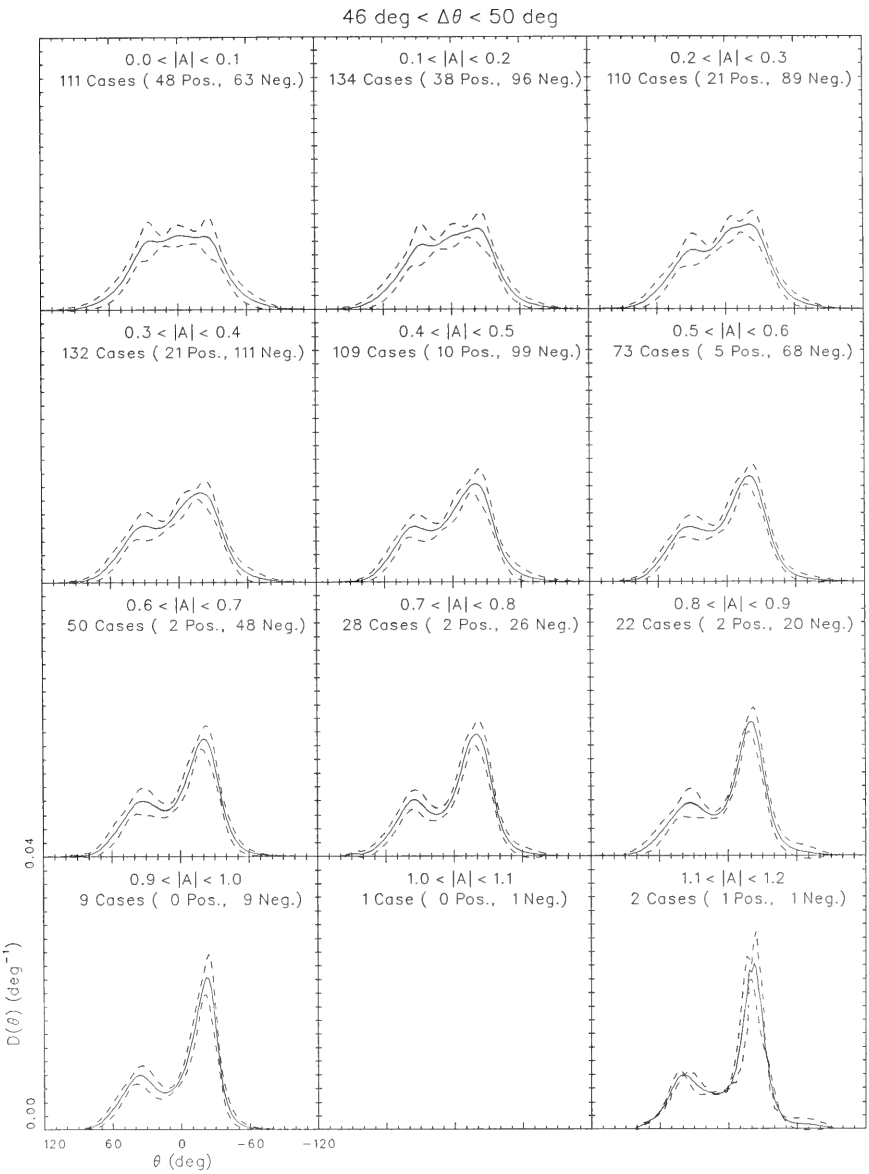


Figure 41. Composite directional distribution functions for spread parameter in the range 46 to 50 deg and for all asymmetry classes

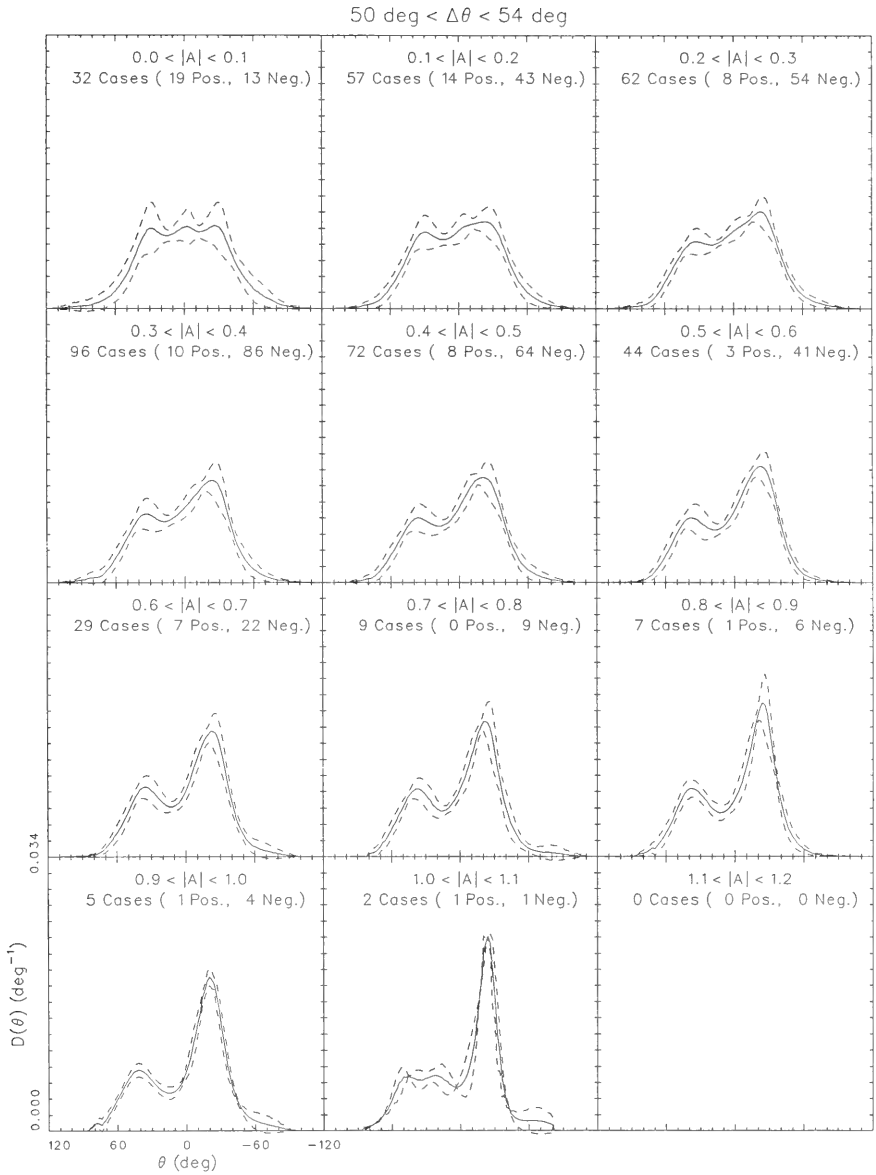


Figure 42. Composite directional distribution functions for spread parameter in the range 50 to 54 deg and for all asymmetry classes

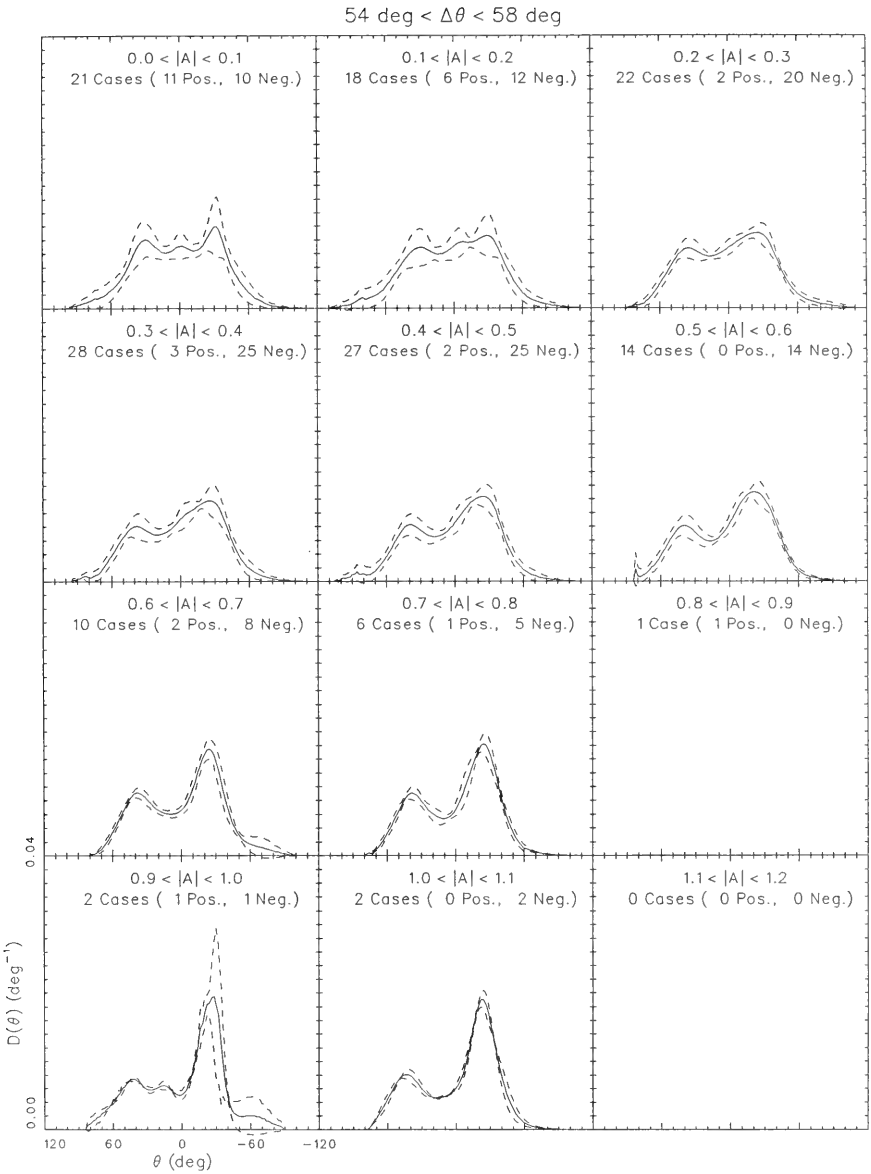


Figure 43. Composite directional distribution functions for spread parameter in the range 54 to 58 deg and for all asymmetry classes

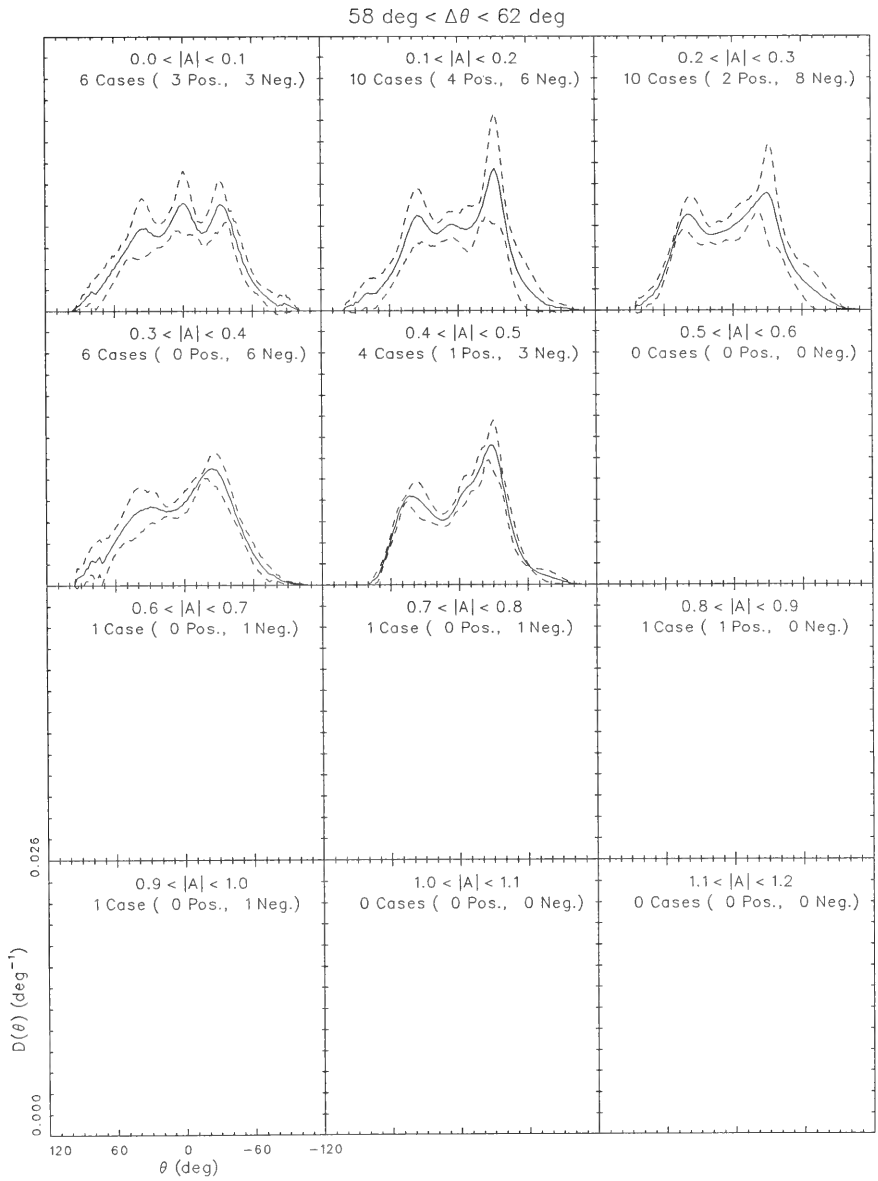


Figure 44. Composite directional distribution functions for spread parameter in the range 58 to 62 deg and for all asymmetry classes

one side of the distribution peak. As shown in Figures 32 to 44, it is on the left, but the negative contributions, reflected in these figures, have a lobe on the right. It is not pronounced in the two groups with smallest spread (Figures 32 and 33) because the arcs bounding the second and third quarters of the energy (the ratio of which leads to the asymmetry parameter) are very small. The effect of asymmetry in these two figures is visible as a more gradual decay of the distribution on the left side as compared to the right side.

238. This effect becomes slightly more pronounced in the next two spread groups (Figures 34 and 35), especially at higher asymmetries (bottom two rows of each figure). Here, there is a suggestion of a distinct change in the decay rates to the left of the distribution peaks. A better-defined lobe of energy becomes apparent throughout the next four spread groups (Figures 36, 37, 38, and 39). Seen as a small secondary maximum in the distributions, it is strongest at high asymmetries. It becomes more pronounced at lower asymmetries as spread increases (i.e., in the sequential progression from Figure 36 to 39). As a group, this set of four figures represents the most common directional distributions. Based on case count, about 66 percent of the low-noise, unimodal distributions are represented in these figures. The range of spread parameter included in this set is 26 deg $< \Delta\theta <$ 42 deg , consistent with the peak in distribution of spread parameter found in Parts VI and VIII. Figures 36 to 39 illustrate that asymmetry, as a subdivision beyond spread, is an important classifier of directional distributions.

239. In the next two spread-parameter groups (Figures 40 and 41), the side lobe becomes even more pronounced. It appears in the lowest-asymmetry class (upper-left subplot) as a distinct increase in curvature at the shoulders of the distribution curves. It also becomes apparent that asymmetry cannot be ignored. If, in the interest of modeling, the symmetric distribution (upper-left subplot) is forced to represent the remainder of the classes in each of the two groups shown in Figures 40 and 41, two important errors occur. First, if the symmetric distribution is centered at the peaks of the remaining distributions, the overall energy distribution would be shifted by about 20 deg. This is a typical angular difference between the middle of the energy distributions (0 deg in the plots) and the distribution peaks. This angle is about the same size as one direction bin used in much of the Wave Information Study (WIS) results (Ragsdale 1983). A shift in energy direction

by this amount could have a significant influence on any subsequent engineering study. Second, energy levels and directional locations are very different as asymmetry increases. Energy density is more than twice as high at the peaks of the most asymmetric classes (lower-right subplots) than it is at the peak of the symmetric class (upper-left subplot) at the same spread. Though the two groups represented by Figures 40 and 41 include only about 3.3 percent of the data (based on case count), the same types of behavior are evident in the most common groups shown in Figures 36, 37, 38, and 39.

240. The groups with the greatest spread (Figures 42, 43, and 44) show a continuation of the trends just described. They are relatively uncommon, representing only about 1.2 percent of all cases, but they do suggest the large-spread asymptotes of directional shapes. Here, the extreme shift in peak direction is about 30 deg relative to center-of-energy direction (Figgure 44). The symmetric members of this group are characterized by broad, relatively flat peaks in the directional distributions; that is, the energy density is nearly uniform over a span ranging from about 60 deg in Figure 42 to about 80 deg in Figure 44.

241. This property illustrates a problem in trying to characterize distributions with a parameter denoting peak direction. Compared with the narrow distributions (Figures 32, 33, and 34, for example) which have well-defined peak directions, the broad, symmetric distributions of Figures 42, 43, and 44 have rather diffuse peaks. In two of these cases (Figures 42 and 43), peak directions deduced from the solid lines occur on distibution shoulders. This shifts the angle which might be called peak direction by 30 to 40 deg from the center of the energy distributions (0 deg on the $\theta$-axis). Such curves are much less ambiguously characterized by integral measures of energy distribution such as the derived parameters $\Delta\theta$ , A , and $\bar{\theta}$ used in this report.

242. There is natural concern that the distributions classified here as asymmetric are not common, but occur so rarely that they may be ignored in practical application. If this was true, only the symmetric curves would need to be considered, and the bulk of data could be characterized with directional spread alone. Based on the case counts, this does not appear to be true. Symmetric distributions (as defined here) occur in only about 24 percent of all cases and in about 26 percent of the most common cases (Figures 36, 37, 38, and 39). If the first nonsymmetric classes are added to the symmetric

classes as being nearly symmetric, the fractions increase to about 47 percent for all cases and about 50 percent for the most common cases. This result means that at least half of the distributions have sufficient asymmetry that they cannot be ignored. Given the energy positioning and density errors that can occur by ignoring asymmetry, as discussed above, this suggests strongly that asymmetry should be included in modeling and engineering structural response studies.

Applicability of the Model of Longuet-Higgins, Cartwright, and Smith (1963)

243. The characteristic directional distribution functions shown in Figures 32 to 44 are in the form of empirical results. Ideally, these results would be fitted with analytic functions so they could be easily incorporated in process models and so that better interpolation could be done for more concise distribution definitions given specific spread and asymmetry parameters. While this has not yet been done, a subset of the results can be compared to an existing model for directional distributions. The subset consists of those classes identified as symmetric, i.e., those with $0.0 < |A| < 0.1$ (small asymmetry). As members of the low-asymmetry asymptote of the overall group of classes, their shapes depend only on one parameter, directional spread. These symmetric shapes can be compared to the one-parameter model proposed by Longuet-Higgins, Cartwright, and Smith (1963) and defined by Equations 31 and 32.

244. Figure 45 illustrates the shapes of several members of this class of function. In this model, directional spread is determined indirectly by the parameter $s$. As $s$ increases, the spread becomes smaller. Heights of the distribution peaks necessarily become larger with increasing $s$ to satisfy the constraint of unit area under the distribution. To see if this class of function can represent the present empirical observations, curves are fitted to the data in each spread class by varying the parameter $s$. Least square difference between curve and data is used as the fitting criterion.

245. Figure 46 illustrates the results of this fitting procedure. One subplot is shown for each of the 13 classes of directional spread. Data mean values are shown as solid circles spaced at 2-deg intervals. Variations of one standard deviation of the data about its mean values are shown as dashed

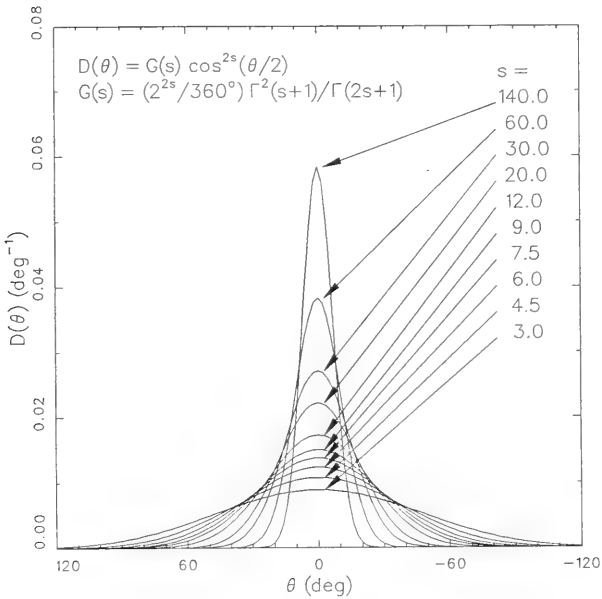


Figure 45. Examples of model directional distribution function proposed by Longuet-Higgins, Cartwright, and Smith (1963) for several values of parameter s

lines. Directional spread classification and value of fitted parameter s are listed in each subplot.

246. Examination of Figure 46 reveals that the model characterizes the data quite well for spread parameter in the range 22 deg $< \Delta\theta <$ 34 deg . At all spreads narrower than this, 10 deg $< \Delta\theta <$ 22 deg , the fitted curves might be considered reasonable. They underestimate the distribution peaks, by as much as about 10 percent for the narrowest class, and fall off faster than the distribution tails. Fitted curves could resolve the peaks better by restricting the set of fitted data to peak regions of the direction axis (near 0 deg). This would make the model distributions narrower still, which would degrade the fit on the tails of the observed distributions. Since these tails are regions of low energy, this approach would allow the model to characterize data at these spreads with reasonable verity.

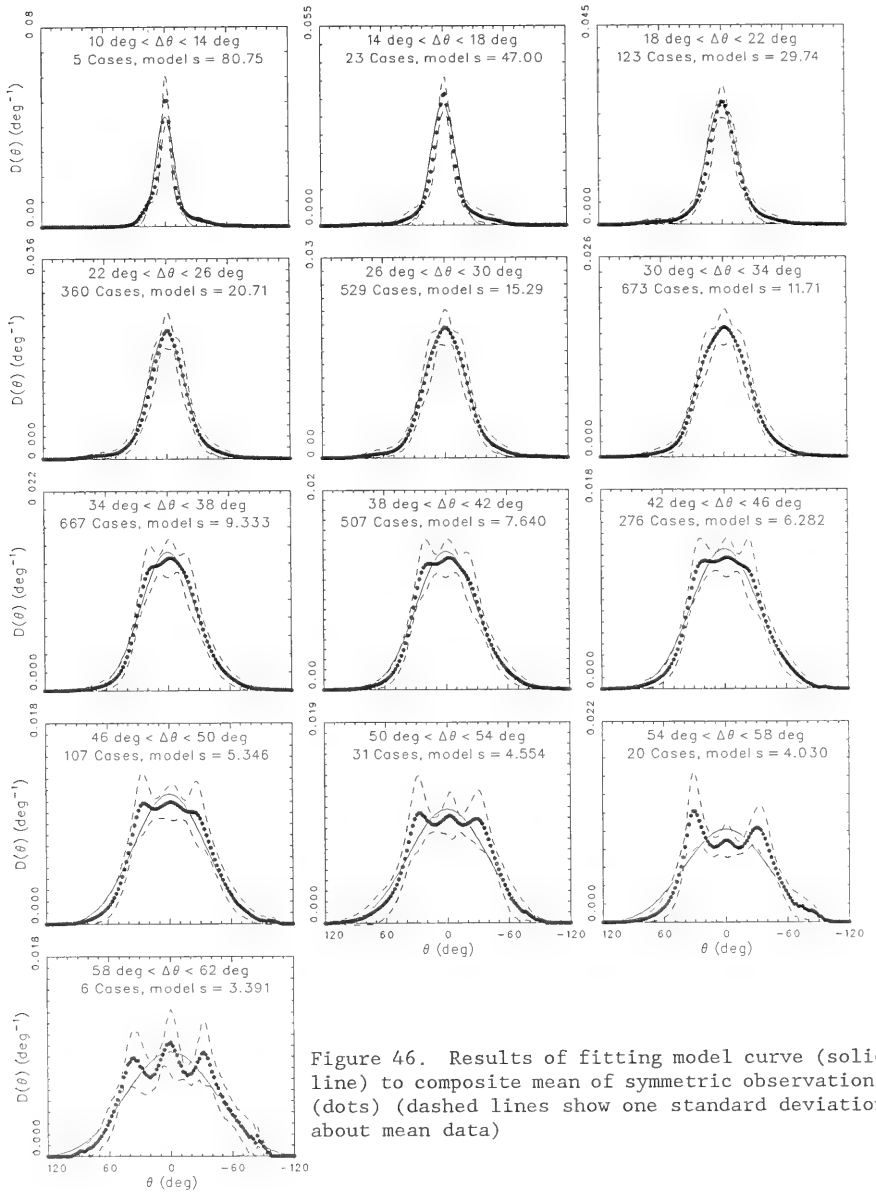


Figure 46. Results of fitting model curve (solid line) to composite mean of symmetric observations (dots) (dashed lines show one standard deviation about mean data)

247. For directional spreads greater than 34 deg, the character of the observed distributions seems to differ from the model curves. The composite data appear to evolve relatively flat distributions in the ranges of their maximum values, high curvature at the ends of these ranges, and tail distributions that appear less dependent on directional spread than the model distributions. It is difficult to assert with much confidence that this indicated behavior is true. There are few observations at the larger spreads (only six at the largest); and data confidence, as indicated by the standard deviation curves, is not high. Flat regions strongly indicated for the largest spreads are not as wide for slightly smaller spreads where there are more observations and therefore higher confidence.

248. Note that the reference to flat regions means the somewhat sinuous curves at the peaks of the broad distributions. As explained earlier, the IMLE method can result in small lobes of energy which deviate from true distributions, especially where distributions are flat. It could well be that deviations of observations from the fitted model curves are, in these cases, simply an artifact of the data processing algorithm. If this is so, model curves can be considered to approximate the data reasonably well at the larger directional spreads. A proper way to state this is that the model curves are within one standard deviation of the data mean curves (with a few exceptional points) but that the standard deviations are large, approaching 30 percent of mean values in some locations.

249. These results suggest that the model proposed by Longuet-Higgins, Cartwright, and Smith (1963) can give a reasonable characterization of the symmetric directional distributions found in the present data set. However, since the symmetric observations account for only one-quarter to one-half of all observations, the model is not complete. Furthermore, the simple shape of the model does not lend itself to representation of the asymmetric classes of data which account for the other one-half to three-quarters of the observation set. This means that further research is necessary to find a class of mathematical functions with which to characterize these observations. It appears that a reasonable starting point in such research would be an extension or modification of the tested model, subject to the constraint that it revert to the form given by Equation 31 for symmetric distributions of narrow-to-intermediate spreads.

## Summary

250. In this section, measured data were examined for systematic order at the level of directional distribution shapes. Using unimodal distributions where low energy cases were excluded as a basis for examination, it was found that the shapes were readily classified by parameters of directional spread and asymmetry. Similar distributions were observed at all frequencies. Classes with low asymmetry were found to conform reasonably well to a one-parameter mathematical function proposed by Longuet-Higgins, Cartwright, and Smith (1963), at least in the low-to-intermediate ranges of spread. Strongly asymmetric distributions, for which this model could not work well, were found to occur in at least half the observations.

## PART X: CONCLUSION

251. Guidance for engineering design of coastal structures which can withstand or modify attacking wind waves must ultimately rely on a proper description of sea state. In view of the paucity of complete, shallow-water, sea state observations and the demonstrable importance of wave directionality described by the experiments of Vincent and Briggs (1989) and Kaihatu and Briggs (in preparation), a long-term series of detailed wave field observations has begun at the CERC FRF. A preliminary analysis of 1,046, high-resolution, frequency-direction spectra from the first year of data collection has been done.

252. Directional distribution characteristics of the observed wave fields have been defined in terms of integral properties of the angular distributions of wave energy at three levels of detail: (a) total energy in the form of the integrated direction spectrum, (b) energy at each frequency from subdivision of the frequency-direction spectra, and (c) energy in isolated modes from subdivision of distributions at each frequency. Distribution parameters have been defined in terms of the angles that bound the four quarters of the directional energy distribution at any given level of detail. In particular, a measure of directional spread is the arc bounding the central half of total energy. A measure of the extent to which a distribution is skewed (higher concentration of energy on one side of a distribution) is determined from the ratio of the arc length bounding the second quarter of total energy to the arc length bounding the third quarter.

253. This study consists of basic correlation of parameters and evaluation of information from the observed frequency-direction spectra alone, primarily to isolate the geometric properties of spectral shape. Little consideration was given to wave generation or transformation processes. Working data are the set of observed directional distribution functions and an extensive but obviously necessary set of parameters with which to characterize the observed sea states.

254. In terms of bulk conventional parameters, the observed ocean-wave climate is in the normal ranges of behavior for a shallow, nearshore site adjacent to a broad, shallow continental shelf and subject to forcing by high winds from a preferred quadrant. Bulk peak direction tends to have wide scatter at low energy, reflecting the effects of light, variable winds and

day-to-day, deep-ocean background swell. At high energy, peak directions are more shore normal, suggesting the influence of refraction on the low-frequency, energetic waves in well-developed seas. In terms of peak period, short-period (high-frequency) wave fields tend to arrive from the northeast quadrant, consistent with patterns of predominant local wave-generating winds. Long-period wind waves which are likely from distant sources tend to arrive from shore normal to slightly south of shore normal.

255. The observed range of peak directions is about 70 deg on either side of shore normal. Characteristic wave heights range from about 0.3 to 4.4 m. Peak periods cover the full range allowed in the effective filtering by the Fourier analysis used here, from about 3.1 to 18.5 sec. As a whole, the data set is dominated by day-to-day low-energy observations. Fewer than 10 percent of observations represent storms.

256. One of the most important results of this study is the behavior of the new parameter characterizing directional spread. It was found never to be small (no unidirectional wave fields). The range was from about 20 to 60 deg. For the data set as a whole, there was a well-defined peak in the spread parameter at about 40 deg. This peak appeared to occur in all sea states, being nearly independent (statistically) of energy level, peak period, peak direction, or bulk steepness (as a dimensionless combination of wave height and wavelength deduced from peak period). Given the sensitivity of system response to directional spread deduced in the laboratory studies of Vincent and Briggs (1989) and Kaihatu and Briggs (in preparation), this result is a strong indication that directional spread must be taken into account in sea state description.

257. Frequency-by-frequency examination of the data indicates that roughly a third of all directional distributions are multimodal. Where multimodal distributions occur, the tendency is for energy to be evenly distributed among the modes. Though some multimodal distributions at high frequencies may be attributable to noise contamination, the occurrence is too high at intermediate frequencies to ignore. This means that multimodal distributions are a very important aspect of wave directionality. Ignoring secondary modes in an attempt to simplify the problem is highly likely to give a poor representation of wave energy. This result indicates that further study is required concerning this aspect of wave directionality.

258. Examination of peak directions and directional spreads of spectra at the frequency-by-frequency level gives results which tend to verify the characteristic properties found in the bulk parameter analysis. High-frequency waves tend to arrive from a broad range of directions, and low-frequency waves tend to be aligned with the shore-normal direction. Directional spreads at the frequency level tend to have a broader range than that found for bulk spread parameter (20 to 60 deg). Spreads as small as 10 deg and as large as 90 deg are not uncommon. However, peaks in the spread distributions are more tightly constrained. Low-frequency waves have spreads commonly in the 20- to 30-deg range; high-frequency waves are spread commonly in the 40- to 50-deg range. Waves at intermediate frequencies have spreads at intermediate levels, more like the distribution of the parameter characterizing bulk spread. When the data set is restricted to unimodal distributions, the only change in results is that spreads for high-frequency waves tend to become more like those for intermediate frequencies. This means that the spread properties at each frequency are rather like the bulk properties. The occurrence of unidirectional waves (spreads of less than about 10 deg) are extremely rare at any frequency.

259. Finally, a computation has been done to define the fundamental shapes that constitute directional distributions. It was assumed that multimodal distributions can be constructed from properly scaled, unimodal shapes. Low-energy, potentially noisy data were eliminated. About half of all observed distributions remained after application of these constraints. Fundamental shapes were then found from composite means of individual distributions, and classified by spread and asymmetry parameters.

260. The result is a set of well-defined (generally having low standard deviations) empirical functions which illustrate and characterize the way wave energy is distributed in direction. The range of spread parameter is 10 to 62 deg, covering the full range of spreads found in the bulk characterization. It was found that only one-fourth to one-half of the distributions could be considered symmetric (having roughly equally distributed energy on both sides of the peak). The remaining one-half to three-fourths of the cases were strongly asymmetric. This property may be as important as directional spread in modeling coastal processes and computing system responses to coastal modifications. It was found that the symmetric distributions could be reasonably fitted with a mathematical function proposed by Longuet-Higgins,

Cartwright, and Smith (1963), at least for classes with low-to-intermediate spread. This suggests that such a model might serve as a basis for an extended model which includes all of the shapes found.

261. The rather exciting consequences of these results are as follows:

a. There is not an infinite variety of directional distribution shapes. The composite curves indicate that there is a distinct order in the way wave energy behaves in shallow water.

b. At least half of all distributions can be represented by a simple, two-parameter mathematical function. It has yet to be defined analytically; but it exists. At a minimum, the empirical shapes published here can be used for modeling even though they are somewhat awkward, being in discrete form.

c. Quite probably, all of the distributions can be represented by this two-parameter function. By scaling and positioning one of these for each mode in a multimodal distribution, a complete distribution of any degree of modality can be constructed. Consequently, the shapes found in this study may be used as fundamental building blocks with which to construct a complete frequency-direction spectrum. This makes a complete spectrum much easier to characterize than having to consider energy separately at all locations in the frequency and direction domains.

d. It is evident that asymmetry in the distributions is as important a parameter as directional spread, especially at the larger spreads. While failure to account for it may lead to serious errors in spectral interpretation and model results, the fact that it has been found and quantified in the present results means that this type of structure can be included in future studies.

262. Together, these results and ideas suggest that there is potential to characterize and describe in detail entire classes of frequency-direction spectra with just a few parameters. This would be an extremely useful result for engineering design because it would allow detailed definition of all, including the most destructive, wave environments to be characterized in a simple way. What is striking about the present results is the strong suggestion of order in what could potentially be a highly irregular system.

263. Compared to what is desired for knowledge of wave directionality in shallow water, the present results are clearly of the most rudimentary variety. A great deal of work remains to be done. In the first place, the present results need to be incorporated into the realm of characterizing the detailed structure of complete frequency-direction spectra. This means

ensuring that the shapes found in this first, simple examination apply, as hypothesized, to all directional distributions. Whole spectra then need to be described in terms of these shapes and the resulting patterns examined for common structure. Observed spectra need to be related to the forcing and transformation mechanisms active at the present site. Further studies need to be performed to see how variability in parameters relating to directional spread affects other guidance regarding sea state description. These include wave height distribution models, correlation of frequency-spectral structure with directional structure, and models of the evolution of high-energy (stormy) seas.

264. The present results simply make it clear that such studies are needed. The laboratory studies of Vincent and Briggs (1989) and Kaihatu and Briggs (in preparation) demonstrated the importance of seas with directional spread in shallow, bounded environments typical of Corps projects. The present field studies show that such seas are normal. This introduces a new and more realistic dimension in describing processes affecting coastal engineering design. Results presented here are an initial foray in trying to understand and quantify these processes.

## REFERENCES


Abramowitz, M., and Stegun, I. A. 1970. Handbook of Mathematical Functions, Dover, NY.

Barber, N. F. 1961. "The Directional Resolving Power of an Array of Wave Detectors," *in* Ocean Wave Spectra, Prentice Hall, Englewood Cliffs, NJ, pp 137-150.

Birkemeier, William A. 1984. "Time Scales of Nearshore Profile Changes," Proceedings of the 19th Coastal Engineering Conference, American Society of Civil Engineers, September 3-7, 1984, Houston, TX, pp 1507-1521.

Birkemeier, William A., and Mason, Curtis. 1984. "The CRAB: A Unique Nearshore Surveying Device," Journal of Surveying Engineering, Vol 110, pp 1-7.

Birkemeier, William A., Miller, H. Carl, Wilhelm, Stanton D., DeWall, Allen E., and Gorbics, Carol S. 1985. "A User's Guide to the Coastal Engineering Research Center's (CERC's) Field Research Facility," Technical Report CERC-85-1, US Army Engineer Waterways Experiment Station, Coastal Engineering Research Center, Vicksburg, MS.

Bouws, E., Günther, H., and Vincent, C. L. 1985. "Similarity of the Wind Wave Spectrum in Finite Depth Water 1. Spectral Form," Journal of Geophysical Research, Vol 90, pp 975-986.

Capon, J., Greenfield, R. J., and Kolker, R. J. 1967. "Multidimensional Maximum-Likelihood Processing of Large Aperture Seismic Arrays," Proceedings of the IEEE, Vol 55, pp 192-211.

Cartwright, D. E., and Smith, N. D. 1964. "Buoy Techniques for Obtaining Directional Wave Spectra," Buoy Technology, Marine Technology Society, Washington DC, pp 112-121.

Cote, L. J., Davis, J. O., Marks, W., McGough, R. J., Mehr, E., Pierson, W. J., Jr., Ropek, J. F., Stephenson, G., and Vetter, R. C. 1960. "The Directional Spectrum of a Wind Generated Sea as Determined from Data Obtained by the Stereo Wave Observation Project," Meteorological Papers, New York University College of Engineering, Vol 2, pp 1-88.

Crowson, Ronald A., Birkemeier, William A., Klein, Harriet M., and Miller, Herman C. 1988. "SUPERDUCK Nearshore Processes Experiment: Summary of Studies, CERC Field Research Facility," Technical Report CERC-88-12, US Army Engineer Waterways Experiment Station, Coastal Engineering Research Center, Vicksburg, MS.

Davis, Russ E., and Regier, Lloyd A. 1977. "Methods for Estimating Directional Wave Spectra from Multi-Element Arrays," Journal of Marine Research, Vol 35, pp 453-477.

Donelan, M. A., Hamilton, J., and Hui, W. H. 1985. "Directional Spectra of Wind Generated Waves," Philosophical Transactions of the Royal Society of London, Series A, Vol 315, pp 509-562.

Elgar, Steve, and Guza, R. T. 1985a. "Shoaling Gravity Waves: Comparisons Between Field Observations, Linear Theory, and a Nonlinear Model," Journal of Fluid Mechanics, Vol 158, pp 47-70.

_____. 1985b. "Observations of Bispectra of Shoaling Surface Gravity Waves," Journal of Fluid Mechanics, Vol 161, pp 425-448.

Goda, Yoshimi. 1985. Random Seas and Design of Maritime Structures, University of Tokyo Press, Japan.

Hasselmann, K., Barnett, T. P., Bouws, E., Carlson H., Cartwright, D. E., Enke, K., Ewing, J. A., Gienapp, H., Hasselmann, D. E., Kruseman, P., Meerburg, A., Müller, P., Olbers, D. J., Richter, K., Sell, W., and Walden, H. 1973. "Measurements of Wind-Wave Growth and Swell Decay During the Joint North Sea Wave Project (JONSWAP)," Ergänzungsheft zur Deutschen Hydrographischen Zeitschrift, Reihe A(8°), Number 12, Hamburg.

Horikawa, Kiyoshi. 1988. Nearshore Dynamics and Coastal Processes, University of Tokyo Press, Japan.

Howd, Peter A., and Birkemeier, William A. 1987. "Storm-Induced Morphology Changes During DUCK85," Proceedings of Coastal Sediments '87, American Society of Civil Engineers, 12-14 May 1987, New Orleans, LA, pp 834-847.

Kaihatu, J. M., and Briggs, M. J. "Diffraction by a Semi-Infinite Breakwater: Numerical and Experimental Comparison," in preparation, Journal of the Waterway, Port, Coastal, and Ocean Division, American Society of Civil Engineers.

Kitaigorodskii, S. A. 1983. "On the Theory of the Equilibrium Range in the Spectrum of Wind-Generated Waves," Journal of Physical Oceanography, Vol 13, pp 186-827.

Leffler, Michael W., Hathaway, Kent K., Scarborough, Brian L., Baron, Clifford F., and Miller, Herman C. 1989. "Annual Data Summary for 1987, CERC Field Research Facility," Technical Report CERC-89-10, US Army Engineer Waterways Experiment Station, Coastal Engineering Research Center, Vicksburg, MS.

Longuet-Higgins, M. S., Cartwright, D. E., and Smith, N. D. 1963. "Observations of the Directional Spectrum of Sea Waves Using the Motions of a Floating Buoy," *in* Ocean Wave Spectra, Prentice Hall, Englewood Cliffs, NJ, pp 111-132.

Miller, H. C., Birkemeier, W. A., and DeWall, A. E. 1983. "Effects of CERC Research Pier on Nearshore Processes," Proceedings of Coastal Structures '83, American Society of Civil Engineers, 9-11 March 1983, Arlington, VA, pp 769-784.

Miller, H. C., and Vincent, C. L. 1990 "FRF Spectrum: TMA with Kitaigorodskii's $f^{-4}$ Scaling," Journal of the Waterway, Port, Coastal, and Ocean Division, American Society of Civil Engineers, Vol 116, pp 57-78.

Mitsuyasu, H., Tasai, F., Suhara, T., Mizuno, S., Ohkusu, M., Honda, T., and Rikiishi, K. 1975. "Observations of the Directional Spectrum of Ocean Waves Using a Cloverleaf Buoy," Journal of Physical Oceanography, Vol 5, pp 750-760.

Oltman-Shay, Joan, and Guza, R. T. 1984. "A Data-Adaptive Ocean Wave Directional-Spectrum Estimator for Pitch and Roll Type Measurements," Journal of Physical Oceanography, Vol 14, pp 1800-1810.

Pawka, S. S. 1982. "Wave Directional Characteristics on a Partially Sheltered Coast," Ph.D. Dissertation, Scripps Institute of Oceanography, University of California, San Diego, CA.

_____. 1983. "Island Shadows in Wave Directional Spectra," Journal of Geophysical Research, Vol 88, pp 2579-2591.

Pawka, S. S., Inman, D. L., and Guza, R. T. 1984. "Island Sheltering of Surface Gravity Waves: Model and Experiment," Continental Shelf Research, Vol 3 pp 35-53.

Phillips, O. M. 1958. "The Equilibrium Range in the Spectrum of Wind-Generated Waves," Journal of Fluid Mechanics, Vol 4, pp 426-434.

Pierson, W. J., and Moscowitz, L. 1964. "A Proposed Spectral Form for Fully Developed Windseas Based on the Similarity Theory of S. A. Kitaigorodskii," Journal of Geophysical Research, Vol 69, pp 5181-5190.

Ragsdale, Danielle S. 1983. "Sea-State Engineering Analysis System (SEAS)," WIS Report 10, US Army Engineer Waterways Experiment Station, Coastal Engineering Research Center, Vicksburg, MS.

Shore Protection Manual. 1984. 4th Edition, 2 Vols, US Army Engineer Waterways Experiment Station, Coastal Engineering Research Center, US Government Printing Office, Washington, DC.

The IAHR Working Group on Wave Generation and Analysis. 1989. "List of Sea-State Parameters," Journal of the Waterway, Port, Coastal, and Ocean Division, American Society of Civil Engineers, Vol 115, pp 793-808.

US Army Engineer District, Wilmington. 1980. Manteo (Shallowbag) Bay, North Carolina, General Design Memorandum, Phase II, Wilmington, NC.

Vincent, Charles L., and Briggs, Michael J. 1989. "Refraction-Diffraction of Irregular Waves over a Mound," Journal of the Waterway, Port, Coastal, and Ocean Division, American Society of Civil Engineers, Vol 115, pp 269-284.

# APPENDIX A: LINEAR ARRAYS - THEORY AND APPLICATION

## Introduction

1. This section is intended to provide the reader and/or potential user of the Field Research Facility (FRF) linear array with a fundamental understanding of linear array theory and its application to wind wave directional estimation. The appendix will discuss: (a) bottom-mounted pressure sensors and their limitations, (b) directional information contained in arrays of pressure sensors, and (c) problems in directional resolution and aliasing.

## Wave Information from Bottom-Mounted Pressure Sensors

2. Bottom-mounted pressure sensors measure fluctuations about hydrostatic pressure caused by passing surface waves. These fluctuations can be translated to surface elevation using linear wave theory, which indicates how wave-induced pressure fluctuations are attenuated with depth. When a sensor is at a depth of half the wavelength of a surface wave, pressure fluctuations from that wave are so small as to be imperceptible to many pressure sensors. Therefore, the shorter the wavelength (the higher the wind wave frequency), the greater is the pressure attenuation with depth. Since a pressure sensor detects each wave frequency in a composite sea differently, there is no simple equivalence between time series of elevation and pressure. Pressure fluctuations caused by each frequency component of a wind wave field will require a specific *surface correction* to extract the surface elevation amplitude.

3. Two important points are to be learned from this: (a) if the sensors are placed too deep, high-frequency, small-wavelength wind waves will be filtered out (fluctuations will be too small to be detected at the bottom); and (b) if the interest is not in the bottom pressure field but in surface elevations, a pressure time series must be decomposed into its Fourier coefficients and the coefficients *surface corrected* to obtain the elevation amplitude for each frequency of wind wave.

4. For this discussion, surface elevation information will be considered in terms of its complex Fourier coefficients (one pair of coefficients for each frequency). The frequency variance spectrum (proportional to and

sometimes called the *energy spectrum*) of surface elevation can be obtained from these coefficients. Relative phase information, which is used to estimate wave propagation directions, can also be extracted.

Estimating Propagation Direction of a Single Plane Wave with Two Sensors

5. Propagation directional distributions are estimated frequency by frequency, i.e., information at one frequency is assumed to be independent of information at any other frequency. A frequency-direction spectrum is simply the two-dimensional (2-D) presentation of each of these independent directional estimates. Therefore, the following discussion will deal with directional estimation at a single wind wave frequency.

6. Phase difference between sensors is used to estimate wave propagation direction. How propagation direction is extracted from phase is best shown in the simple case of a single plane wave passing through an array of two pressure sensors (Figure A1). The pressure sensors are in a line parallel to the shoreline and are separated by some known distance. A plane wave normally incident to the beach will have its crests and troughs arrive at both sensors at the same time (Figure A1a). Wave signals at the sensors will then have equal phase; and their phase difference will be zero, independent of their longshore separation. If the plane wave is incident at some angle off the normal to the array, one sensor would see wave crests and troughs before the other (Figure A1b). The phase difference would then be nonzero and would depend on the longshore separation of the two pressure sensors.

7. To understand how phase differences can translate to directional angle requires some trigonometry. The water surface $\eta$ of a progressive plane wave is represented as a cosine function,

$$\eta = a \cos(2\pi ft - \mathbf{k}\cdot\mathbf{x}) \tag{A1}$$

where $a$ is amplitude, $f$ is cyclic frequency (equal to $1/T$ ; where $T$ is wave period), $t$ is time, $\mathbf{k}$ is wave number vector (having cross-shore and longshore components $k_x$ and $k_y$ , respectively), and $\mathbf{x}$ is the coordinate location vector (having components $x$ and $y$ as cross-shore and longshore positions, respectively). The $\mathbf{k}\cdot\mathbf{x}$ term in the cosine argument of Equation A1 is constant if the plane wave is being observed from a fixed

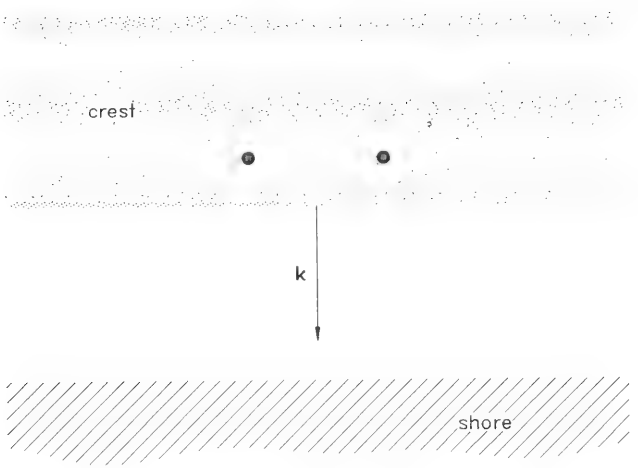


a. normal incidence

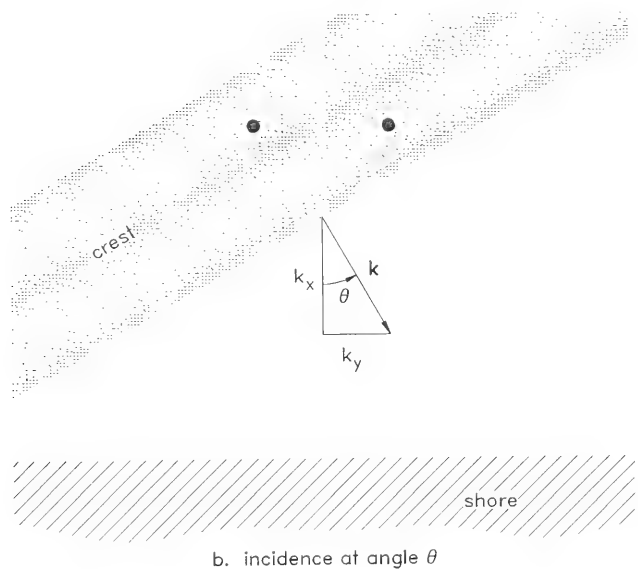


b. incidence at angle $\theta$

Figure A1. Plan view of waves incident on the array and beach

(x,y) location. This term is identically the phase of the plane wave when $t = 0$ for that (x,y) location. Rewriting the plane wave equation by expanding the $\mathbf{k}\cdot\mathbf{x}$ term gives

$$\eta = a \cos(2\pi ft - k_x x - k_y y) \tag{A2}$$

where the wave number and position vectors are converted to component form (Figure A1). The phase term in the cosine argument for $t = 0$ and an arbitrary (x,y) location is

$$\phi = k_x x + k_y y \tag{A3}$$

8. For two sensors located on a line parallel to the shoreline, the offshore coordinates $x = x_1$ and $x = x_2$ will be the same. The longshore coordinates $y = y_1$ and $y = y_2$ will differ. The sensors will have the following respective phase terms

$$\phi_1 = k_x x_1 + k_y y_1 \tag{A4a}$$

$$\phi_2 = k_x x_2 + k_y y_2 \tag{A4b}$$

and phase difference

$$\Delta\phi = \phi_1 - \phi_2$$

$$= k_y (y_1 - y_2) \tag{A5}$$

since $x_1 = x_2$ . This phase difference contains the information needed to obtain the propagation direction of the wave. Application of trigonometry to the vector diagram in Figure A1b gives the relation

$$k_y = k \sin (2\pi\theta/360) \tag{A6}$$

where $\theta$ is the plane wave propagation direction (in degrees), measured from shore normal, and k is the magnitude of the wave number vector $\mathbf{k}$ . Equation A5 then can be written

$$\Delta\phi = k\ (y_1 - y_2)\ \sin\ (2\pi\theta/360) \tag{A7}$$

In Equation A7, $(y_1 - y_2)$ is known, $\Delta\phi$ is measured with the two sensors (as discussed below), and $k$ can be found, using linear wave theory, from knowledge of wave frequency (which is also measured with the two sensors). Linear wave theory relates wave number magnitude $k$ to wave frequency $f$ and water depth $d$ through the surface gravity wave dispersion relationship

$$4\pi^2 f^2 = gk \tanh kd \tag{A8}$$

where $g$ is gravitational acceleration. Thus, the only unknown variable left in Equation A7 is $\theta$, for which the solution is

$$\theta = \frac{360}{2\pi} \sin^{-1} \left[ \frac{\Delta\phi}{k(y_1 - y_2)} \right] \tag{A9}$$

9. In combination, two sensors detect the amplitude and relative phase of a plane wave that passes over them. With a little help from linear wave theory, those data are used to estimate the propagation direction of the plane wave. This is quite a simple result. Obviously, real ocean waves are not that easy to analyze, or two sensors would always be used instead of larger arrays.

## Requirements for More than Two Sensors

10. In application of Equation A9, it is desirable to be able to resolve, for example, a wave incident at 20 deg from another at 30 deg. To do this, it is necessary to resolve the phase of the 20-deg incident wave from that of the 30-deg wave. The longshore separation of the sensors is critical in this regard. Defining an ideal gage separation is called the *resolution* problem. Unfortunately, there is no single ideal separation. This is because the longshore component $k_y$ of the wave number vector $k$ is a factor in the phase differences observed by the sensors (Equation A5), and it varies with propagation direction Equation A6).

11. To illustrate this problem, Figure A2a shows a vertical cross-section (along the sensor array) of a wave incident at direction $\theta_1$ as it

passes by the two sensors. This figure represents a snapshot of the pattern of crests and troughs along the array at, say, $t = 0$. Solid circles mark the two sensor locations. The sensor at $y = 0$ sees the full amplitude $a$ of a wave. The sensor at $y = y_2$ sees a smaller amplitude $a \cdot \cos(k_y y_2)$, as defined by Equation A2 with both $x$ and $t$ set to zero.

12. Figure A2b shows a vertical cross section of the same wave, but it is now incident at direction $\theta_2$, where $\theta_2 < \theta_1$. Sensor locations are the

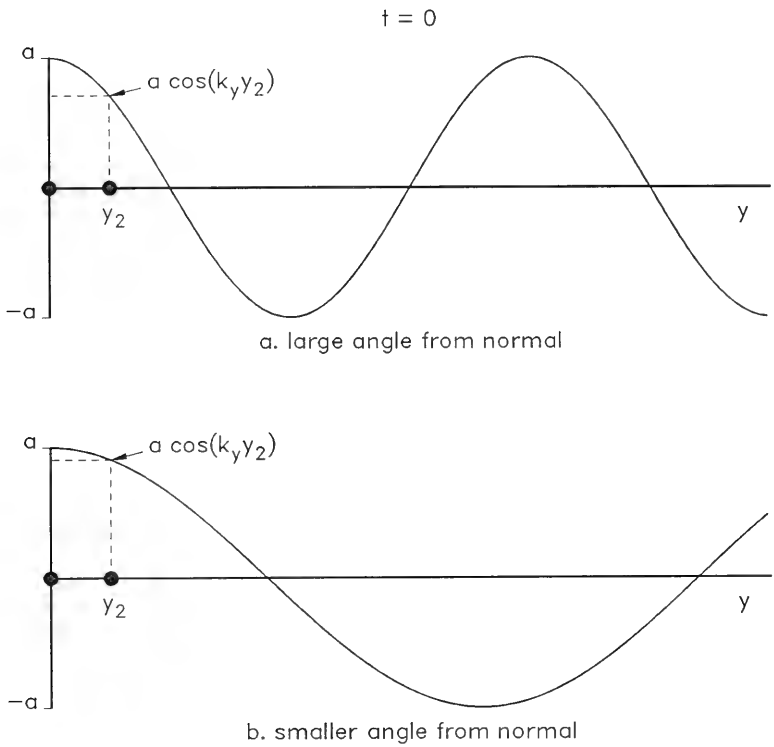


Figure A2. Vertical sections through water surface along two-element array (dots) of waves incident at two different angles

same as in Figure A2a. The wave in Figure A2b, however, has a different $k_y$ in the direction along the array. The signal detected by the sensor at $y = y_2$ is different from that in Figure A2a. To distinguish between the $\theta_1$ and $\theta_2$ propagation directions, the pressure sensors need to be sensitive enough to distinguish the two amplitudes at $y = y_2$. One obvious solution may be to place the sensors farther apart. However, there is a risk of another problem, called *aliasing*.

13. Aliasing occurs when the sensors are separated by more than half the wavelength of the shortest wave that may be encountered. If this occurs, a short wave cannot be distinguished from a longer wave through the phase information available; both give the same phase difference for a given sensor separation. It is impossible to determine which one is present (Figure A3).

14. At a given frequency, the longshore component of an incident wave is shortest when its direction is 90 deg off the normal. To avoid aliasing, it is necessary to make sure that the sensors are not separated any farther than one-half of this wavelength. The trade-off is that this separation may not be large enough to give the desired directional resolution.

15. Actually, the problem is more severe than that. In a real ocean environment, it is desirable to measure waves at all wind wave frequencies. Resolution of high frequency (short wavelength) waves requires a small sensor separation. Lower frequency (long wavelength) waves will, therefore, be sorely deficient of any directional resolution because, for them, the separation is too small.

16. This situation can be improved by using more than two sensors. The number of sensors required will depend both on the range of wind wave frequencies covered and the degree of directional resolution desired.

## Linear Array with Four Sensors

17. This section explains the advantages of using more than two sensors to improve resolution and avoid aliasing. The concept of coincident and quadrature (Co and Quad) computations is introduced for analyzing data from multielement linear arrays. An array of four sensors is considered.

18. The problem becomes one of determining sensor placement so that gage response is optimized. A set of four sensors could be placed so they are separated by equal distances with spacing between adjacent sensors given the

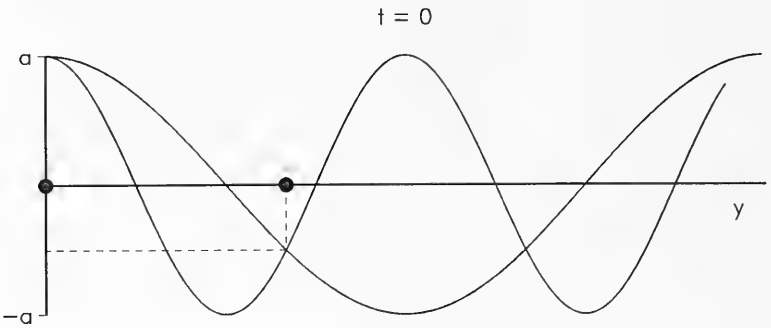


Figure A3. Example of aliasing (the short wave is not aliased)

symbol YLAG . By Equation A5, phase differences between equally spaced sensors in a well-behaved wave field are the same. This would lead to three independent but redundant estimates of $\theta$ from Equation A9. However, the most serious need is not redundancy but measurement of nonaliased, well-resolved phase differences for all wind wave frequencies.

19. With four, equally spaced sensors, it can be seen that phase differences between the end sensors, whose separation is 3·YLAG , can also be detected. While this may give an aliased phase measurement for high-frequency waves, it would provide not only a nonaliased phase for low-frequency waves but also a more effective sensor separation for directional resolution of low-frequency waves. This suggests that better use of the four sensors can be made by trying to make all sensor separations unique. Such an arrangement avoids redundant measurements and provides a variety of spacings which lead to nonaliased, better-resolved phase measurements for a variety of wave frequencies. A good design might be what is referred to as a *1-2-4* array. In this design, the first and second sensors are separated by YLAG , the second and third are separated by 2·YLAG , and the third and fourth are separated by 4·YLAG . The total possible combinations of sensor pairs would allow phase estimates from sensors separated by (1, 2, 3, 4, 6, and 7)·YLAG . This arrangement increases the range of wind wave frequencies at which good direction resolution can be obtained.

20. The above discussion introduces the concept of *lag-space*, which is a convenient way to discuss and design linear arrays. Instead of thinking about linear arrays in terms of absolute (x,y) sensor locations, arrays can

be considered in terms of combinations of sensor separations, or *lags*. The lag axis ranges from a value of 0 (the separation of a sensor with itself) to the length of the array (the separation of the end sensors). It is usually labeled in terms of minimum lag, which is the separation of the two closest sensors. In the case of a 1-2-4 array, the lag unit would be YLAG , and the lag axis would range from 0 to 7·YLAG .

21. A useful mechanism often employed to understand the potential of a linear array is to graph phase differences between sensors as a function of lag separation for ideal waves having various $L_y$ (longshore component of wavelength, equal to $2\pi/k_y$ ). To fully appreciate this, some of the details in obtaining phase information from the sensors must be examined.

22. Phase information is extracted from the coefficients of a Fourier series representation of time series of sea surface elevations at wind wave frequencies. A Fourier transform of the plane wave signal given by Equation A2 yields the complex Fourier coefficient

$$F(f) = a(f)\,[\cos(k_x x + k_y y) + i \sin(k_x x + k_y y)] \tag{A10}$$

where $i = \sqrt{-1}$ and indicates complex notation.

23. The phase difference between one sensor located at $(x,y_1)$ and a second at $(x,y_2)$ is found from the Fourier coefficients, called $F_1(f)$ and $F_2(f)$ , respectively, of signals from the two sensors. The product of the Fourier coefficient of one sensor with the complex conjugate of the other is

$$\begin{aligned} F_1(f)\cdot F_2^*(f) = [a(f)]^2 \cdot &[\cos(k_x x + k_y y_1) + i \sin(k_x x + k_y y_1)] \\ \cdot &[\cos(k_x x + k_y y_2) - i \sin(k_x x + k_y y_2)] \end{aligned} \tag{A11}$$

where the asterisk (*) denotes complex conjugation. With some trigonometry this can be written as

$$F_1(f)\cdot F_2^*(f) = [a(f)]^2 \cdot \{\cos[k_y(y_1 - y_2)] + i \sin[k_y(y_1 - y_2)]\} \tag{A12}$$

24. The terms in braces contain the phase difference information. The real part of Equation A12 is the in-phase or *coincident* component and the imaginary part is the *quadrature* component. These are commonly called the *Co* and *Quad* terms, respectively. Note that these terms are modulated by sensor

separation [the $(y_1 - y_2)$ in Equation A12]. A little more trigonometry reveals

$$\tan^{-1}\left[\frac{\text{Quad}}{\text{Co}}\right] = \tan^{-1}\left\{\frac{\sin[k_y(y_1 - y_2)]}{\cos[k_y(y_1 - y_2)]}\right\}$$

$$= k_y (y_1 - y_2)$$

$$= \Delta\phi \qquad \text{(A13)}$$

where $\Delta\phi$ is the same as that expressed in Equation A5.

25. Note that if the Fourier coefficient of one sensor is multiplied by its own complex conjugate, Equation A12 reduces to an expression for the squared amplitude (variance) at that frequency, since $y_1 = y_2$. The in-phase, cosine term would have a value of one and the quadrature, sine term would be zero, indicating, correctly, that the sensor is completely in-phase with itself.

26. The phase characteristics of a multi-directional wave field are more easily interpreted if one examines the Co and Quad components of Equation A12 instead of the phase term of Equation A13. The Co and Quad terms can be graphed in terms of the array lag space. To illustrate this, Figure A4a shows a snapshot of a plane wave passing through a 1-2-4 array. The sinusoid is a cross section of the pattern of crests and troughs along the array as a function of absolute $(x,y)$ coordinates. The Co and Quad plots for the same wave are shown in Figure A4b and A4c, respectively. The crests and troughs of the Co plot indicate lag separations where signals from two sensors would be in-phase and 180 deg out of phase, respectively. Similarly, the crests and troughs of the Quad plot indicate sensor separations where signals would be 90 and 270 deg out of phase, respectively.

27. The Co and Quad plots of a single plane wave are sinusoids with wavelengths equal to the longshore component of the incident wavelength; that is, they provide an estimate of $k_y$. Knowledge of $k_y$, $f$, and $d$ allows an estimate of $\theta$ by way of Equations A6 and A8. This shows how all the sensor separations may be used together to get an estimate of the longshore wavelength of an incident wave and, from this, its propagation direction.

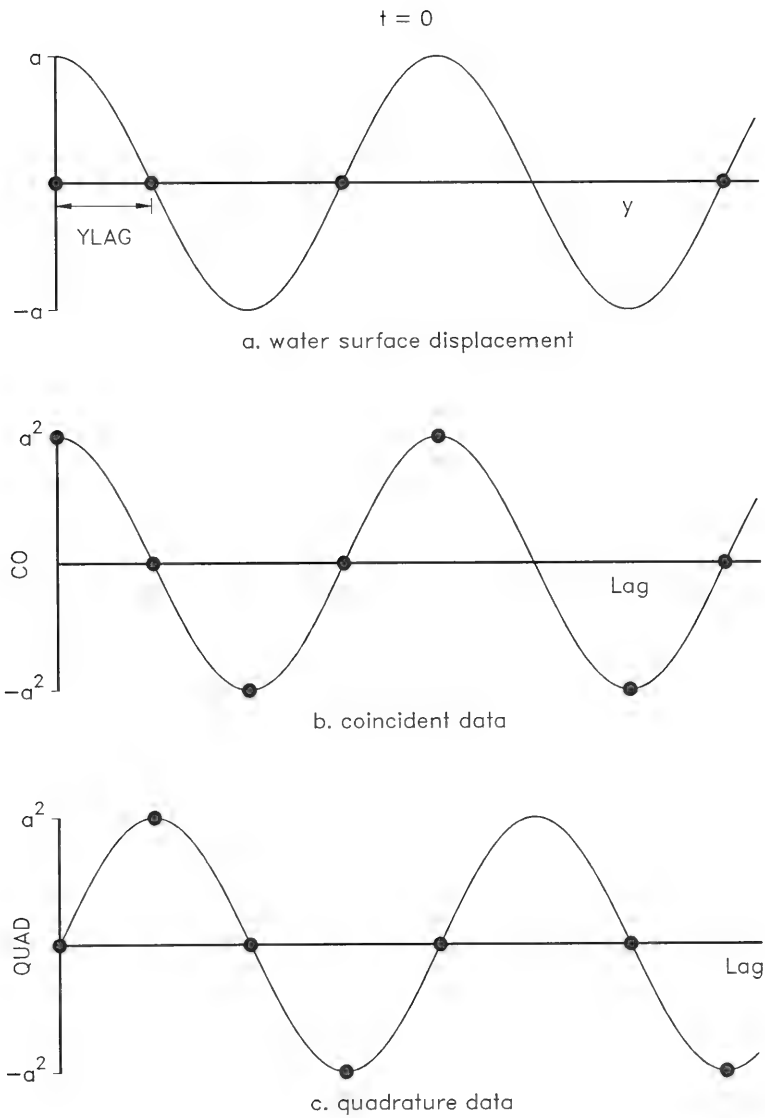


Figure A4. Coincident and quadrature spectra in terms of array lag space

28. The advantage of a multi-element linear array is that it gives phase measurements from many different sensor separations. Whereas some of these separations may be too small or too large to use in Equation A9, the sinusoidal patterns in the Co and Quad plots show that all phase differences from all sensor separations can be used. This avoids the aliasing problem for short waves (as long as the minimum gage spacing is small enough) and allows good resolution of longer waves (if the overall array is long enough). Expected patterns in Co and Quad plots allow the fitting of model curves to Co and Quad data. This improves resolution since multiple samples of the wave directional pattern are realized in the Co and Quad data.

## Directional Spectra from Longshore Wave Number Estimates

29. To this point, discussion has been about the contents of the Co and Quad data for a single plane wave incident on the array. Nature does not work like that; a real wave field contains a directional distribution of waves incident on an array. The Co and Quad plots would then contain a superposition of longshore wavelength signatures of all the incident waves, with each signature representing a directional angle of incidence. To resolve these directions, it is necessary to decompose the Co and Quad plots into a variance distribution as a function of longshore wave number (or directional angle) of the total wave field.

30. This is the same problem encountered when a time series is decomposed into cosines and sines (Fourier components) in order to estimate the frequency distribution of variance (or wave energy). A reasonable approach might be to decompose the Co and Quad data into Fourier components. However, there are physical restrictions that make this approach untenable.

31. For Fourier analysis of the Co and Quad data to work, the full length of the array must be at least equal to the longest longshore wavelength to be resolved. Everything would be in good shape if wind waves all traveled parallel to the shore. For wind waves in the frequency range 0.05 to 0.33 Hz and in a nominal water depth of 8 m, the largest wavelength to be resolved would be 175 m. An array of this length can be constructed easily. However, wind waves typically do not travel parallel to the shore so longshore wavelengths to be resolved are much larger.

32. For instance, if a 0.05-Hz wave was incident at 10 deg from shore normal, its longshore wavelength would be about 1 km. This means an array of length 1,000 m would be needed to distinguish this wave from one that was normally incident. Additionally, some sensor separations would have to be as small as 10 m to avoid aliasing high-frequency, shorter waves. Hence, use of Fourier analysis in directional estimation would require an unrealistic number of sensors and an extremely challenging gage installation and maintenance program.

33. For this reason, alternate analysis methods know as *high-resolution estimators* must be used to estimate longshore wave number and directional content of signals at an incident wind wave frequency. These methods are capable of resolving wavelengths that are approximately three times the array length. This allows wave directional estimation to be performed with an array of reasonable length. High-resolution methods are somewhat complicated mathematically, and care is required when implementing them and interpreting their estimates. Nonetheless, with proper use, these methods have proven extremely effective in yielding reliable directional spectral estimates of wind waves incident on a beach. Details of high-resolution estimators are not given here but can be found in the literature. One of the classic approaches is described by Davis and Regier (1977).* An improved adaptation of this is derived by Pawka (1983). A summary of both these methods is in the paper by Oltman-Shay and Guza (1984).

## Linear Array with Nine Pressure Sensors

34. The FRF linear array consists of nine bottom-mounted pressure sensors placed along the 8-m, shoreline parallel contour. A tenth sensor was placed 5 m offshore of the main array to form a slope (or Sxy) array in combination with two of the linear array sensors.

35. Historical records at the FRF field site indicate that peak wind wave frequencies typically fall within the 0.06- to 0.35-Hz range (2.8- to 16-sec periods). To measure the high-frequency waves with bottom-mounted pressure sensors, the sensors must be in rather shallow water because of the

---

* Sources of these works are given in the References of the main body of this report.

signal attunuation problem. Conversely, the sensors should also be outside the surf zone so that linear wave theory can be used with some confidence. It was determined that the 8-m contour was the shallowest deployment site which was also outside of the surf zone in typical storm conditions. Pressure sensing elements are mounted approximately 1 m above the bottom and so are at a nominal depth of 7 m. Attenuation of surface wave signals at this depth is such that the signal-to-noise ratio of the pressure sensors permits observation of waves with frequencies up to 0.33 Hz.

36. Figure A5 maps the relative locations of all 10 sensors. The full array length is 255 m. The minimum sensor separation is 5 m. In light of the lag-increment naming of the four-element array discussed above, the FRF array can be called a 7-5-21-2-3-1-7-5 array. The 5-m minimum separation ensures that aliasing will not occur for the highest frequency waves (those most sensitive to aliasing). The wavelength of a 0.33-Hz wave in 8 m of water is

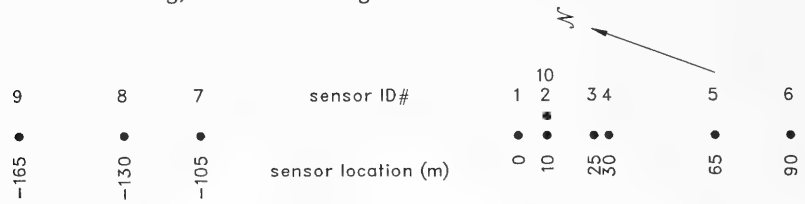


Figure A5. Spacing and numbering of gages in the FRF linear array

about 14 m. Since minimum gage separation is less than half this wavelength, aliasing will not occur.

37. It may be noticed that the sensor identification (ID) numbers are not sequential. The reason for this is that the full array is actually broken into subarrays, divided as follows:

| Subarray Name | Sensors Used, ID# | Length of Subarray, m |
|---|---|---|
| Short Array | 1,2,3,4,5 | 65 |
| Short-Intermediate Array | 1,2,3,4,5,6 | 90 |
| Long-Intermediate Array | 1,2,3,4,5,6,7 | 195 |
| Long Array | 1,2,3,4,5,6,7,8,9 | 255 |

38. The short and intermediate arrays are nested within the long array and are tuned to ranges of wavelengths to be resolved. The short arrays are used to measure directional distributions of shorter wavelength wind waves; the longer arrays are used to measure longer wavelengths. The frequency and corresponding wavelength groupings are:

| Subarray Name | Frequencies, Hz | Wavelengths, m (in 8 m of water) |
|---|---|---|
| Short Array | 0.19 to 0.33 | 38 to 14 |
| Short-Intermediate Array | 0.14 to 0.19 | 57 to 38 |
| Long-Intermediate Array | 0.08 to 0.14 | 107 to 57 |
| Long Array | 0.05 to 0.08 | 175 to 107 |

39. Detailed analysis of the behavior of high-resolution spectral estimators has suggested the design of these nested subarrays. When waves are directionally spread about a central angle, superposition of the different longshore wavelengths makes the Co and Quad data appear as sinusoids which decay exponentially with increasing lag. If the sensors are too far apart, the exponential decay causes Co and Quad curves to approach zero. If too much of the lag axis contains these low values, high-resolution estimators misbehave and directional spectra are less reliable.

40. The FRF linear array has been designed to avoid this problem by proportionally truncating the size of the array for different ranges of wavelength. This limits the amount of decay in the Co and Quad curves and so increases reliability of estimation algorithms.

# APPENDIX B: NOTATION

| | |
|---|---|
| $*$ | Complex conjugation operator |
| $a$ | Wave amplitude |
| $a_{mn}$ | Wave amplitude at $n^{th}$ frequency and $m^{th}$ direction |
| $A$ | Asymmetry parameter |
| $A_n$ | Asymmetry parameter of a 180-deg directional distribution function at frequency $f_n$ |
| $A_n^{(k)}$ | Asymmetry parameter of mode $k$ within a directional distribution function at frequency $f_n$ |
| Co | Coincident or in-phase part of product of Fourier coefficients of two signals |
| $d$ | Water depth |
| $df$ | Frequency increment |
| $d\theta$ | Direction increment |
| $D(f_n,\theta_m)$ | Directional distribution function at frequency $f_n$ and direction $\theta_m$ |
| $E$ | Mean wave energy per unit crest length |
| $E'$ | Sea surface variance per unit crest length |
| $f$ | Wave frequency |
| $f_n$ | $n^{th}$ frequency of a set of $N$ discrete frequencies |
| $f_N$ | Highest frequency of a set of $N$ discrete frequencies |
| $f_p$ | Peak frequency |
| $f_{p,FD}$ | Frequency at peak of frequency-direction spectrum |
| $f_{p,IFS}$ | Frequency at peak of integrated frequency spectrum |
| $f_1$ , $f_2$ , ... | Specific wave frequencies |
| $F$ | Fourier coefficient (complex) |
| FD | Frequency-direction |
| $F_1$ , $F_2$ | Specific (complex) Fourier coefficients |

| | |
|---|---|
| $g$ | Gravitational acceleration |
| $G(s)$ | Coefficient in an analytic model of directional distribution which has $s$ as a parameter |
| $H_{mo}$ | A characteristic wave height |
| $i$ | $\sqrt{-1}$ , indicates complex notation |
| $I(\theta_j)$ | Cumulative distribution function of integrated direction spectrum at direction $\theta_j$ |
| $I(f_n,\theta_m)$ | Cumulative distribution function at frequency $f_n$ and direction $\theta_m$ |
| $I^{(k)}(f_n,\theta_j)$ | Cumulative distribution function for mode $k$ at direction $\theta_j$ from a directional distribution at frequency $f_n$ |
| $k$ | Wave number vector; components $(k_x,k_y)$ |
| $k$ | Magnitude of wave number vector; counting index of modes in a distribution |
| $k_n$ | Magnitude of wave number corresponding to $n^{th}$ frequency |
| $k_x$ | Cross shore component of wave number |
| $k_y$ | Longshore component of wave number |
| $K$ | Number of modes in a directional distribution |
| $L$ | Wavelength |
| $L_{p,IFS}$ | Wavelength associated with the peak frequency of the integrated frequency spectrum |
| $L_y$ | Longshore wavelength |
| $m$ | Index associated with discrete direction |
| $M$ | Integer number of discrete directions |
| $n$ | Index associated with discrete frequency |
| $N$ | Integer number of discrete frequencies |
| $P_n^{(k)}$ | Fraction of total energy at frequency $f_n$ contained in mode $k$ of a directional distribution |
| Quad | Quadrature or out-of-phase part of product of Fourier coefficients of two signals |
| $r$ | Index of a discrete direction bounding a mode on the left (counter-clockwise) side |

| | |
|---|---|
| $s$ | Index of a discrete direction bounding a mode on the right (clockwise) side;<br>a parameter in an analytic directional distribution model |
| $S$ | Spectral density |
| $S(f)$ | Frequency spectral density (continuous) |
| $S(f_n)$ | Integrated frequency spectral density at frequency $f_n$ |
| $S(\theta)$ | Direction spectral density (continuous) |
| $S(\theta_m)$ | Integrated direction spectral density at direction $\theta_m$ |
| $S(f,\theta)$ | Frequency-direction spectral density (continuous) |
| $S(f_n,\theta_m)$ | Frequency-direction spectral density at frequency $f_n$ and direction $\theta_m$ |
| SW | Spectrally weighted |
| $t$ | Time |
| $T$ | Wave period |
| $T_p$ | Spectral peak period |
| $T_{p,IFS}$ | Peak period from the integrated frequency spectrum |
| $\mathbf{x}$ | Position vector; components (x,y) |
| $x$ | Cross shore position |
| $x_1$ , $x_2$ | Specific cross shore positions |
| $y$ | Longshore position |
| $y_1$ , $y_2$ | Specific longshore positions |
| YLAG | Basic unit of linear array gage spacing |
| $\beta$ | A parameter in an analytic model of directional distributions |
| $\Gamma$ | The Gamma function |
| $\Delta\theta$ | Directional spread parameter |
| $\Delta\theta_n$ | Directional spread parameter of a 180-deg directional distribution at frequency $f_n$ |
| $\Delta\theta_n^{(k)}$ | Directional spread parameter of mode $k$ within a directional distribution at frequency $f_n$ |

| | |
|---|---|
| $\Delta\theta_{IDS}$ | Directional spread parameter of integrated direction spectrum |
| $\Delta\theta_{SW}$ | Spectrally weighted directional spread parameter |
| $\Delta\phi$ | Phase difference |
| $\eta$ | Sea surface elevation |
| $\theta$ | Wave direction (in degrees), equals $360\cdot\theta'/2\pi$ |
| $\overline{\theta}$ | Positioning parameter |
| $\theta_j$ | $j^{th}$ direction of a set of M discrete directions |
| $\theta_m$ | $m^{th}$ direction of a set of M discrete directions |
| $\theta_{min}$ | Direction at which there is a minimum of energy |
| $\theta_M$ | Extreme direction of a set of M discrete directions |
| $\overline{\theta}_n$ | Positioning parameter of a 180-deg directional distribution function at frequency $f_n$ |
| $\overline{\theta}_n^{(k)}$ | Positioning parameter of mode k within a directional distribution at frequency $f_n$ |
| $\theta_p$ | Peak direction |
| $\theta_{p,n}$ | Direction of peak in directional distribution function at frequency $f_n$ |
| $\theta_{p,n}^{(k)}$ | Peak direction within mode k of a directional distribution at frequency $f_n$ |
| $\theta_{p,FD}$ | Direction at peak of frequency-direction spectrum |
| $\theta_{p,IDS}$ | Direction at peak of integrated direction spectrum |
| $\theta_{r,n}^{(k)}$ | Discrete direction bounding left side of $k^{th}$ mode of directional distribution at frequency $f_n$ |
| $\theta_{s,n}^{(k)}$ | Discrete direction bounding right side of $k^{th}$ mode of directional distribution at frequency $f_n$ |
| $\theta_o$ | Peak direction in analytic models of directional distribution functions |
| $\theta_1$ , $\theta_2$ , ... | Specific wave directions |
| $\theta_{25\%,n}$ | Direction at which cumulative distribution function equals 0.25 at frequency $f_n$ |

| | |
|---|---|
| $\theta_{50\%,n}$ | Direction at which cumulative distribution function equals 0.50 at frequency $f_n$ |
| $\theta_{75\%,n}$ | Direction at which cumulative distribution function equals 0.75 at frequency $f_n$ |
| $\theta_{25\%,IDS}$ | Direction at which integrated direction spectrum cumulative distribution equals 0.25 |
| $\theta_{50\%,IDS}$ | Direction at which integrated direction spectrum cumulative distribution equals 0.50 |
| $\theta_{75\%,IDS}$ | Direction at which integrated direction spectrum cumulative distribution equals 0.75 |
| $\theta^{(k)}_{25\%,n}$ | Direction at which cumulative distribution function at frequency $f_n$ and for mode $k$ equals 0.25 |
| $\theta^{(k)}_{50\%,n}$ | Direction at which cumulative distribution function at frequency $f_n$ and for mode $k$ equals 0.50 |
| $\theta^{(k)}_{75\%,n}$ | Direction at which cumulative distribution function at frequency $f_n$ and for mode $k$ equals 0.75 |
| $\theta'$ | Wave direction (in radians), equals $2\pi\theta/360$ |
| $\rho$ | Water density |
| $\phi$ | Wave phase |
| $\phi_{mn}$ | Wave phase at $n^{th}$ frequency and $m^{th}$ direction |
| $\phi_1$ , $\phi_2$ | Specific wave phases |

DEPARTMENT OF THE ARMY
WATERWAYS EXPERIMENT STATION, CORPS OF ENGINEERS
3909 HALLS FERRY ROAD
VICKSBURG, MISSISSIPPI 39180-6199

Official Business

SPECIAL

FOURTH-CLASS
U.S. POSTAGE PAID
VICKSBURG, MS
PERMIT NO. 85

37907/012/01
DOCUMENTS LIBRARY/SMITH 206
WOODS HOLE OCEANOGRAPHIC INSTITUTION
WOODS HOLE MA 02543-1098